Membrane fouling in waste water filtration

causes, consequences and prevention

Emile Cornelissen

41

MEMBRANE FOULING IN WASTE WATER FILTRATION

Causes, consequences and prevention

PROEFSCHRIFT

ter verkrijging van
de graad van doctor aan de Universiteit Twente,
op gezag van de rector magnificus,
Prof.dr. F.A.van Vught,
volgens besluit van het College voor Promoties
in het openbaar te verdedigen
op vrijdag 16 mei 1997 te 13.15 uur.

door

Emile Robin Cornelissen

geboren op 11 augustus 1968
te Apeldoorn

Dit proefschrift is goedgekeurd door de promotoren prof.dr.ing. H.Strathmann en prof.dr.ir. T.Reith en de assistent-promotor dr.ir. Th.v.d.Boomgaard.

Acknowledgements

Unilever Research Laboratory Vlaardingen is gratefully acknowledged for their co-operation in and financial support of the work described in this thesis.

Thanks are due to dr. F.F.Stengaard from Dow Denmark Separation who kindly supplied the membrane samples.

Cornelissen, Emile Robin

Membrane fouling in waste water filtration: Causes, consequences and prevention
Emile Robin Cornelissen. -[S.l. : s.n.]. - Ill.
Thesis Enschede. - With Ref. - With Summary in Dutch.

ISBN 90-9010598-0

Printed by: Alfa, Enschede, The Netherlands

Voorwoord

De eenzame auteursnaam die op de voorzijde van dit proefschrift prijkt, suggereert ten onrechte dat de produktie van dit proefschrift een solistische aangelegenheid is geweest. Niets is minder waar in mijn geval. In de afgelopen vier jaar heeft een aantal personen een belangrijke bijdrage geleverd aan de totstandkoming van dit proefschrift, die hier niet onvermeld mogen blijven. De volgorde van de lijst van namen is zeker geen rangorde naar belangrijkheid.

Allereerst ben ik mijn promotoren Heiner Strathmann en Tom Reith mijn dank verschuldigd, zonder wie er geen promotieopdracht was geweest in de eerste plaats. Thonie van den Boomgaard heeft als begeleider een belangrijke bijdrage geleverd aan het werk, met name tijdens het (her)schrijven van het proefschrift.

Tijdens vele bezoeken aan het Unilever Research Laboratorium te Vlaardingen kon een aantal mensen altijd tijd vrij maken voor een discussie over membranen, ondanks volle agenda's. Hieronder valt in de eerste plaats Remko Boom, die ik wil bedanken voor vele ideeën en nuttige suggesties die mede richting hebben gegeven aan het onderzoek. Zijn enthousiaste begeleiding in de afgelopen vier jaar heeft mij een eind op weg geholpen. Vele interessante en leerzame discussies waren er met Theo Verbeek en Ard Leerink die vaak met dezelfde problemen kampten als ik.

Het spreekwoord, "vele handen maken licht werk", geldt zeker in mijn geval. Allereerst kon ik twee jaar op de hulp en inzet bouwen van Betty Folkers, die voor mij een vliegende start betekende. Verder had ik het geluk om vier afstudeerders te mogen begeleiden. Ruben Sander, Peter Haverkort, Arianne Moraal en Caroline Bruinsma verschenen de afgelopen vier jaar na elkaar. Hun enthousiasme en inzet betekende voor mij van elk van hen een hoofdstuk vol aan experimenteel geweld en resultaten. HTS en HBO stagaires waren Kitty Nijmeier, Patrick Wuis en Lydia Versteeg die elk op hun beurt veel experimenteel werk verzetten met evenveel enthousiasme en inzet. Aan BKp-studenten, die bij mij hun technische opdracht van zes weken uitvoerden, ook geen gebrek. Dankzij het experimentele werk van Albert Kassies, Jeroen Mulder, Harry Gruben en Jappe v.d. Zwan konden vele losse eindjes aan elkaar worden geknoopt. Verder wil ik al de andere studenten hierbij bedanken die, meestal in het kader van een practicum, een bijdrage hebben geleverd.

De membraantechnologie groep is een leuke en gezellige groep. In elk voorwoord van een verslag uit deze groep valt dit te lezen, wat wel de waarheid moet bewijzen van deze stelling. Vele uitstapjes, excursies, barbecues, borrels, etc. zijn de oorzaak en het gevolg van deze gezelligheid. In het bijzonder wil ik John(ny), Christel, Willem en

Franca noemen, die ieder op hun beurt de afgelopen vier jaar erg plezierig en aangenaam hebben gemaakt. Dezelfde namen kunnen bovendien worden genoemd als het gaat om vakinhoudelijke zaken en het corrigeren van (een gedeelte van) het proefschrift. Voor dit laatste dank ik ook Joost en Michiel. Sander, die in hetzelfde schuitje zat als ik, ben ik dankbaar voor zijn enthousiaste inbreng in bijna elk hoofdstuk van dit proefschrift. Ondersteuning bij allerlei praktische zaken tijdens het werk kon altijd worden gevonden bij John Heeks, Erik Rolevink en Greet v.d.Voort.

Tenslotte wil ik mijn familie en vrienden bedanken voor al hun interesse en geduld, met name tijdens het laatste jaar, waarin sociale contacten soms in de weg werden gezeten door het schrijven van het proefschrift. In het bijzonder mijn ouders voor al hun steun en begrip, wat voor mij altijd veel betekent. Dit geldt ook zeker voor Hilde, die ondanks de grote afstand altijd in de buurt was voor mij.

Emile

Contents

Chapter 1

Treatment of laundry waste water by micro- and ultrafiltration

1.1 Introduction

Due to an increasing demand of clean water and an ever decreasing amount of natural clean water resources, the use of water has to be controlled more carefully and the re-use of it is of increasing importance (Shuval, 1977). In the future, water will become a scarce and valuable product. Therefore, many domestic and industrial waste water streams have to be cleaned.

A variety of techniques is available to clean water (Judsen King, 1971). They can be divided into mechanical, thermal and biological treatments. Examples of mechanical waste water treatments are the use of settlers, filters and sieves. Settlers for example are used to separate components on the basis of a difference in density between the components and water (e.g. sedimentation of sand, creaming of oil). This technique is sometimes supported by adding chemical compounds to increase the settling effect. This is called flocculation in enhancing sedimentation or flotation in enhancing creaming. Examples of thermal treatments are evaporation and distillation techniques. A drawback of these techniques is a very high energy consumption to evaporate water from waste. Biological treatment in cleaning waste waters is carried out by using oxidation beds or active slabs.

A selection of a certain waste water treatment technique depends on many aspects, such as the type of waste water, cost (Rogers, 1984), available space, lifetime, necessity of adding extra chemicals, etc. For example, waste water can be polluted with particles (e.g. sand, oil-droplets), heat (e.g. cool water from heat exchangers), salts (e.g. sulphate, nitrates, phosphates), heavy metals (e.g. lead, mercury, cadmium), complex chemical agents (e.g. pesticides, detergents) and biological pollutants (e.g. viruses, bacteria). In this thesis waste waters from laundry processes are investigated. Particularly the possibility of the application of a waste water treatment device within a domestic laundry machine is studied.

The total amount of water used in a wash load can be reduced if the waste water stream could be purified and recycled. Furthermore, some of the detergent components

could be regenerated and re-used, thus reducing the strain on the environment. Water usage can be reduced by the introduction of a water saving system.

Waste water streams from a washing machine have a low suspended solid weight fraction. In this thesis the application of membrane separation techniques for the removal of the solid weight fraction will be investigated (Fane, 1995). These techniques are usually very compact and do not need an extra energy source, apart from a pressure gradient along the membrane filtration unit. This is supplied by a pump already available in a washing machine. Furthermore, membrane separation techniques usually do not require any change in aggregation state (unlike evaporation and distillation) or additives (unlike flocculation and flotation).

Several problems arise when membrane filtration will be used in a household washing machine. The membrane filtration device has to operate at temperatures between 20 – 90°C and has to filtrate a batch of about 20 ℓ domestic waste wash water in approximately one hour. Furthermore, the device needs to have a lifetime in the order of magnitude of the lifetime of the washing machine with a constant performance. Components in waste water will have a different interaction with the membrane material, which will lead to a complex problem of membrane fouling. This has an influence on the membrane selectivity and permeability. It is this phenomenon which affects the lifetime and performance of a membrane filtration device in a washing machine. It is therefore the main topic of this thesis.

A brief introduction on membrane filtration will be given in §1.2. The laundry process and the composition of the waste water from laundry processes will be discussed shortly in §1.3 and §1.4 respectively.

1.2 Membrane filtration

A membrane can be defined as a permselective barrier between two homogeneous phases (Mulder, 1991). As a result of a driving force across the membrane, the components tend to be transported through the membrane, but due to its selectivity, the membrane will allow some components to permeate faster than others. Hereby, a separation can be achieved.

A classification of different membrane processes can be made according to this driving force.

- pressure driven membrane processes (e.g. reverse osmosis, nano-, ultra- and microfiltration, gas separation)
- electrically driven membrane processes (e.g. electrodialysis)
- concentration driven membrane processes (e.g. dialysis, pervaporation)
- temperature driven membrane processes (membrane distillation)

Another classification can be made on the basis of the separation mechanism. Membranes can act as filters which separate components in a feed solution because of a difference in solute size or membranes can act as barriers in which feed materials selectively are

dissolved and transported through the membrane. In the first case, membranes contain pores, contrary to the second case in which the membrane is usually a dense film.

In this thesis only porous membranes are used in a membrane process with a pressure difference as the driving force. In Chapter 9 of this thesis also an additional electric force will be used.

1.2.1 Ultra- and microfiltration

Pressure driven membrane processes using porous membranes can be subdivided into reverse osmosis, nanofiltration, ultrafiltration and microfiltration. In this thesis only the last two techniques are studied.

For filtration of waste water streams, both processes can be used depending on the diameter of solutes in the feed solution to be separated from the medium. In ultrafiltration, solutes with a diameter in the order of $1 - 100\ nm$ can be separated from the medium (usually water). In microfiltration the solute diameters are in the order of $0.1 - 10\ \mu m$ (Mulder, 1996). There is however no distinct border between the two processes.

Both ultra- and microfiltration membranes contain pores which differ enormously in diameter range. These pores are in the nanometer range for ultrafiltration membranes and in the micrometer range for microfiltration membranes. Ultrafiltration membranes are usually characterised by membrane manufacturers by a so-called molecular weight cut-off (mwco). Mwco which is defined as the molecular weight of standard solutes (polyethyleneglycol or dextranes) that are for 90% rejected by the membrane. This definition, however, strongly depends on the process circumstances and the solutes and concentration which are used, and is therefore only a qualitative characterisation parameter (Koops, 1995). Microfiltration membranes are usually characterised by an experimentally determined mean pore diameter.

1.2.2 Flux and retention

An important property of a membrane is its flux, which is defined as the permeate mass (or volume) flow through the membrane per unit membrane area. The membrane mass (or volume) flux or simply the flux J through the membrane is given by:

$$J = \frac{1}{A_m}\frac{dm}{dt} \tag{1.1}$$

Here is m the total collected mass of the permeate during a time t, and A_m the membrane area.

Another important characteristic of a membrane is selectivity. This can be expressed as the retention R which is defined as:

$$R = 1 - \frac{c_p}{c_f} \tag{1.2}$$

Here is c_p and c_f respectively the concentration in the permeate and the concentration in the feed solution. When solutes are completely retained by the membrane, the membrane has a retention of $R = 1$.

1.2.3 Concentration polarisation and fouling

When during a separation process, an aqueous solution is brought to a porous membrane surface, water will permeate through the membrane under a given driving force while solutes are retained. This leads to an accumulation of the retained solutes at the membrane surface. The increased concentration will be counterbalanced by a back diffusion into the bulk and consequently a concentration gradient is formed in the boundary layer. This phenomenon is called concentration polarisation (Jonsson, 1984; Strathmann, 1979) and is schematically depicted in Figure 1.1. In this figure, the feed solution is well mixed and the concentration build up takes place in the boundary layer adjacent to the membrane surface.

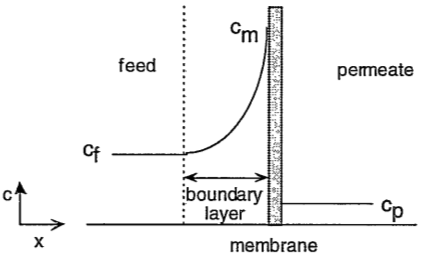

Figure 1.1: Schematic drawing of the concentration profile in the feed solution and in the permeate, illustrating the concentration polarisation phenomenon

The concentration at the membrane surface is c_m. A distinction has to be made between the observed retention R as defined above by equation 1.2 and the intrinsic membrane solute retention R^* given by:

$$R^* = 1 - \frac{c_p}{c_m} \tag{1.3}$$

As can be seen from Figure 1.1, R^* is larger than R.

Concentration polarisation is a reversible process and will disappear when the driving force is removed. Concentration polarisation results in a fast reduction in flux through the membrane and eventually in adsorption, precipitation or gelation of the solutes on the membrane surface. These phenomena are referred to as membrane fouling and are normally related to a long time flux decline. Contrary to concentration polarisation, fouling can be irreversible and is a complex phenomenon which depends on many factors, such as membrane material, temperature, pressure, type and concentration of the feed solution. Fouling will be discussed more thoroughly in Chapter 2. The laundry process itself is shortly described in the following paragraph.

1.3 Laundry process

A washing process is a batchwise operated process which is meant to separate soils (such as small particles and oils) from fabrics (i.e. the laundry). Dirty laundry is put into a

vessel which is then partially filled with water. After this, the system is agitated by rotation. To enhance the cleaning process, a mixture of chemicals (detergent) is added to the system. Processes in the vessel are carried out at temperatures of $20 - 90°C$. These are the basic actions of a washing machine (Brekel, 1987). For economical, environmental and technological reasons, it is interesting to have a closer look at the process and try to improve the efficiency, i.e. by using less energy, chemicals and water per wash load.

A typical household washing machine uses approx. 75 ℓ water per load, which is discarded as waste water after washing. Apart from this, $50 - 200$ g of detergent (i.e. washing powder) is added to the system. In some older designs, because of mechanical imperfections, approximately 25% of the detergent is directly flushed away. The function of water is first to act as a solvent for the detergent and secondly after being in contact with the fabrics to act as a solvent for some of the soil components and a dispersing medium for the rest of the insoluble soil components. At the end of the process, water is used for removing all components (detergents and soil) from the fabrics.

Some chemical compounds in detergents are known to affect the quality of ground- and surface water (Jakobi and Löhr, 1987). Some of these compounds may lead to an undesirable foam formation in natural waters. Another problem is the eutrophication of natural waters by phosphates which have been added to detergents to decalcinate water.

In the past decades, the composition of detergents has changed considerably, for a variety of reasons. Through these changes it became possible to use high-agitation machines as the typical European horizontal-axis machine, to wash at ever lower temperatures and thus with a lower energy consumption, and with less detergent, while the wash result has constantly improved. The main groups of ingredients of the detergent are described in the following paragraph.

1.4 Composition of the waste water

Waste water from laundry machines consists of the ingredients of detergents and removed waste components from dirty laundry. It may further contain components removed from the fabric itself. Because of variations in the kind of fabric encountered world-wide, the diversity in washing machine technology and different regional customs for fabric use and care, there is a remarkable variety in detergents. Detergents are complex formulations and contain several different types of substances, classified in the following major types (Jakobi and Löhr, 1987):

- surfactants
- builders
- bleaching agents
- auxiliary agents

The composition and amount of removed waste from the laundry also shows large variations and depends on many factors.

1.4.1 Surfactants

The most significant component in a detergent is a mixture of surface active agents (i.e. surfactants). The function of surfactants is multiple. They lower the surface tension of water, leading to a better wetting of the laundry, play an important role in the soil removal mechanisms and hinder redeposition of soil that already has been removed.

A surfactant molecule consists of a hydrophobic and a hydrophilic part. The hydrophobic part usually is an aliphatic chain, while the hydrophilic part differs for the type of surfactant. Depending on the charge, surfactants can be subdivided into four groups : anionic, nonionic, cationic and amphoteric surfactants.

Anionic surfactants are present in large amounts in detergents. The hydrophilic part of an anionic surfactant consists of a negative charged head-group with a cationic counter-ion. The first applied detergent was soap (sodiumstearate). It is very sensitive to water hardness, i.e. the amount of Ca^{2+} and Mg^{2+} in the water, and forms so-called limesoap, which prevents soil removal to take place effectively and has a number of other disadvantages. It was replaced by synthetic surfactants such as alkylbenzene sulphonates (ABS) which show better characteristics in many aspects. Generally, these synthetic anionic surfactants are relative inexpensive compared to nonionic surfactants (see later). Furthermore, they show little redeposition of removed soils onto the substrate and a good particle soil removal, both contrary to nonionic surfactants and soap. Drawbacks of synthetic anionic surfactants are a high foaming tendency and a poor oily soil removal. Also relative large amounts of surfactant are necessary at high ionic strength for a good washing effect.

Nonionic surfactant molecules contain a hydrophilic part which usually consists of a chain of ethylene oxide groups. Contrary to anionic surfactants, nonionic surfactants do not show electrostatic interactions. An advantage of nonionic surfactants is that they can be tailored to a certain need, with respect to washing effectiveness simply by changing the degree of polymerisation of the ethoxylate chain. Other advantages are a good oily soil removal and a low foaming tendency. Drawback are, that they are expensive, show a lot of redeposition of soil onto the substrate and have a poor particle soil removal.

Cationic surfactants have a positive charged head-group which is compensated by an anionic counter-ion. This group is not of great commercial importance for detergency, because cationic surfactants reduce the mutual repulsion of soil (dirt) and laundry because of electrostatic attractions. They are used as a fabric softener, sometimes in the presence of a nonionic surfactant. Cationic surfactants have an opposite effect in comparison with anionic surfactants, therefore mixtures of these two surfactants show no washing effect, in fact, they precipitate.

Amphoteric surfactants can display good detergency performance, but are too expensive for commercial application. Apart from this they are in general toxic.

In laundry detergents the trend is to use surfactant mixtures which enhance each other. Especially mixtures of anionic and nonionic surfactants are used. The choice of which surfactants to use in a detergent depends on the washing performance, but also on toxicological and ecological aspects.

1.4.2 Builders

The main function of builders in a washing powder is supporting the detergent action by extracting calcium and magnesium ions from wash water. These bivalent ions are present in tap water, in soil, and in fabrics. These ions form undesirable precipitates, e.g. with anionic surfactants or soaps originating in the soil, giving rise to poor soil removal, formation of unwanted residues and encrustation of machine parts. Three groups of builders can be distinguished: alkalis (e.g. soda, silicates and sodiummonophosphate), complexing agents (e.g. sodiumtriphosphate) and ion exchangers (e.g. sodium aluminum silicates or zeolites).

Contrary to alkalis, complexing agents are builders which do not precipitate with calcium and magnesium ions, but form water-soluble complexes (chelates). Ion exchangers have many similarities with complexing agents (see Chapter 7 of this thesis). The main difference is that ion exchangers are not soluble in water, in contrast to the relatively low molecular weight complexing agents.

1.4.3 Bleach system

A detergent may contain components for bleaching action. Bleaching is introducing a change towards a lighter shade in the colour of an object. Coffee-, tea- or ink stains have to be decomposed by oxidation or reduction by bleach agents.

Two types of bleaches that are commonly used are peroxide bleaches and hypochlorite bleaches. Hypochlorites are far more powerful bleach-agents than peroxides. A bleach activator is often used to obtain bleach activity at a lower temperature.

1.4.4 Auxiliary agents

Auxiliary agents are present in detergents in small amounts. Important auxiliary agents are enzymes which decompose proteins, hydrocarbons and fatty or oily soils.

Other auxiliary agents are optical brighteners (i.e. whitening agents) which transform UV radiation of sunlight to larger wavelengthes or absorb yellow light to increase the overall brightness. In this way washed laundry will look brighter than without whitening agents.

Fragrances provide a detergent and the washed laundry with an agreeable odour. Fillers are used for several reasons, such as providing good flowing properties, prevention of cake forming and prevention of dusting (Brekel, 1987) as well as providing to correct ionic strengths.

1.4.5 Dirt

Waste water of a washing process contains only upto about hundred grams of dirt, which results in a very low concentration. This dirt originates from soil in dirty laundry which stems from dust from the atmosphere, bodily excretion and impurities derived from domestic, commercial and industrial activities (Jakobi and Löhr, 1987). This soil consists

of a wide range of compounds, which can be classified into several groups such as water-soluble soils, fats, proteins, pigments and dyes. All these groups have to be removed from the substrate. Detergent action and mechanisms of soil removal are however beyond the scope of this work and will not be discussed here.

1.5 Objective of the research

The main problem that arises during waste water filtration in general is the occurrence of concentration polarisation and membrane fouling, resulting in a decrease in membrane performance. The aim of this thesis is to gain insight into the causes, consequences and prevention of membrane fouling. Emulsions are chosen as a model for waste waters. Membrane fouling is controlled in this thesis by a proper membrane selection, surface modification of membranes, the use of prefilters, the application of low transmembrane pressures in cross-flow filtration and the use of electrical forces.

1.6 Structure of this thesis

In Chapter 2 the state-of-the-art of membrane fouling is given. Several methods to reduce fouling and to enhance the membrane flux will be discussed.

Because waste water streams of domestic laundry machines are very complex mixtures with varying compositions, an oil-in-water emulsion has been chosen as a model for the waste water. The preparation of this emulsion is described in Chapter 3.

Several strategies to identify a low or non fouling membrane system have been investigated in this thesis. In Chapter 4 the selection of a suitable commercial membrane is studied. Both membrane material and membrane filtration aspects will be assessed.

A suitable membrane material which has both low fouling properties as well as good thermal and chemical stability properties is often unavailable. In Chapter 5 several surface modification techniques are discussed to obtain a thermally and chemically stable membrane with low surface fouling properties.

The mechanism of emulsion fouling of ultrafiltration membranes is the topic of Chapter 6. The use of prefilters on the feed side of ultrafiltration membranes to avoid fouling of the membranes will be investigated in Chapter 7.

Membrane fouling in cross-flow membrane modules is minimised by operating at low transmembrane pressures (Chapter 8) and by using electric forces (Chapter 9).

1.7 List of Symbols

Symbol	Quantity	Units
A_m	membrane area	$[m^2]$
J	permeate flux	$[kg \cdot m^{-2} \cdot h^{-1}]$
R	observed retention	$[-]$
R^*	intrinsic retention	$[-]$

c_f	bulk feed concentration	$[kg \cdot m^{-3}]$
c_m	concentration at the membrane face	$[kg \cdot m^{-3}]$
c_p	concentration of the permeate	$[kg \cdot m^{-3}]$
m	permeate mass	$[kg]$
t	time	$[s]$

Chapter 2

Fouling and fouling control - state-of-the-art

2.1 Introduction

During ultra- and microfiltration a decline in flux is observed, which is caused by concentration polarisation and fouling. Concentration polarisation is the accumulation of particles (or solutes) at the membrane surface as a result of the transmembrane pressure. This phenomenon is reversible and causes the flux to decline in the first seconds of the filtration process (Berg, 1988). As a result of accumulation near the membrane, particles (or solutes) might precipitate onto the membrane surface to cause membrane fouling, which is a collective term for phenomena that cause a long term flux decline (Lund and Sandu, 1981). Some of these phenomena are cake layer formation on top of the membrane, pore blocking, pore narrowing, adsorption, particle deposition, etc., which are often irreversible phenomena.

The state of the art of membrane fouling and fouling control is discussed in this chapter. First in §2.2 some models from literature are discussed which describe flux behaviour during ultra- and microfiltration. Second in §2.3 membrane fouling mechanisms are summarised and the influence of feed solution properties, membrane properties and process conditions on membrane fouling are discussed. Finally, in §2.4 several methods are discussed to control membrane fouling at three different levels, i.e., at the feed solution, the membrane and the process level.

2.2 Flux models

In literature, various models have been reported which describe the observed flux decline. In most of these models concentration polarisation and fouling are not discussed separately but taken together. Excellent articles exist, which review these flux models (Belfort *et al.*, 1994; Bruin *et al.*, 1980; Field, 1993; Lojkine *et al.*, 1992) and in this section a brief overview of these models is given.

2.2.1 Film model

As discussed before, concentration polarisation is caused by accumulation of solutes being retained by the membrane while solvent is passing. Because of this accumulation, solutes tend to diffuse back into the bulk solution. Concentration polarisation with low molecular weight solutes without precipitation at the membrane surface can be mathematically described by the so-called film model (Jonsson, 1984; Strathmann, 1979). The film model can be used in the case of reverse osmosis. It is assumed that a laminar boundary layer is established adjacent to the membrane surface in which longitudinal mass transport is negligible. Therefore mass transport within the boundary layer (i.e. the film) can be regarded one dimensional. During filtration a steady state situation is reached as a result of the balance between convective transport of solutes towards the membrane surface and diffusive back transport of retained solutes into the feed solution. This is schematically shown in Figure 2.1.

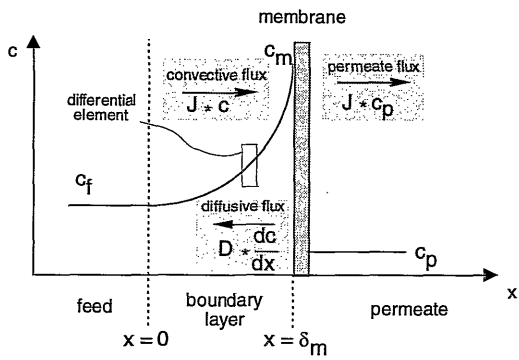

Figure 2.1: Schematic drawing of the concentration profile in the feed solution and in the permeate, illustrating the concentration polarisation phenomenon and the convective and diffusive transport terms

A material balance for the solute in a differential element (see Figure 2.1) of the film is given by:

$$J \cdot c = D\frac{dc}{dx} + J \cdot c_p \tag{2.1}$$

Here is c the concentration in the boundary layer at a certain distance from the membrane surface, c_p the concentration of the permeate, x the distance from the membrane surface, D the diffusion coefficient and J the convective flux towards the membrane which is identical with the permeate flux. Both the diffusion coefficient and the convective flux are assumed constant. This equation is integrated over the boundary layer in which concentration build up is assumed to take place with the following boundary conditions:

$$\begin{aligned} c &= c_f \quad \text{at} \quad x = 0 \\ c &= c_m \quad \text{at} \quad x = \delta_m \end{aligned}$$

Here is c_f the feed concentration, c_p the permeate concentration and δ_m the thickness of the laminary boundary layer. After integration, the film model relation can be found (Berg, 1988; Bowen and Jenner, 1995; Matthiason and Sivik, 1980):

$$J = k_m \ln\left(\frac{c_m - c_p}{c_f - c_p}\right) \tag{2.2}$$

In which:

$$k_m = \frac{D}{\delta_m} \tag{2.3}$$

Here is c_m the concentration at the membrane surface, c_f the uniform bulk concentration, k_m the mass transfer coefficient and δ_m the thickness of the boundary layer. The mass transfer coefficient k_m can be estimated from empirical correlations which are a function of the flow conditions in a membrane system (expressed by the Reynolds number), the nature of the feed solution (expressed by the Schmidt number) and the geometry of the system. For different filtration systems these relations are reviewed by Gekas et al. (Gekas and Hallström, 1987).

The film model can be used to study the effect of some characteristic filtration parameters on the permeate flux during reverse osmosis. If, for example, the cross-flow velocity increases, the model predicts higher fluxes, because of an increase in k_m. This is in accordance with experimental findings (Bauser *et al.*, 1982; Le and Howell, 1984). A temperature rise increases the diffusion coefficient and results in an increase in flux according to the film model. This is also observed in practice (Marshall *et al.*, 1993).

A drawback of this model is that the concentration at the membrane surface c_m is not limited. For all solutes there is, however, an upper solubility limit. Other simplifications are the assumption of a steady state situation, i.e., no variations in the concentration profile with time, no mass transport parallel to the membrane surface due to concentration or density gradients and a fully developed velocity profile in the turbulent flow regime. Despite these shortcomings the film model has proved to be quite useful to describe concentration polarisation in reverse osmosis under various flow conditions (Strathmann, 1979).

2.2.2 Gel formation

In ultrafiltration and especially microfiltration the simple film model is no longer applicable. This is because of a low diffusive back transport of macromolecules into the feed solution and a high transmembrane flux compared to reverse osmosis. If the diffusive back transport can not counterbalance the convective transport towards the membrane surface, the solute concentration at the membrane surface exceeds its solubility or gel concentration c_g (Michaels, 1968; Strathmann, 1979). This results in the precipitation and formation of a solid gel layer on the membrane surface, which adds an additional resistance to the transmembrane flux. This is schematically drawn in Figure 2.2, in which the concentration profiles are given of the feed solution, boundary layer and gel layer.

Increasing the transmembrane pressure, when a gel or cake layer has been established, results in a temporary flux increase and in an increase in solute deposition and thickening

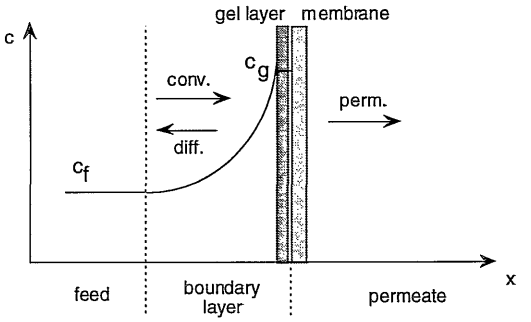

Figure 2.2: Schematic drawing illustrating the concentration polarisation with solutes which form a gel layer

of the gel or cake layer, which results again in a decrease of the flux to its original value (Jonsson, 1986). This means that in ultrafiltration and microfiltration the transmembrane flux will be independent of the transmembrane pressure as soon as a gel layer is formed. This transmembrane flux is called the limiting flux which is often observed in practice (Aimar and Field, 1991; Doshi, 1985; Sridhar, 1991). This is given by:

$$J_{\text{lim}} = k_m \cdot \ln\left(\frac{c_g}{c_f}\right) \tag{2.4}$$

Here is J_{lim} the limiting membrane flux, k_m the mass transfer coefficient, c_g the gel concentration and c_f the concentration in the feed solution.

This model is known as the gel layer model and was proposed by Michaels (Michaels, 1968). It has been used by many researchers in dead-end filtration (Blatt *et al.*, 1970; Trettin and Doshi, 1980) and in cross-flow filtration (Blatt *et al.*, 1970; Porter, 1972). The gel layer concentration can be found by plotting J versus $\ln(c_f)$ from which a straight line can be found with slope $-k_m$ and $\ln(c_g)$ as intercept.

A drawback of this model is that it can not be applied to solutes which do not precipitate or gelate. Furthermore, sufficient diffusion data are often lacking (Bowen and Jenner, 1995).

2.2.3 Osmotic pressure model

For solutes which do not precipitate or gelate, the flux behaviour can be described by an osmotic pressure model (Field and Aimar, 1993; Goldsmith, 1971; Jonsson, 1984). Until now, the osmotic pressure difference (always opposite to the pressure difference) across the membrane has been neglected. The reason for this is that contrary to low molecular weight solutes, macromolecular weight solutes have a very low osmotic pressure. Due to accumulation of solutes near the membrane during filtration, it is assumed that the effect of an osmotic pressure can no longer be neglected. The basis for the osmotic pressure

model is the flux equation:

$$J = L_p \cdot (\Delta P - \Delta\Pi) \tag{2.5}$$

Here is ΔP the transmembrane pressure, $\Delta\Pi$ the osmotic pressure difference over the membrane and L_p the hydrodynamic permeability. The magnitude of the osmotic pressure depends on the type of solute and on the concentration at the membrane surface (c_m). The relation between these parameters is expressed in the van 't Hoff equation for dilute solutions (Berg, 1988). More concentrated solutions behave non-ideal, resulting in a more complex relation:

$$\Pi = \frac{RT}{M_w}\left(c + B_2c^2 + B_3c^3 + \ldots\right) \tag{2.6}$$

Here is c the concentration of the solutes, M_w the molecular weight of the solutes, T the temperature, R the gas constant, B_2 and B_3 are respectively the second and third virial coefficients specific for the kind of solute. From this relation $\Delta\Pi(=\Pi(c_m)-\Pi(c_p))$ can be calculated if the concentration at the membrane surface c_m is known. This concentration can be found by using the film model (see equation 2.2). The osmotic pressure model also predicts the occurrence of a limiting flux. By increasing the transmembrane pressure, the flux through the membranes increases, which leads to an accumulation of solutes at the membrane surface. This results in an increase in the osmotic pressure difference, counteracting the transmembrane pressure. These two counteracting phenomena lead to a limiting flux. A drawback of this model is that in most practical situations in ultrafiltration and especially in microfiltration the osmotic pressure is negligible (Song and Elimelech, 1995).

2.2.4 Resistance models

Pressure driven membrane filtration can also be expressed in the resistance-in-series model (see also equation 2.5). The decline in flux in this model is caused by an increase in resistance against mass transfer. Transport through the membrane is described by the flux equation by Darcy's law for porous membranes:

$$J = \frac{\Delta P}{\eta R_{\text{tot}}} \tag{2.7}$$

Here is R_{tot} the sum of several resistances which are assumed to be additive and independent of each other. Reversible resistances (such as the reversible cake or gel layer) and irreversible resistances (such as the fouling resistance R_f) can be distinguished (Chudacek and Fane, 1984). The formation of a reversible gel-layer is the result of concentration polarisation (see §2.2.3 and §2.2.1). Fouling can be the result of many phenomena, such as pore blocking, pore narrowing, adsorption, internal fouling and formation of a cake layer and will be discussed in more detail in §2.3.1. A well-known model (Belfort, 1989; Blatt *et al.*, 1970; Cain, 1988; Kim *et al.*, 1992; Krijgsman, 1994; Reihanian *et al.*, 1983) based on the resistances in series approach is the cake layer model and will be discussed below.

Cake layer model

The cake filtration theory assumes that the diameter of the solutes is larger than the pore diameter of the membrane, so that no internal fouling can occur and a cake layer can be formed on top of the membrane (Baker *et al.*, 1985; Chudacek and Fane, 1984; Fane, 1984; Howell and Velicangil, 1982). Transport through the membrane is described by equation 2.7, in which the resistance is given by the sum of the membrane resistance and the cake layer resistance:

$$J = \frac{\Delta P}{\eta \left(R_m + R_c\right)} \tag{2.8}$$

Here is R_m the membrane resistance and R_c the cake layer resistance, which depends on the thickness of the cake layer given by:

$$R_c = r_c \delta_c \tag{2.9}$$

Here is r_c the specific cake resistance and δ_c the thickness of the cake layer. A well-known model for the specific resistance of a cake layer consisting of identical spherical particles is the Kozeny-Carman relation:

$$r_c = \frac{180(1-\epsilon)}{\rho_p d_p^2 \epsilon^3} \tag{2.10}$$

Here is d_p the diameter of the spheres, ϵ the void fraction of the cake layer and ρ_p the density of the particles. This model, however, does not account for compressibility of the cake layer.

If a cake layer is compressible, the cake layer resistance will increase as a function of the pressure. This will result in a decrease in transmembrane flux (Kawakatsu *et al.*, 1993). Cake compressibility has been reviewed by Tiller (Tiller and Yeh, 1987). Two compressibility mechanisms are distinguished. The first one being cake consolidation by degradation of particle aggregates with movement of particles into open spaces in the cake layer (nonelastic mechanism). The second one is cake compressibility by deformation of particles (elastic mechanism). Cake layer compressibility is expressed in a variation in the specific cake layer resistance as a function of the pressure given by (Tiller and Yeh, 1987):

$$r_c = r_{c,0} \cdot \Delta P^n \tag{2.11}$$

In which $r_{c,0}$ is the cake layer resistance at zero pressure and n is the compressibility index, expressing the degree of compressibility. If $n = 0$, no compression occurs.

2.2.5 Particle interaction models

In the models described so far, interparticle interactions such as electrostatic, dispersion and hydration forces have been neglected. Anomalies between calculated fluxes and experimental fluxes can be ascribed to neglecting these effects (Bowen and Jenner, 1995; McDonough *et al.*, 1989; McDonough *et al.*, 1992). In literature attempts have been made to incorporate these interactions, for example by taking electrokinetic effects in a cake layer into account (McDonough *et al.*, 1989). McDonough et al. added an extra

term to the film model which depends on the particle charge and the ionic environment. Reasonable good predictions have been found using this modified film model for particle sizes ranging from 0.01 to 0.2 μm.

A rigorous approach was given by Bowen et al. (Bowen and Jenner, 1995) in which a modified cake layer model is presented in which electrostatic, dispersion and hydration forces, electroviscous and entropy effects are incorporated. The model takes variations in time and place of the local specific resistance of the cake into account. It can thus be considered as a compressible cake filtration model. A good agreement has been found between theory and experiments for a broad range of solutes with different zeta potentials and ionic strengths. The main conclusion from this work is that the interparticle interactions are essential in the quantitative description of ultrafiltration, especially for particles in the range of $5 - 500$ nm. The effect was smaller with larger particles, for example in the microfiltration range (particles larger than 500 nm).

2.2.6 Back transport models

The film model describes the steady state flux in cross-flow ultrafiltration experiments quite reasonable. According to this theory, the permeate flux is expected to decrease for particles with increasing size, due to a decrease in the diffusion coefficient for larger particles. This is contrary to experimental findings. The underestimation of the permeate flux for larger particles (> 10 μm) is known in literature as the 'flux paradox' (Blatt *et al.*, 1970; Fane, 1984; Porter, 1972).

Blatt et al. (Blatt *et al.*, 1970) found that actual back transport during cross-flow filtration was substantially larger than would be expected from simple Brownian diffusion. These findings were confirmed by Porter (Porter, 1972) who argued that an extra mechanism for back diffusion exists during filtration. Different theories have been developed to describe particle transport in cross-flow filtration (Belfort, 1989; Belfort *et al.*, 1994; Bowen and Jenner, 1995; Field, 1993). Three of those, lateral migration, shear enhanced diffusion and flowing cake layers, will be discussed in more detail.

Lateral migration model

The first hydrodynamic theory to explain the observed flux paradox is lateral migration or the 'tubular pinch effect' (Altena *et al.*, 1983; Green and Belfort, 1980; Porter, 1972). Particles are dragged away from the membrane wall, because of forces which arise from the shear gradient. These forces are counterbalanced by convection of the particles to the wall by filtration. Dependent on the balance between these forces, particles are dragged towards the membrane and can cause a fouling layer or are swept away from the surface without fouling the membrane. Altena et al. (Altena *et al.*, 1983) theoretically showed that the mechanism of lateral movement from the surface is only possible for relatively large particles ($> \pm 1$ μm). Smaller macromolecules are not affected by this mechanism.

Shear-enhanced diffusion

This approach describes the re-entrainment of settled particles in a cake layer which tumble over each other as the layer is sheared. Because of movement of the particles, the diffusion of these particles is enhanced. This was observed for small rigid and neutral spheres dispersed in a viscous oil in shear flow. The following relations were found for the shear enhanced diffusion coefficient (Eckstein *et al.*, 1977):

$$D = \begin{cases} 0.1\phi r_p^2\gamma & 0 < \phi < 0.2 \\ 0.025 r_p^2\gamma & 0.2 < \phi < 0.5 \end{cases} \tag{2.12}$$

Here is r_p the radius of the particles, γ the shear rate and ϕ the volume fraction of the particles. Zydney and Colton (Zydney and Colton, 1986) used the description of the diffusion coefficient of Eckstein et al. and derived the following flux equation:

$$J = 0.078 \left(\frac{r_p^4}{L}\right)^{\frac{1}{3}} \gamma\rho \ln\frac{c_m}{c_f} \tag{2.13}$$

Here is L the length of the membrane channel. This equation, however, assumes a constant viscosity over the boundary layer, which is in general not correct in a practical microfiltration situation.

Flowing cakes and surface transport

As a result of imposed stress by cross-flow, the build-up foulant layer shears in the cross-flow direction. Particles are able to roll or slide along the membrane, giving rise to a "flowing cake". Leonard and Vassilief (Leonard and Vassilieff, 1984) were the first to apply this theory to cross-flow microfiltration.

This concept of a flowing cake is often combined with theories about shear enhanced diffusion. Davis and Leighton (Davis and Leighton, 1987) and Romero and Davis (Romero and Davis, 1988) developed a model combining the two theories. They were able to predict flux and cake layer thickness in a stationary state as a function of the membrane module length. For the length mean flux the following equation is obtained:

$$J = 0.06 \left(\frac{r_p^4}{\phi_f L}\right)^{\frac{1}{3}} \gamma\rho \tag{2.14}$$

Here is r_p the radius of the particles, γ the shear rate, ϕ_f the volume fraction of the particles in the feed and L the membrane module length.

2.2.7 Alternative models

A recent model was developed by Song and Elimelech (Song and Elimelech, 1995) to describe concentration polarisation in cross-flow systems, by using force, energy and mass balances. Particles were assumed to be incompressible and monodisperse.

This model distinguishes two regions : a concentration polarisation region and a cake-forming region. With help of the so-called filtration number N_f, it can be calculated which region is applicable. This number can be considered as the ratio of energy needed to bring a particle from the membrane surface to the bulk solution and thermal (dissipative) energy of the particle (Song and Elimelech, 1995) and is given by:

$$N_f = \frac{4\pi d_p^3}{3kT}\Delta P_p \tag{2.15}$$

Here is N_f the filtration number, d_p the particle diameter, T the temperature, k the Boltzmann constant and ΔP_p the pressure drop across the concentration polarisation layer. According to the authors it is justified to neglect the membrane resistance and ΔP can be taken instead of ΔP_p. If $N_f > 15$, the cake-formation theory applies and the following overall flux equation is applicable:

$$J = \left(\frac{2.25 \cdot D^2 \cdot \gamma(1+N_c)\Delta P_p \cdot M_w}{23.559 \cdot kT \cdot c_f \cdot L}\right)^{\frac{1}{3}} \tag{2.16}$$

Here is D the particle diffusion coefficient, γ the fluid shear rate, L the length of the membrane channel, c_f the bulk (feed) concentration. N_c is a dimensionless cake-forming number which expresses the effect of the cake layer thickness on accumulation of retained particles in the polarisation layer.

In this model, also local and average flux equations are given for the concentration polarisation region, together with the concentration distribution of accumulated particles in the cross-flow channel. For the cake-formation region, equations are given for the local fluxes and for the thickness of the cake layer as a function of the length of the channel. These are not given here but can be found in the reference.

An excellent agreement has been found between this theory and experimental observations. The theory predicts an increase in permeate flux with increasing particle size without incorporating a back transport model.

2.3 Membrane fouling

Membrane fouling is defined as a process resulting in performance loss due to the deposition of suspended or dissolved substances on external surfaces, at pore openings or within the internal structure of a membrane (Koops, 1995). The definition is not unambiguous but normally is concerned with a long-term flux decline (Jonsson, 1984). It is a very complex phenomenon which depends on a lot of factors. Different fouling mechanisms, such as internal fouling, pore blocking, pore narrowing and surface fouling by the formation of a cake layer are discussed in §2.3.1. Factors which influence membrane fouling are usually divided into feed solution, membrane and process parameters, which are discussed in §2.3.2, §2.3.3 and §2.3.4, respectively.

2.3.1 Fouling mechanism

Depending on the ratio between the solute diameter and the pore diameter of the membrane, different types of fouling can occur. If the pores are very small in comparison to the solute diameter, the formation of a so-called cake layer is favourable. This is often the case in ultrafiltration. If the pores are bigger than the solute diameter, different mechanisms can occur. This is the case in microfiltration where complete and partial pore blocking can occur. Also an internal fouling of the pores is possible, leading to pore narrowing. The different fouling mechanisms are schematically drawn in Figure 2.3.

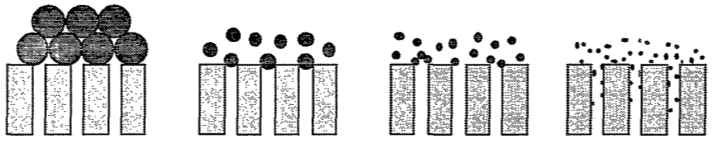

Figure 2.3: Different fouling mechanisms

The formation of a gel or cake layer creates an extra resistance to mass transport on top of the membrane phase and influences the flux and retention of the membrane. The difference between a fouling gel (or cake) layer and a gel (or cake) layer caused by concentration polarisation (see §2.2.2) is that the gel layer caused by concentration polarisation is formed on the membrane surface because the gel concentration is reached, whereas the fouling gel (or cake) layer is formed by other mechanisms (such as adsorption) and that it is more closely bound to the membrane surface (Jonsson, 1984). The density of the fouling cake layer can increase with the proximity to the membrane surface (Chudacek and Fane, 1984; Matthiasson, 1983) and the density may be higher around the pores (Kim *et al.*, 1992). The cake layer is affected by a lot of parameters, such as pH, ionic strength, transmembrane pressure, hydrodynamic conditions etc. An increased pressure for example can lead to a compaction of the layer and a decrease in thickness. During multicomponent filtration, smaller components can deposit within the structure of the cake layer lattice formed by larger components.

If pores are of about the same size as the solutes, complete or partial pore blocking can occur. Because of deposition at the pore entrance, obstruction of solvent passing occurs. This mechanism plays also a part in the first few seconds during (ultra)filtration (Fane, 1984; Fontyn, 1991). The biggest pores get plugged first, resulting in an immediate steep flux decline. This was shown by the application of the Hagen-Poiseuille equation for flow through capillaries. Due to pore plugging a loss in effective membrane porosity is observed.

Partial pore plugging is described by Le and Howell (Le and Howell, 1984) who developed a pore bridging model. Initial partial blocking can lead to bridges over the pore openings. This model has been used to explain the lack of truly pressure independent flux with colloidal suspensions.

Internal fouling of the membrane structure leads to pore narrowing. The amount of

internal fouling is small in ultrafiltration. In microfiltration a greater deposition within the pores exists. Deposition in larger pores dominates over smaller pores. Internal fouling is shown by radiolabeling (Hanemaaijer *et al.*, 1989). The amount of protein adsorbed onto nonporous polysulfone surfaces was 100-400 times less than the amount adsorbed in a membrane.

2.3.2 Feed properties

The occurrence and extent of membrane fouling depends on the type of feed solution that is used. In this paragraph the influence of the feed solution concentration, *pH* and ionic strength on the amount of membrane fouling is discussed. Also interactions between different components can affect the fouling behaviour.

Concentration

An increase in the feed concentration results in a decrease of the permeate flux (Bhattacharjee, 1993; Doulia *et al.*, 1992). This becomes clear from different models described in §2.2, in which c_f appears in the denominator of all equations. An exception to this 'rule' applies when solutes tend to cluster at higher concentrations (Bhattacharjee, 1993; Jönsson and Jönnson, 1991). This, or another effect that changes the solute size in the feed as a function of the concentration, can increase the flux and changes also the retention.

If internal fouling occurs, an increase in concentration leads to a more rapid flux decline in time, because the rate of deposition is increased. At increasing concentration the formation of a cake layer, however, is more likely.

If surface fouling dominates, an increase in the concentration increases the total hydrodynamic resistance to the membrane flux. This is due to an increase in the gel or cake layer thickness. This is also supported by the fact that retentions increase with increasing concentrations (Strathmann, 1979).

pH and ionic strength

The influence of the pH and ionic strength on membrane fouling is very complex and can be subdivided into four main aspects: molecular size changes, solute shape and flexibility changes, solute-solute interaction changes and solute-membrane interaction changes (Cheryan and Merin, 1981).

For proteins it is known for example that at the iso-electric point (IEP) the overall charge of proteins is zero (Marshall *et al.*, 1993). This results in the formation of a compact cake layer during filtration, leading to a low flux.

At higher or lower pH the proteins are charged which causes a mutual repulsion preventing clustering of proteins. Furthermore, if solutes are charged, the solubility in water increases and the affinity for the membrane decreases (Nyström, 1989). This leads to a looser cake layer during filtration leading to a higher flux. The charge of solutes is affected by the ionic strength that causes a charge shielding.

Component interaction

In multicomponent mixtures, filtration of one solute can affect the flux and retention behaviour of another solute (Oers, 1994). The presence of larger components in the solution can increase the retention of smaller molecules (Blatt *et al.*, 1970). A possible mechanism for this behaviour is the formation of a cake layer by larger molecular weight components that has a smaller porosity than the original membrane. Another mechanism is pore narrowing by one of the solutes affecting the filtration behaviour of other solutes. Also feed conditions might be changed due to different solute-solute interaction.

2.3.3 Membrane properties

Membrane related properties can be divided into membrane material related factors (e.g. hydrophobicity and charge) and into membrane structure related factors (e.g. roughness, pore size, pore size distribution and porosity). Both factors are discussed in this paragraph.

Hydrophobicity

Solutes tend to adsorb less onto hydrophilic membranes compared to hydrophobic membranes (Fane, 1987; Hanemaaijer *et al.*, 1989; Hanemaaijer *et al.*, 1988; Reihanian *et al.*, 1983; Stengaard, 1988; Wahlgren, 1989). Due to a lower degree of adsorption, higher permeate fluxes are observed with hydrophilic membranes (Müller and Krieger, 1981). According to Howell (Howell and Nyström, 1993) adsorption onto hydrophobic membranes leads to more compact structures and increased pore-blocking.

When concentration polarisation dominates, the effect of the hydrophobicity of membranes on the flux decline is obscured. In rotary systems where concentration polarisation effects are minimised, the flux behaviour of hydrophilic membranes is superior compared to hydrophobic membranes (Lopez-Leiva and Matthiasson, 1981).

Charge

The presence of charge is another membrane material related property that affects flux and retention behaviour of membranes. The charge of a membrane is strongly affected by the pH and the ionic strength of the feed solution (see also §2.3.2) and depends on the membrane material itself.

Charges on the membrane can achieve a retention of equally sized solutes. Nakao (Nakao *et al.*, 1988) filtrated a mixture of two equally sized proteins at a pH of the IEP of one protein. The other protein was of the same charge as the membrane. High retentions were found for the charged solutes.

Higher retentions have been found for charged solutes with a diameter smaller than the pore diameter for equally charged membranes compared to uncharged membranes (Marshall *et al.*, 1993). Even very small ions can be retained with relatively open ultrafiltration membranes if electrostatic repulsion is established.

Roughness

If the membrane roughness increases, the flux decline and the degree of fouling is observed to increase (Howell and Nyström, 1993). By using Langmuir-Blodgett layers a smoothing of the membrane surface leads to a decrease of flux loss and fouling (Kim *et al.*, 1989).

Surface roughness can alter the fouling mechanism. Extreme surface roughness hinders the formation of a complete cake layer, because solutes have to fill and bridge irregularities on the surface. This was found by Marshall et al. (Marshall *et al.*, 1993) who found lower retention for an open side up membrane compared to the same membrane with the tight side up.

Pore size

Initial permeate fluxes increase with increasing pore size (Bansal *et al.*, 1991). During filtration, however, the flux declines more rapidly for membranes with larger pores. In general it can be said that membrane fouling is more severe with increasing pore size because the degree of internal fouling increases.

Sometimes, however, an optimum pore size is found with respect to permeate flux. Below this optimum pore size the permeate flux is restricted by the membrane resistance or by the resistance of the fouling layer. Above the optimum pore size severe internal membrane fouling reduces the flux.

With increasing pore size the initial retention of the membrane decreases. During filtration the retention increases due to fouling (e.g. pore plugging and cake layer formation). In general, this is more severe as the pore size increases. This is shown by Meireles et al. (Meireles *et al.*, 1991) who filtrated different proteins with three different ultrafiltration membranes with a variation in pore size (cut-off value). During the first few minutes the retention was lowest for the membrane with the largest pores. After steady-state conditions all the retentions were similar regardless of the membrane.

Porosity and pore size distribution

In general, ultrafiltration membranes have relatively low surface porosities (approx. 0.10) compared to microfiltration membranes. Due to a low porosity, solvent flowing towards an ultrafiltration membrane will not meet a homogeneously permeable surface, but will have to follow streamlines to the opening of isolated pores (Fane and Fell, 1987). This is different for microfiltration membranes which have higher porosities (0.75–0.80). Because of the low porosity, ultrafiltration membranes show high local polarisation and fouling effects at the pore entrances.

Apart from this, membranes have a wide distribution of pore sizes. Fane et al. (Fane and Fell, 1987) calculated that the solvent flow is higher at the larger pores, resulting in a higher local concentration polarisation leading to a higher susceptibility to fouling. Therefore the overall membrane flux is very sensitive to the presence and population of large pores. In general the largest deposition (fouling) occurs with membranes with the lowest porosity and the highest heterogeneity. Except for the higher sensitivity of the

permeate flux to fouling, due to a wide pore size distribution, the selectivity is also poor (Jonsson, 1985).

Because of fouling phenomena both the pore size distribution and the porosity of the membrane change in time. According to Fontyn *et al.* (Fontyn, 1991) the number of largest pores decreases because of pore narrowing and the number of the smaller pores decreases because of pore plugging during filtration. Due to these phenomena, the flux and retention behaviour of the membrane alters during fouling. A striking example of this phenomenon is given by Gatenholm *et al.* (Gatenholm *et al.*, 1988) who compared protein filtration with a 0.2 μm microfiltration membrane to a 100 kDa ultrafiltration membrane. During filtration the retention for the microfiltration membrane was found to be much lower than the retention for the ultrafiltration membrane, but the final flux was higher for the ultrafiltration membrane. A possible explanation for this phenomenon is that the number of open pores is more reduced for the microfiltration membrane, resulting in a lower flux. Some of the largest pores, however, are still open resulting in a lower retention for the microfiltration membrane.

2.3.4 Process properties

The extent of membrane fouling is also affected by process related factors, such as temperature, transmembrane pressure and cross-flow velocity. These factors are the topic in this paragraph.

Temperature

Increasing the temperature generally leads to an increase in the flux, due to a lowering of the viscosity and an increase in the diffusivity (Grieves *et al.*, 1973; Yamagiwa *et al.*, 1993). This becomes clear from the different models as described in §2.2, which have an inverse proportional relation to the viscosity (e.g. film model, osmotic pressure model, lateral migration model) and a proportional relation to the diffusion coefficient. The flux can also decrease as a result of a temperature increase, if the feed properties are changed. For example by clustering and aggregation of solutes at high temperature, fouling is more severe in filtration of proteins than at low temperatures. The retention usually decreases with increasing temperature because of an increase in concentration polarisation (due to the increase of the permeate flux) resulting in higher solute concentrations at the membrane surface.

Transmembrane pressure

In general an increase in the transmembrane pressure results in an increase in the permeate flux. However, if the solubility limit of solutes during filtration is reached, a gel or cake layer is formed (see §2.2.2). If the pressure is increased when a gel or cake layer is established, a temporary flux increase causes the gel or cake layer to thicken, which results again in a decrease of the flux to its original value (Jonsson, 1986). Because of these phenomena, a limiting flux region exists above the so-called critical transmembrane pressure. This critical transmembrane pressure decreases as the mean pore size of the

membrane increases (Marshall *et al.*, 1993). If the increase in fouling rate is much higher than the increase in permeate flux, the permeate flux can even decline when the transmembrane pressure increases (e.g. by compaction of the fouling cake). This is sometimes the case in microfiltration. The rate of flux decline is also affected by the transmembrane pressure and increases with increasing pressure. The influence of the transmembrane pressure on the fouling will be discussed in Chapter 8 of this thesis in more detail.

Cross-flow velocity

Increasing the cross-flow velocity results in a flux improvement for both ultra- and microfiltration membranes (Blatt *et al.*, 1970; Le and Gollan, 1989; Yamagiwa *et al.*, 1993), owing to a reduction in concentration polarisation and fouling. This is due to the reduction in the boundary layer thickness δ_m, resulting in an increase of the mass transfer coefficient in the film model. For particle transport, an increase in the cross-flow velocity results in a higher shear rate (enhancing the back transport mechanisms).

In ultrafiltration, fouling due to the formation of a cake layer dominates. Increasing the cross-flow velocity leads to a reduction of the cake layer thickness because of re-entrainment of settled cake layer particles resulting in higher fluxes. Evidence for a diminished fouling layer at higher cross-flow velocity is given by a decreased retention.

For internal fouling mechanisms (e.g. pore narrowing) the cross-flow velocity has almost no effect on the flux and retention behaviour of the membrane. In some cases increased cross-flow velocities even lead to an increase in internal membrane fouling. This is caused by an increased pressure drop along a membrane module at higher cross-flow velocities.

2.4 Fouling control

A flux decline in time is the result of the occurrence of concentration polarisation and fouling during filtration, and leads to a loss in membrane performance. Membrane fouling is a complex phenomenon depending on a lot of factors which can be divided into feed solution, membrane and process related factors as are discussed in §2.3. Ways to reduce or even prevent the degree of fouling and enhance the membrane flux can also be divided into these three categories and are discussed in this paragraph.

2.4.1 Feed properties

Feed solutions usually are multicomponent mixtures, consisting of compounds with a wide range of molecular weights. It is known that the largest molecular weight compounds in these mixtures, can block the largest membrane pores resulting in a steep flux decline in the first few seconds of filtration. Apart from this, these largest molecular weight compounds can act as seeds or catalysts for the formation of a cake layer on top of the actual membrane resulting in lower fluxes. By prefiltration of the feed solution the permeate flux can be improved, because of removal of large molecular weight compounds

(Fane and Fell, 1987). This method of prefiltration is also referred to as clarification of the feed.

2.4.2 Membrane properties

The first fouling layer on a membrane is the result of the interaction between the feed solutes and the membrane material. This interaction will have a negative effect on the membrane performance and the separation characteristics, depending on the type of feed solutes. From literature it is known that hydrophobic materials show a stronger interaction with most solutes than hydrophilic materials (Fane, 1987; Hanemaaijer *et al.*, 1989; Hanemaaijer *et al.*, 1988; Reihanian *et al.*, 1983; Stengaard, 1988; Wahlgren, 1989).

Flux enhancement can be achieved by a proper membrane material selection or by changing the properties of the membrane (see Chapter 4 and 5 of this thesis). Hydrophilic membranes have a lower fouling tendency compared to hydrophobic membranes. These hydrophilic membranes, however, usually have a limited chemical and thermal stability. Therefore, hydrophobic membranes are used and flux enhancement can be achieved by modifying the surface properties of the membrane. This surface modification can be either irreversible (e.g. chemical reaction, plasma treatment, UV-irradiation) or reversible (e.g. adsorption coating) and will be discussed in chapter 5 of this thesis in more detail.

2.4.3 Process conditions

Turbulent flow

One of the easiest ways to improve fluxes is to increase the cross flow velocity, and change the flow field in a membrane module from laminar to turbulent flow. Due to this, concentration polarisation effects diminish as a result of increased mass transfer resulting in an improved flux. Turbulent flow can also reduce fouling because of an increase in wall shear rate at the membrane surface.

Turbulence promoters

Turbulence promoters present in a membrane module alter the flow field, resulting the membrane module to operate in a turbulent flow regime at lower cross flow velocities than for empty channel. This means that the pressure drop due to frictional forces is similar to (or smaller than) empty systems. Apart from this, turbulence promoters induce the formation of eddies at high flow velocities which enhance fluid mixing. All these factors decrease concentration polarisation and fouling.

Turbulence promoters appear in many shapes and sizes. Static rods, wire spiral, plastic mesh, metal grills and fluid beds inserted into the membrane channel are some examples of different kinds of turbulence promoters. All these types of turbulence promoters create an enhanced turbulence at the membrane surface and some of them also induce some sort of scouring action at the membrane surface. Nyström and Howell (Nyström, 1993) give an overview of plastic mesh turbulence promoters (spacers). They conclude

that an optimum cross-flow velocity exists because of an increase in pressure drop and an increase of the mass transfer as the cross-flow velocity increases.

Futselaar (Futselaar, 1993) developed a transverse flow membrane module for microfiltration hollow fibres, in which improved fluxes were found due to a reduction of a cake layer thickness on top of the membranes. Hollow fibre membranes were placed perpendicular to the feed flow and act as inserts which change the flow field in a membrane module from laminar to turbulent flow.

Backflushing

Backflushing serves to clean membranes by forcing the permeate periodically back through the membranes (Paul, 1984). As a result of this the accumulated cake on the membrane loosens and lifts off. According to Marshall *et al.* (Marshall *et al.*, 1993) removal of fouling by backflushing is possible if the accumulation takes place on the surface of the membrane rather than in the pores. If solutes are strongly adsorbed onto the membrane (e.g. in the case of protein adsorption) backflushing is not very effective. Typical backflush periods of several seconds in every few minutes are found to be very effective during filtration. Good results have been found by Wenten *et al.* (Wenten *et al.*, 1994) in using backflushing in beer filtration with very short backflushing intervals (within seconds). The disadvantage of backflushing is the energy consumption and the loss of permeate.

Pulsed flow

Unlike backflushing, neither filtrate nor much energy is required for pulsed flow (Nyström, 1993). Pulsed flow may be induced by pulsing of the feed solution by pump vibration, ultrasound or by other means. Pulsed flow enhances mass transfer and modifies the laminar turbulent transition. It was found that higher fluxes are favoured by higher frequencies and shorter pulse duration. There is however an optimum range of values for the frequency and pulse duration.

Alternatives

Another way to reduce membrane fouling is removing the gel layer at the membrane surface. This can be done mechanically by using sponge balls (mechanical cleaning). Also natural convection in the vicinity of the membrane can be used. Centrifugal forces can be used perpendicular or parallel to the boundary layer and are used in rotating membrane modules (Lopez-Leiva and Matthiasson, 1981). In a Couette flow system with an internal rotating cylinder high velocity gradients along the membrane can be achieved. Due to the small annulus, increased radial mixing occurs because of formation of counter rotating Taylor vortices. In this rotating membrane system concentration polarisation can be minimised. In a recent study by Ophoff et al. (Ophoff *et al.*, 1996) the use of a helically twisted modules are used to create Dean vortices to minimise concentration polarisation and fouling. Dean vortices in membrane modules are also studied by Belfort *et al.* (Belfort, 1989).

2.5 Conclusions

Flux decline during membrane filtration is the result of concentration polarisation and fouling, resulting in a loss of membrane performance. Concentration polarisation is the accumulation of solutes at the membrane surface which can result in a deposition of these solutes. This phenomenon can be described by the film model, gel or cake layer model using Brownian diffusion coefficients. These models describe the flux behaviour well for small solutes or particles ($< 0.1\ \mu m$), contrary to larger solutes or particles ($> 1\ \mu m$) for which a flux paradox has been observed and Brownian diffusion coefficients are too low. This flux paradox has been explained by several theories in literature, such as tubular pinch effect, shear enhanced diffusion and flowing cakes. In recent models interparticle interactions (e.g. electrostatic, dispersion and hydration forces) are incorporated to obtain a better description of the flux behaviour.

Deposition of solutes on the membrane surface can lead to fouling of the membrane, such as pore blocking, pore narrowing, irreversible cake layer formation, adsorption, etc. Membrane fouling is a very complex phenomenon, which depends on feed solution properties (e.g. concentration, pH, ionic strength and component interactions), membrane related properties (e.g. hydrophobicity, charge, roughness, pore size (distribution) and porosity) and process related properties (e.g. temperature, transmembrane pressure and cross-flow velocity).

Control of fouling to reduce or prevent a loss of membrane performance can be performed on these three levels. On the membrane level, for example, membrane fouling is minimised for hydrophilic membranes with a charge equal to the charge of the feed solutes. Furthermore, a membrane structure with small pores with a narrow pore size distribution is preferred with a high porosity. This depends, however, on the type and composition of the feed solution. Furthermore, high cross-flow velocities, low transmembrane pressures, pulsing of the feed and backflushing are effective to improve the membrane flux and reduce fouling.

2.6 List of Symbols

Symbol	Quantity	Units
B_2	second virial coefficient (equation 2.6)	$[m^3 \cdot kg^{-1}]$
B_3	third virial coefficient (equation 2.6)	$[m^6 \cdot kg^{-2}]$
D	diffusion coefficient	$[m^2 \cdot s^{-1}]$
J	permeate flux	$[kg \cdot m^{-2} \cdot h^{-1}]$
L	length of the membrane channel	$[m]$
L_p	hydraulic permeability	$[kg \cdot m^{-2} \cdot h^{-1} \cdot bar^{-1}]$
M_w	molecular weight	$[g \cdot mol^{-1}]$
N_c	dimensionless cake-forming number (according to equation 2.16)	$[-]$
N_f	filtration number (according to equation 2.15)	$[-]$
R	gas constant (= 8.3144)	$[J \cdot K^{-1} \cdot mol^{-1}]$

R_{cp}	concentration polarisation resistance	$[m^{-1}]$
R_c	cake layer resistance	$[m^{-1}]$
R_f	fouling resistance	$[m^{-1}]$
R_m	membrane resistance	$[m^{-1}]$
R_{tot}	total resistance	$[m^{-1}]$
Re	Reynolds number $(\frac{\rho v d_h}{\eta})$	$[-]$
Sc	Schmidt number $(\frac{\nu}{D})$	$[-]$
T	temperature	$[K]$
ΔP	transmembrane pressure	$[bar]$
ΔP_p	pressure drop across the concentration polarisation layer	$[bar]$
$\Delta\Pi$	osmotic pressure difference	$[bar]$
Π	osmotic pressure	$[bar]$
δ_c	thickness of the cake layer	$[m]$
δ_m	thickness of the mass boundary layer	$[m]$
ϵ	cake layer porosity	$[-]$
η	dynamic viscosity of the medium	$[Pa \cdot s]$
γ	shear rate	$[s^{-1}]$
ν	kinematic viscosity	$[m^{-2} \cdot s^{-1}]$
ϕ	particle volume fraction	$[-]$
ϕ_f	feed particle volume fraction	$[-]$
ρ	density	$[kg \cdot m^{-3}]$
c	concentration	$[kg \cdot m^{-3}]$
c_f	feed concentration	$[kg \cdot m^{-3}]$
c_g	gel layer concentration	$[kg \cdot m^{-3}]$
c_m	concentration at the membrane face	$[kg \cdot m^{-3}]$
c_p	concentration of the permeate	$[kg \cdot m^{-3}]$
d_h	hydraulic diameter	$[m]$
d_p	particle diameter	$[m]$
k	Boltzmann constant $(= 1.38062 \cdot 10^{-23})$	$[J \cdot K^{-1}]$
k_m	mass transfer coefficient	$[m \cdot s^{-1}]$
r_c	specific cake layer resistance	$[m^{-2}]$
$r_{c,0}$	cake layer resistance at zero pressure	$[m^{-2} \cdot bar^{-n}]$
r_p	particle radius	$[m]$
t	time	$[s]$
v	cross-flow velocity	$[m \cdot s^{-1}]$
x	distance from the membrane surface	$[m]$

Chapter 3

Oil-in-water emulsions as a feed solution for model studies

3.1 Introduction

Filtration of waste water streams is a relevant application of membrane processes (Vigo *et al.*, 1984). The major problem encountered during the filtration of waste water is a decline in membrane flux resulting in a loss of performance. Flux decline is caused by concentration polarisation and fouling of the membrane by waste water constituents (Fane and Fell, 1987; Jonsson *et al.*, 1996).

Waste water streams differ widely in composition and are strongly dependent on the process which generates the waste water. In this work, filtration of waste water from laundry processes will be investigated. The composition of these waste waters fluctuates strongly. For this study a model solution has been chosen for waste water from domestic laundry processes.

Nowadays, waste wash water contains anionic and nonionic surfactants (Jakobi and Löhr, 1987). Although usually mixtures of nonionic (alkyl ethoxylates) and anionic (alkyl sulphonates and alkylbenzene ethoxylates) surfactants are applied, in some processes only nonionic surfactants are used. Therefore, in this study, a choice was made to use only nonionic surfactants, for the sake of simplicity.

Apart from surfactants, waste wash water contains other membrane fouling constituents. The most severe foulants in waste wash water are proteins and especially oils (Bhattacharyya *et al.*, 1979; Lee *et al.*, 1984). In this study an oil was chosen as the model foulant for waste wash water.

Oil in waste wash water is usually present as surfactant stabilised droplets with a diameter of about 1 μm, created during the washing action of the detergent (Jakobi and Löhr, 1987). In this study, these oil droplets are manufactured in this diameter-range by an emulsification process. The droplet diameter and diameter distribution depend on several parameters during the emulsification process, dependent on the type of emulsification technique. This chapter deals with the theory and practice of emulsion preparation.

3.2 Theory

3.2.1 Definition of terms

An emulsion is a colloidal dispersion and is defined as an opaque, heterogeneous system which consists of two immiscible liquid phases, usually an 'oily' phase and a 'water' phase, in which one of the phases is dispersed as droplets in the other phase (Griffin, 1979; Heusch, 1987). Two situations can exist. An O/W emulsion exists when an 'oily' phase is dispersed in the 'water' phase which is the continuous phase. Vice versa the 'water' phase is dispersed in a continuous 'oily' phase resulting in a water-in-oil (W/O) emulsion. The diameter of the droplets in an emulsion is in the range of $0.01 - 10\ \mu m$. An everyday example of an emulsion is fresh milk, in which oil droplets are dispersed in water. These droplets have an average diameter of $3 - 4\ \mu m$ (Walstra, 1983).

Emulsions are thermodynamically metastable but stable in colloidal sense, which means that the droplets do not aggregate at a significant rate. Aggregation is the process or the result of the formation of aggregates. According to Everett (Everett, 1972) this is also called coagulation or flocculation for unstable colloidal dispersions, such as emulsions (see Figure 3.1 c).

In case of a density difference between the oil phase and the water phase, separation may occur, depending on the droplet diameter. When the droplets have a lower density than the continuous phase, creaming will occur dependent on the droplet diameter, which is the macroscopic separation of a dilute emulsion into a highly concentrated emulsion (Everett, 1972) (see Figure 3.1 a). When the droplets possess a higher density, sedimentation will occur (see Figure 3.1 b). These phenomena of separation are a function of time. A coarse emulsion, mainly droplets with a large droplet diameter, will separate faster than a fine emulsion with small droplets. In dairy technology this is used to delay creaming by reducing the droplet diameter by homogenisation (§3.2.3).

In principle both separation and aggregation are reversible processes and will lead to a closer packing density of the droplets. In some cases the formation of aggregates (flocculation of the emulsion) may be followed by coalescence (see Figure 3.1 d). Coalescence is the disappearance of the boundary between two particles, followed by changes of shape leading to a reduction of the total surface area. This phenomenon is irreversible without an additional energy input. If coalescence is extensive, it leads to the formation of a macrophase and the emulsion is said to break.

Coalescence of emulsion droplets can be prevented by the use of a proper emulsifier, which has several functions. An emulsifier facilitates emulsion formation by lowering the interfacial tension between the oil and water surface and prevents direct coalescence during emulsion formation. Emulsifiers can also assist the formation of a 'new' structure during emulsion formation. Depending on the chemical nature, the emulsifier is capable of stabilising water droplets in oil or oil droplets in water. The form of emulsions (W/O or O/W) is determined by the so-called 'Bancroft rule', which states that the continuous phase is the one in which the emulsifier is most soluble (Dickinson, 1994).

Emulsifiers can also provide a long-term stability of emulsions. Compounds that can function as emulsifier are polymers, surfactants or finely divided particles (Pickering

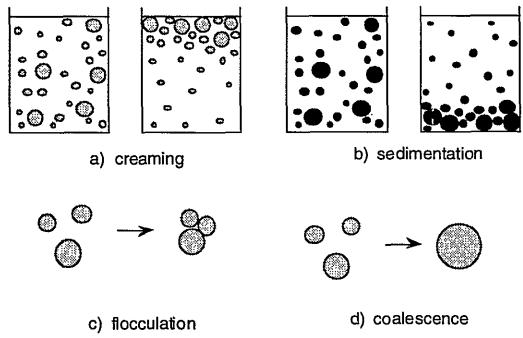

Figure 3.1: a) creaming, b) sedimentation, c) flocculation and d) coalescence

stability (Tadros, 1983)). This is the topic of the next paragraph.

3.2.2 Stability of emulsions

In oil-in-water emulsions, the oil droplets are dispersed in water (see §3.2.4). Because water is a poor solvent for oil, the colloidal system is called lyophobic according to IUPAC definitions (Everett, 1972). For these systems special measures are required to stabilise them. Without these measures the droplets will coalesce and the system will be colloidally unstable.

Colloid stability arises from the balance between repulsive and attractive forces between two approaching droplets. This stability can be drastically influenced by stabilisers, e.g., surfactants and polymers. Usually these substances adsorb strongly on the colloid particles and change the double-layer and/or introduce a steric component to the particle interaction.

For charged surfactants or charged polymers, colloid stability is achieved by the balance between attractive van der Waals forces and repulsive double-layer or electrostatic forces (Tadros, 1983). This is described by the DLVO (Derjaguin, Landau, Verwey and Overbeek) theory which is the basic theory for the stability of lyophobic colloids (Tadros, 1983; Walstra, 1996). The theory will not be discussed here, since in the system discussed in this work no electrostatic forces are present.

In this work, oil droplets are stabilised by nonionic surfactants. In this case, a strong adsorption of the lyophilic part to the oil droplets results in a hydrophilic coating by the hydrophilic surfactant parts. Colloid stability is in this case achieved by so-called 'steric stabilisation' (Lyklema, 1991; Napper, 1977) by a balance between attractive van der Waals forces and repulsive forces arising from interpenetration of polymer chains (see Figure 3.2).

Quantification of these repulsive forces can be carried out by calculation of the free energy of interpenetration as was shown by Flory-Krigbaum (Napper, 1977). This free energy of interpenetration strongly depends on the interaction parameter between the solvent (in this work water) and the polymer chains. When two polymer layers interpen-

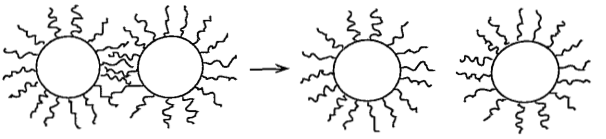

Figure 3.2: Schematic drawing of stabilisation due to repulsive forces by interpenetration of polymer chains attached to oil droplets

etrate, repulsion occurs when the polymer solvent interactions are more favourable than polymer polymer interactions (Lyklema, 1991). The solvent polymer interaction strongly depends on the conditions of the solvent (type of solvent, temperature and pressure). Other steric stabilisation theories explain the repulsive interpenetration forces in terms of osmotic pressure increase during overlap (Luckham, 1991). A significant disagreement has been found when comparing experimental findings to these steric stabilisation theories (Napper, 1977). Especially in the case of low molecular weight stabilisers, of which the degree of polymer interpenetration is low, stabilisation phenomena can not be explained by the steric stabilisation theories, and will not be used in this work.

A rather new approach to colloid stability is the VCG-theory (Van Oss, Chaudhury and Good) (Oss, 1994), in which colloid stability is given by three instead of two components. Colloid stability is a function of attractive van der Waals forces, repulsive electrostatic forces and acid-base or polar forces which can be both attractive or repulsive (Oss, 1996).

3.2.3 Preparation of emulsions

Emulsions are normally prepared by dispersion, thus by breaking down the droplet diameter by external forces. The most important techniques for emulsification are homogenisation, colloid milling and stirring (Becher, 1957; Dickinson, 1994; Walstra, 1983).

In a homogeniser emulsification is carried out by forcing oil and water through a fixed small hole at a high velocity and impinging the jet violently on the surface of a flat plate (see Figure 3.3 a). In colloid milling a high shearing force is created in a narrow gap between a stator and a rotor (see Figure 3.3 b).

Simple stirrers create turbulent flow in a tank with baffles near the walls, and may be of various types e.g. propeller and turbine stirrers (Figure 3.3 c). The mean droplet diameter in the emulsion decreases with increasing stirrer speed and with increasing emulsification time if sufficient surface active agents are present. Simple stirrers are often used as a pre-mixer of oil before feeding the mixture into a homogeniser or colloid mill. A special case of a simple stirrer is the ultraturrax which is a rotor-stator device with slits in both the rotor and the stator (see 3.3 d).

Simple stirring has been selected in this work for emulsification because of the simplicity of the technique.

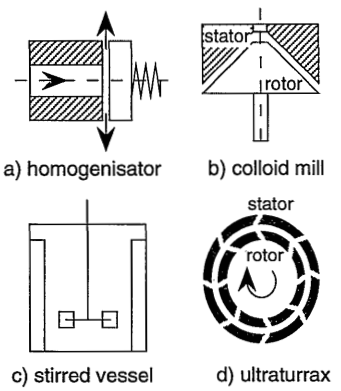

Figure 3.3: Different types of emulsificators

3.2.4 Principles of emulsification

During emulsification three different processes occur simultaneously (Dickinson, 1994). First droplets are deformed and broken up. The mean droplet diameter during emulsification is determined mainly by this mechanism (Donaldson, 1995), which is the topic of the next section.

Furthermore emulsifiers are transported towards the deformed or newly formed surfaces and adsorb onto them (the so-called Gibbs-effect). This adsorption can lead to a stabilising mechanism during emulsification and prevents coalescence of droplets, which occurs when two partially covered droplets encounter each other (the Gibbs-Marangoni effect). The region between the two droplets is depleted of emulsifier during adsorption of emulsifier onto the oil-water interface (Figure 3.4 a). Because of the interfacial tension

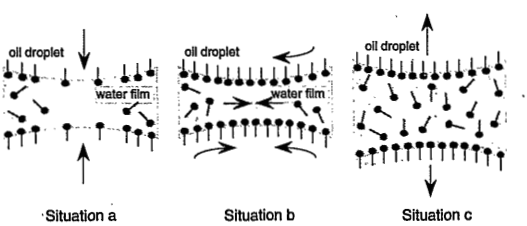

Figure 3.4: The Gibbs-Maragoni effect

gradient along the surface, emulsifier molecules move towards the region of the lowest surface concentration (Figure 3.4 b). These emulsifier movements drags liquid between the two droplets, which drives the droplets away from each other (Figure 3.4 c). This is a non-equilibrium process and is only possible if the droplets are partially covered with emulsifier. When the droplets have been formed and the emulsifier is equally distributed along the surface, recoalescence is prevented by other mechanisms (see §3.2.2).

Finally the droplets encounter each other and might coalesce depending on the stability of the newly formed droplets (see §3.2.2).

Droplet break-up

Emulsions with a droplet diameter of about 1 μm are prepared by introducing high mechanical energies into an oil and water system in order to increase the surface area between the two phases. The energy required for this process is given by:

$$\Delta G = \gamma \cdot \Delta A \tag{3.1}$$

Here is ΔG the energy required for the formation of the additional surface ΔA and γ is the interfacial tension between the two phases.

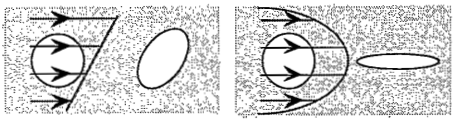

Figure 3.5: simple shear and elongational flow fields

Droplet disruption depends on the properties of the disperse and continuous phases, the interfacial properties and the flow conditions (Donaldson, 1995). In laminar flow, droplets can be disrupted by external shear forces. Examples of laminar flow fields are simple shear and elongational flow (see Figure 3.5). In turbulent flow, external forces arise from velocity gradients and might lead to droplet break-up. In literature both laminar and turbulent break-up mechanisms are described theoretically (Dickinson, 1994; Donaldson, 1995; Walstra, 1993). In this work, only the turbulent break-up mechanism is relevant, because simple stirring is used, and will be discussed in more detail.

Turbulent flow is usually characterised by a local velocity v which fluctuates chaotically around a time averaged value $\bar{v}$. The fluctuations are defined by the root-mean square average between these two values (Kolmogorov, 1949). Large fluctuations of the turbulent flow contain small eddies (i.e. circular or spiral movement of liquid). In the flow, a large spectrum of eddies exists of which the smallest contains the highest energy. Kolmogorov derived the following equation for the diameter ℓ of these eddies (Kolmogorov, 1949); the Kolmogorov length scale:

$$\ell = k \cdot \epsilon^{-\frac{1}{4}} \cdot \eta_c^{\frac{1}{4}} \cdot \rho_c^{-\frac{3}{4}} \tag{3.2}$$

In which k is a constant, ϵ is defined as the power input of a certain emulsification apparatus, η_c is the continuous phase viscosity and ρ_c is the density of the continuous phase.

A droplet which encounters an eddy with the same diameter of ℓ will deform if the external force $\rho\bar{v}^2$ which arises from the eddy velocity exceeds the surface tension force

γ/d_p. This can be expressed in terms of a dimensionless number which represents the ratio between the external and surface tension forces, the Weber-number:

$$We = \frac{\rho_c \bar{v}^2 d_p}{\gamma} \tag{3.3}$$

In which d_p is the droplet diameter, $\bar{v}$ is the time averaged velocity and γ the interfacial tension. The internal forces within the droplets have been neglected in this concept.

Deformed elongated droplets can break up in smaller satellite droplets, because of e.g. surface wave growth mechanisms (Donaldson, 1995). In literature a suitable approach has been found for the maximum stable droplet diameter in turbulent flow (Dickinson, 1994; Donaldson, 1995; Walstra, 1983). For droplets which are larger than the Kolmogorov length scale ℓ (see equation 3.2), it was theoretically found that:

$$d_p = k \cdot \rho_c^{-\frac{3}{5}} \cdot \epsilon^{-\frac{2}{5}} \cdot \gamma^{\frac{3}{5}} \tag{3.4}$$

In which k is a constant which accounts for the effect of a finite disperse phase viscosity and has to be determined experimentally.

In the case of smaller droplets with respect to the Kolmogorov length scale ℓ, shear forces rather than inertial forces dominate. For this case it was theoretically found that:

$$d_p = k \cdot \rho_c^{-\frac{1}{2}} \cdot \epsilon^{-\frac{1}{2}} \cdot \gamma \cdot \eta_d^{-\frac{1}{2}} \tag{3.5}$$

In which η_d is the viscosity of the disperse phase.

For fully developed turbulent flow in baffled vessels (e.g. simple stirrers), the energy input is given by the so-called 'Hinze-Clay' relation (Kumar *et al.*, 1993; Walstra, 1983):

$$\epsilon = \alpha N^3 D^5 \tag{3.6}$$

In which N is the stirring speed, D the diameter of the stirrer and α a constant which can be found in literature (Coulson and Richardson, 1996) for distinct vessel and stirrer geometries. The flow in simple stirrers is turbulent if the modified Reynolds-number exceeds a value of about $1 \cdot 10^4$. This modified Reynolds-number Re^* is given by (Coulson and Richardson, 1996):

$$Re^* = \frac{\rho_c N D^2}{\eta_c} \tag{3.7}$$

For droplet break-up in turbulent stirred vessels in which $d_p > \ell$, the droplet diameter correlates to the stirring speed with the power -1.2, which can be derived from equation 3.4 and 3.6.

3.2.5 The HLB-concept

The selection of a surfactant needed for the preparation of a certain emulsion is usually carried out on an empirical basis. The hydrophilic-lipophilic balance (HLB) concept has been introduced by Griffin for surfactant selection as an emulsifier in combination with

the used oil (Becher, 1966; Tadros, 1983). According to the HLB-concept, a surfactant has to be found with the same HLB-number as the oil, to obtain a good and stable emulsion.

The HLB has been introduced for both surfactants and oils and is based upon the relative percentage of hydrophilic to hydrophobic groups in a molecule. There are several ways to determine HLB-numbers, which are described in literature, but none of them appeared to be applicable to all surfactants or oils (Kirk-Othmer, 1979).

The HLB-concept is a very qualitative method applicable only to the investigated system and cannot be generalised. A reason for this is that obtaining a good and stable emulsion also depends on the method of dispersion (hydrodynamics), emulsifier concentration and the phase volumes of oil and water, which are not taken into account in the HLB-concept. Also the complexity of coalescence, liquid film thinning and shear phenomena are not taken into account. The concept can therefore only be used as an indication for obtaining good and stable emulsions.

3.3 Experimental part

3.3.1 Materials

Emulsions were prepared with Castor oil in ultrapure water stabilised by a nonionic surfactant. Castor oil is a vegetable oil and was selected for its high purity and non-toxicity. Like common vegetable oils it is a triglyceride, but is unique among these oils because of a very high (85 % to 90 %) content of one hydroxy fatty acid, ricinoleic acid. Castor oil is among the world's most versatile natural products and is used in the paint-industry, cosmetic industry and farmaceutical industry (Weiss, 1971). Castor oil was obtained from Merck Chemicals and had a viscosity of $\eta_d = 7 \pm 1$ *Poises* at 25°C . The interfacial tension of Castor oil at 20 °C is $\gamma = 39.0\ mJ \cdot m^{-2}$ in water (Kirk-Othmer, 1979).

The HLB-number for Castor oil in water was found in literature (Becher, 1966) to be 14. According to the HLB-concept (see §3.2.5) a surfactant has to be found with the same HLB-number as the oil, to obtain a good and stable emulsion. Synperonic NP9 was used with a HLB-number of 12.8 according to the manufacturers brochure.

Nonylphenol, with on the average nine ethyleneoxide groups, was used in this study and was obtained from ICI under the trade-name Synperonic NP9. The presence of the benzene-group in these surfactant-molecules was important for UV/VIS spectroscopy analysis. The critical micelle concentration for this nonionic surfactant is 145 $mg \cdot \ell^{-1}$ (Oss, 1994).

Ultrapure-water (from Millipore Milli-Q plus device) was used to prepare the emulsions.

3.3.2 Experimental set-up and methods

Emulsions of Castor oil in water stabilised by a nonionic surfactant were prepared with a simple stirring device (Janke & Kunkel GmbH & Co, type RW20) with a power con-

sumption of $P = 70\ W$ (at $220\ V; 50\ Hz$). The stirrer diameter was $D = 40\ mm$ and was a Rushton-type turbine with six blades with a length of $W = 6\ mm$. The vessel volume was 1000 ml (vessel diameter is $D_V = 100\ mm$) and consisted of four baffles with a length of $W_B = 15\ mm$ (see Figure 3.6). The height of the turbine in the vessel was $h = 50\ mm$ and the liquid height H was 140 mm and 38 mm for a liquid volume of respectively 1100 ml and 300 ml. The power input was found from $\epsilon = \frac{P}{V}$ and was $\epsilon = 64\ kW \cdot m^{-3}$ and $\epsilon = 233\ kW \cdot m^{-3}$ respectively for the two cases.

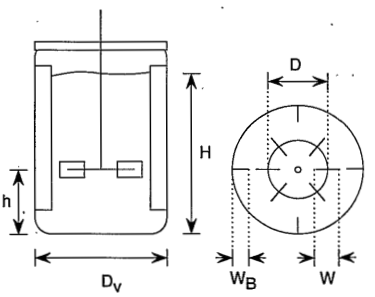

Figure 3.6: The stirred vessel with a Rushton impeller with its specific geometries

Castor oil and Synperonic NP9 were put together in the stirred vessel before water was added with a concentration of respectively 20 $g \cdot \ell^{-1}$ Castor oil and 8 $g \cdot \ell^{-1}$ Synperonic NP9. From preliminary experiments, the amount of nonionic surfactant was found to be sufficient to stabilise this amount of castor oil.

The constituents were mixed using the equipment described earlier. The influence of the stirring speed and the stirring time on the mean droplet diameter were studied for two different volumes of total emulsion. In the first set of experiments, the stirred vessel was completely filled with liquid (approx. 1100 ml) and the vessel was closed by a plastic lid to prevent incorporation of air. In the second set of experiments these precautions had not been taken and the total emulsion volume was 300 ml.

3.3.3 Characterisation of the emulsions

Particle diameter and diameter distribution

If all droplets in the emulsion are of the same diameter, the system is called monodisperse. In the case of a heterodisperse system with a distribution of particle diameters, the system is called polydisperse. The diameter distribution of a polydisperse emulsion solution is very important in the characterisation of the emulsions. The diameter distribution was determined with a Microtrac X100 (Leeds & Northrup) and an adequate sample was taken from the total emulsion which is representative for the continuous distribution.

In literature (Orr, 1983) several different mean diameters are used to characterise polydisperse systems, depending on the method of data determination and on the application of the diameter. A general expression for the mean diameter is given by (Orr,

1983):

$$d_{nm} = \left(\frac{\sum \Delta n_i d_i^n}{\sum \Delta n_i d_i^m} \right)^{\frac{1}{n-m}} \tag{3.8}$$

Here is Δn_i the number of particles per diameter range, d_i is the number based diameter and n and m are constants related to the type of mean particle diameter.

Often used mean diameters are the number mean diameter d_{10}, the surface mean diameter d_{20} and the volume mean diameter d_{30}. In this work, the so-called surface volume mean diameter d_{32} or Sauter mean diameter is used. This diameter relates the amount of available surface to the volume of the droplet and is a measure for the specific surface of the droplets.

Apart from the mean diameter, also a degree for the distribution of the droplet diameters must be found. Analogous to the polydispersity of the molecular weight of polymers, the polydispersity of a particle diameter distribution can be obtained. The polydispersity of molecular weights is given by M_w/M_n, respectively the weight average molecular weight and the number average molecular weight (Hiemenz, 1984). For particles in a normal diameter distribution the polydispersity is given by P_2.

$$P_2 = \frac{d_{21}}{d_{10}} \tag{3.9}$$

If $P_2 = 1$, the system is monodisperse, while for heterogeneous systems $P_2 > 1$.

Structure

To investigate the structure of an emulsion-sample on micro-scale, cryo scanning electron microscopy (cryo-SEM) pictures were made. For cryo-SEM measurements, samples were frozen in liquid nitrogen and were put into the working-chamber of the cryo-SEM device (Philips, 515 cryo-SEM). In this chamber, the samples were etched at $-80°C$ for 15 minutes. After this, the samples were covered by a gold-palladium layer and investigated by the SEM.

3.4 Results and discussion

3.4.1 Completely filled stirred vessel

Stirring time

First the influence of the stirring time on the mean droplet diameter was studied at a constant maximum stirring speed of about 1600 *rpm* (see Figure 3.7). The mean droplet diameter as calculated from equation 3.8 of the prepared emulsion decreased when increasing the stirring time up to 4 hours after which the mean droplet diameter remained constant. An explanation for this phenomenon was that the balance that existed between breaking-up and coalescence of droplets shifted towards breaking-up of droplets which were stabilised by the surfactant which was present. A droplet could only be

broken-up in the mixing zone of the Rushton-propeller. The probability of breaking-up increased when the stirring time was increased resulting in smaller droplets.

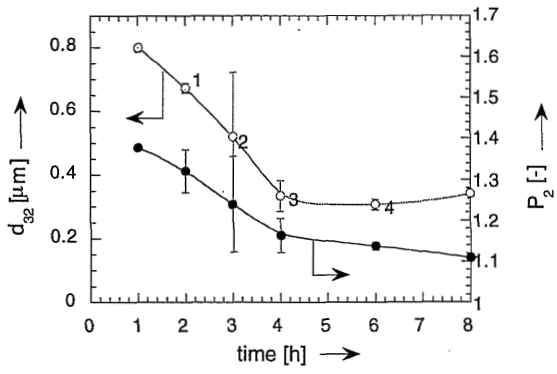

Figure 3.7: Mean droplet diameter d_{32} and distribution P_2 versus the stirring time for a completely filled stirred vessel ($N = 1600\ rpm$)

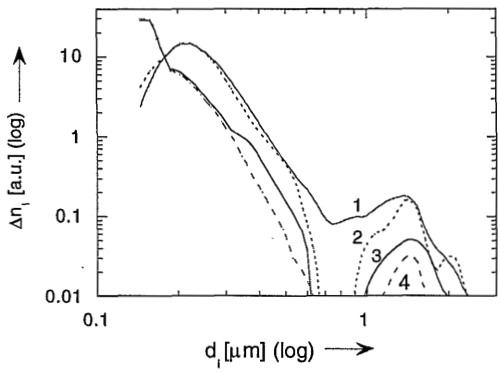

Figure 3.8: The droplet diameter distribution versus the stirring time for a completely filled stirred vessel. The numbers are in accordance with Figure 3.7 and represent 1) two hours, 2) three hours, 3) four hours and 4) six hours of stirring

The decrease in d_{32} with stirring time also becomes clear from Figure 3.8. From this figure it was also observed that two distributions in droplet diameter existed, one around 0.2 μm and a smaller one around 1.5 μm. As a function of the stirring time the peak around 1.5 μm diminished and the peak around 0.2 μm shifted towards smaller droplet

diameters. This indicates that sufficient time was needed to allow all the droplets to pass the mixing zone and break up (Kumar *et al.*, 1993). Still after 8 hours the peak around 1.5 μm did not fully disappear.

In Figure 3.7 also the polydispersity value is plotted versus the stirring time. This value is a measure for the droplet diameter distribution, which decreases with an increasing stirring time. This can also be observed in Figure 3.8. This was explained by a higher break-up probability in the mixing zone when the stirring time increased. This phenomenon was also observed (Dickinson, 1994) in literature.

After 4 hours the minimum mean droplet diameter was reached, which can be seen in Figure 3.7. This is however not clear from Figure 3.8, which indicates that at 4 hours mixing still no final state had been reached. Nevertheless 4 hours was taken as a constant when varying the stirring speed in the next paragraph.

Stirring speed

When the stirring speed is increased, the energy input ϵ increases resulting in smaller droplets. The stirred vessel is operated under fully developed turbulent flow for stirring speeds above 100 *rpm*, which is calculated from the modified Reynolds-number Re^* in stirred vessels (see equation 3.7).

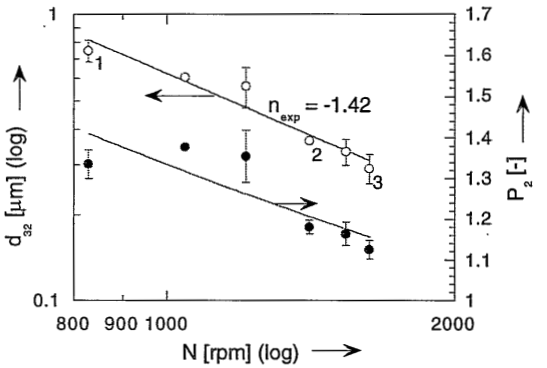

Figure 3.9: Mean droplet diameter d_{32} and distribution P_2 versus the stirring speed for a completely filled stirred vessel ($t = 4$ *hours*)

Assuming that the eddy-diameter is smaller than the emulsion droplet diameter, equation 3.4 is applicable. Combining this equation with the 'Hinze-Clay' relation 3.6 it was found that the droplet diameter correlated with the stirring speed to the power $n = -1.2$. In Figure 3.9 it can be seen that this was reasonably met with the experimentally obtained value $n_{\text{exp}} = -1.42$.

From Figure 3.10 again two droplet diameter distributions were observed. The same trends were visible for increasing stirring speed as for increasing stirring time. The smaller

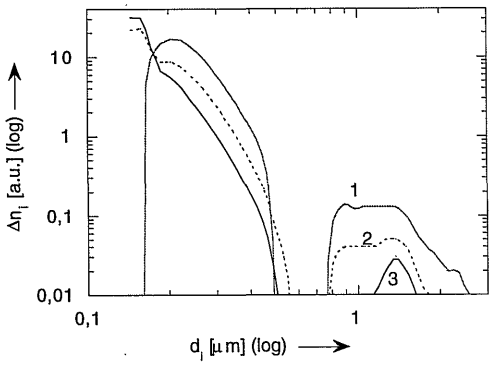

Figure 3.10: The droplet diameter distribution versus the stirring speed for a completely filled stirred vessel ($t = 4$ *hours*). The numbers are in accordance with Figure 3.9 and represent stirring speeds of 1) 830 rpm, 2) 1410 rpm and 3) 1630 rpm

peak around 1.5 μm diminished and the peak around 0.2 μm shifted towards smaller droplet diameters with increasing stirring speed. This was related to the frequency of droplets to enter the mixing zone near the impeller (Kumar *et al.*, 1993), which increased with increasing stirring time and stirring speed.

From Figures 3.9 and 3.10 it can also be seen that the droplet diameter distribution decreased with increasing stirring speed.

3.4.2 Partially filled stirred vessel

Stirring time and stirring speed

The effect of the stirring speed and the stirring time on the mean droplet diameter was studied for the situation that the stirring vessel is not completely filled with emulsion solution. Also the stirred vessel was not closed, so that air entrapment during stirring was observed, which reduced the effectiveness of stirring. In spite of this, emulsions have been obtained which were stable for at least one year.

The time effect on the droplet diameter distribution at 2000 *rpm* becomes clear from Figure 3.11. Both the mean droplet diameter and droplet diameter distribution decreases with increasing stirring time. No difference was found for stirring times of 90 and 120 minutes. Compared to the droplet diameter distribution for completely filled vessels (see Figures 3.8 and 3.10) it was striking that only one distribution existed. This was because of a larger frequency of droplets passing the mixing zone due to the lower liquid height.

In this situation the theory of turbulent break-up is no longer applicable because of incorporation of air into the mixing vessel. The break-up mechanism was complicated because of the occurrence of a gas phase during mixing which probably damped the high

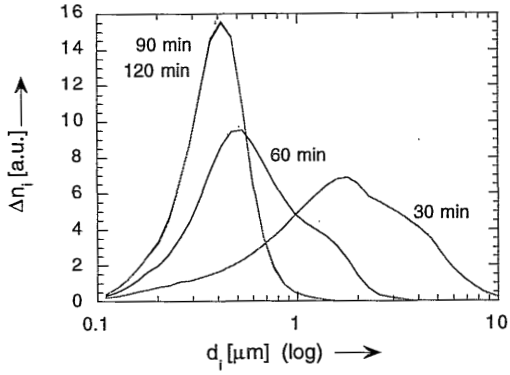

Figure 3.11: The droplet diameter distribution versus the stirring time for a partially filled stirred vessel ($N = 2000\ rpm$).

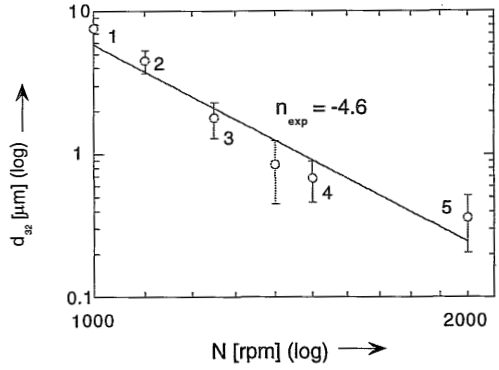

Figure 3.12: Mean droplet diameter versus the stirring speed of a partially filled vessel ($t = 120$ minutes)

turbulence zones in the mixing vessel. From Figure 3.12 it can be seen that the droplet diameter stirring speed dependence is now $n_{exp} = -4.6$ at a constant stirring time of 120 minutes. No explanation could be found for the fact that the droplet diameter decreased more strongly as a function of the stirring speed compared to a completely filled vessel.

The corresponding droplet diameter distributions for the different stirring speeds are given in Figure 3.13. Both the mean droplet diameter and droplet diameter distribution decreased with increasing stirring speed.

Emulsions with a small mean droplet diameter were selected as a suitable standard

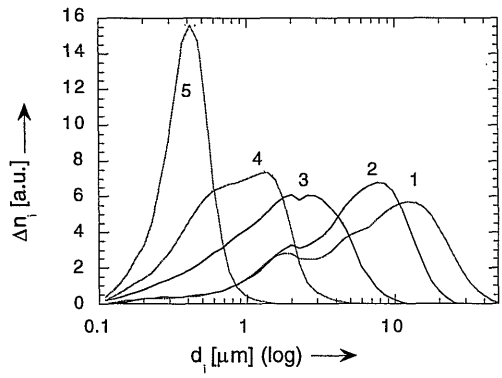

Figure 3.13: The droplet diameter distribution versus the stirring speed for a partially filled stirred vessel (t = 120 minutes). The numbers are in accordance with Figure 3.12 and represent stirring speeds of 1) 1000 rpm, 2) 1100 rpm, 3) 1250 rpm, 4) 1500 rpm and 5) 2000 rpm

(model) emulsion to represent waste wash water for further studies (see §3.1). The standard emulsion is prepared in a partially filled stirred vessel (300 ml) with a stirring speed of 2000 rpm for 90 minutes, because a single droplet diameter distribution was obtained, contrary to the completely filled vessel. The mean droplet diameter of this emulsion was measured by the Microtrac X100 and was $d_{32} = 0.22\ \mu m$.

Structure

A sample of the standard emulsion (90 minutes stirring at 2000 rpm in a partially filled vessel) was investigated by cryo-SEM to study the structure of the emulsion sample.

A high concentration of individual oil-droplets can be seen in Figure 3.14, in which a cryo-SEM picture of the freeze-dried emulsion sample is shown. The diameter of the droplets were estimated to be around $0.3 - 2.5\ \mu m$ from this cryo-SEM picture, which was higher than the droplet diameter determined by light scattering. The reason for this might be coalescence during sample preparation for the cryo-SEM device.

3.5 Conclusions

Emulsions were taken as a model for waste wash water. Stable emulsions were prepared by simple stirring of castor oil in water in the presence of Synperonic NP9. For a completely filled and closed-off stirred vessel, a double droplet diameter distribution was obtained. For a partially filled and not closed-off stirred vessel, air bubbles were influencing the break-up mechanism and a single droplet diameter distribution was obtained.

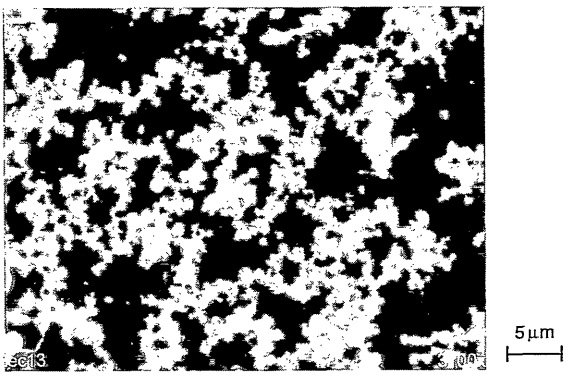

Figure 3.14: Cryo-SEM picture of a freeze-dried emulsion solution

The mean emulsion droplet diameter decreased with increasing stirring speed or increasing stirring time. Also the droplet diameter distribution decreased with increasing stirring speed or increasing stirring time.

Standard emulsions with a mean droplet diameter of about 0.22 μm were prepared in a partially filled stirred vessel (liquid volume of 300 ml) with a stirring speed of 2000 rpm for 90 minutes, which remained stable for at least one year. The diameter of these emulsion droplets was estimated to be around $0.3-2.5$ μm from cryo-SEM pictures.

3.6 Acknowledgements

Thanks are due to prof. M.M.C.G. Warmoeskerken (UT) and dr. R.M. Boom (URL Vlaardingen) for many fruitful discussions about preparing emulsions. Paul Zandbergen (URL Vlaardingen) carried out the Cryo-SEM experiments, Lydia Versteeg and Betty Folkers prepared the emulsions in respectively filled and partially filled stirred vessels.

3.7 List of Symbols

Acronyms

Symbol	Quantity
W/O	water-in-oil
O/W	oil-in-water
$DLVO$	Derjaguin, Landau, Verwey and Overbeek
VCG	Van Oss, Chaudhury and Good
HLB	hydrophilic lipophilic balance
NP	nonylphenol
SEM	scanning electron microscopy

Symbols

Symbol	Quantity	Units
D	length of the stirrer	$[m]$
D_r	vessel diameter	$[m]$
H	liquid height	$[m]$
Re^*	modified Reynolds-number for stirred vessels	$[-]$
W	width of the blades	$[m]$
W_B	width of the baffles	$[m]$
We	Weber-number	$[-]$
ΔA	area	$[m^2]$
ΔG	Gibbs energy of droplet break-up	$[J]$
α, k	constants	$[-]$
ℓ	eddy diameter	$[m]$
ϵ	power input	$[W \cdot m^{-3}]$
η_c	viscosity of the continuous phase	$[Pa \cdot s]$
η_d	viscosity of the disperse phase	$[Pa \cdot s]$
γ	interfacial tension	$[N \cdot m^{-2}]$
ρ_c	density of the continuous phase	$[kg \cdot m^{-3}]$
d_p	droplet diameter	$[m]$
h	distance between bottom of the vessel and the stirrer	$[m]$
N	stirring speed	$[rpm]$
d_i	droplet diameter of i	$[m]$
d_{nm}	mean droplet diameter according to formula 3.8	$[m]$
Δn_i	number of droplets within a class	$[a.u.]$
P_n	polydispersity number	$[-]$
M_w	weight average molecular weight	$[g \cdot mol^{-1}]$
M_n	number average molecular weight	$[g \cdot mol^{-1}]$
v	local velocity	$[m \cdot s^{-1}]$
$\bar{v}$	time averaged velocity	$[m \cdot s^{-1}]$

Chapter 4

Selection of membrane material and structure

4.1 Introduction

One of the major problems encountered during ultra- and microfiltration is the occurrence of flux decline in time due to membrane fouling. This phenomenon leads to a loss in membrane performance which has to be prevented. Membrane fouling is a very complex phenomenon including pore blocking, pore constriction, cake layer formation and adsorption (Jonsson *et al.*, 1993; Kim *et al.*, 1992). By a proper membrane selection these problems can be reduced or even prevented. This selection can be divided into a membrane *material* selection and a membrane *structure* selection, which both are the topic of this chapter.

Fouling of membranes is usually the result of adsorption of feed solution components at the membrane material (Gourley *et al.*, 1994). The general observation in membrane technology is that in aqueous systems, membranes prepared from hydrophilic materials show less adsorptive fouling than those prepared from hydrophobic materials. However, the use of hydrophilic materials is not always possible since the chemical as well as the mechanical stability of most hydrophilic materials is significantly lower than that of hydrophobic materials. The selection of a proper membrane material for a certain feed solution is a matter of optimisation between fouling tendency and chemical stability of the membrane material. The prediction of the fouling tendency is currently still largely empirical. In this chapter the fouling behaviour of polymer membranes by feed solution constituents is predicted by applying a general physico-chemical concept as developed by Van Oss and co workers (Oss, 1993; Oss, 1994). Furthermore, a correlation is established between fundamental surface properties and interactions with the constituents in the feed solution and the tendency of the membrane to foul.

Apart from adsorptive fouling, other fouling mechanisms can be distinguished such as internal fouling, which is highly undesired. Internal fouling can not be reversed completely by cleaning methods such as backflushing, and results in permanent membrane flux decline. It is known that ultrafiltration membranes show less internal fouling than microfiltration membranes (Gatenholm *et al.*, 1988) depending on the feed constituents.

In this chapter, membrane structure selection is carried out by emulsion filtration experiments with both ultra- and microfiltration membranes prepared from a polymeric material selected from the membrane material selection experiments.

4.2 Theory

4.2.1 Physico-chemical aspects of surfaces

Interaction forces in condensed media

The existence of the solid and liquid aggregation states is due to forces of attraction between molecules in these states. Surface forces arise from the net attraction of molecules from the surface towards the bulk. The interfacial tension acts on any interface and tries to minimise the interfacial area. Dimensionally, the interfacial tension is a force per unit length, with no specified direction (Lyklema, 1991). In any direction the interface tries to enlarge, the interfacial tension opposes the action.

Thermodynamically, the interfacial tension equals the differential free energy per unit area at a fixed temperature (T), pressure (p) and mole numbers (n_i) which is also related to the isothermal reversible work. For multicomponent systems this is given by:

$$\gamma = \left(\frac{\partial G}{\partial A}\right)_{p,T,n_i} \tag{4.1}$$

In which γ is the interfacial or surface tension, G the free energy, A the interfacial area and n_i the number of moles of substance i. The *surface* tension is defined at the boundary of two phases of which one of the phases is vacuum, or in practice a gas, while the *interfacial* tension is defined at the boundary of two liquids and at a solid-liquid interface, according to the IUPAC nomenclature (Everett, 1972).

The intermolecular forces, responsible for the surface and interfacial tensions, are subdivided into four classes. According to Van Oss (Oss, 1993; Oss, 1994) these classes are assumed to be additive. The interaction forces or surface tension components are:

1. Apolar or Lifshitz-van der Waals (LW) forces (γ^{LW})
2. Polar or Lewis acid-base (AB) forces (γ^{AB})
3. Electrostatic (EL) forces (γ^{EL})
4. Interaction forces due to Brownian movement (BR) (γ^{BR})

To determine the apolar contribution of the surface tension for a certain solid material (e.g. a flat hard polymer surface), contact angle measurements can be carried out with a high-energy apolar liquid.

Polar or Lewis acid-base (AB) interactions can be divided into an electron-donor and an electron-acceptor part. The polar contribution of the surface tension of a certain material thus consists of two parts, the electron-acceptor parameter part $\gamma^{\oplus}$ and the

electron-donor parameter part $\gamma^{\ominus}$. The total polar surface tension component of the surface tension γ^{AB} can be found from the geometric mean between the two parameters. This is given in equation 4.2:

$$\gamma^{AB} = 2\sqrt{\gamma^{\oplus}\gamma^{\ominus}} \tag{4.2}$$

In order to determine the two parts of this polar surface tension component experimentally, contact angle measurements have to be carried out with two different polar liquids, with a distinct difference in $\gamma^{\oplus}$ and $\gamma^{\ominus}$ values (see §4.3.2).

If a material consists of charged particles or molecules, electrostatic forces have to be taken into account. Electrostatic interactions are determined with the help of electrokinetic measurements, such as streaming potential measurements and electrophoresis (see Chapter 9 of this thesis). In this work, electrostatic interaction forces play a minor role and will be neglected.

Van Oss introduced a fixed contribution for the interaction forces due to Brownian motion, because of the thermal energy of molecules. This contribution is usually very small compared to the other three interaction forces and are neglected in our calculations.

The different interaction forces are assumed to be additive (Oss, 1993). In our case, the total surface tension is thus given by:

$$\gamma = \gamma^{LW} + \gamma^{AB} = \gamma^{LW} + 2\sqrt{\gamma^{\oplus}\gamma^{\ominus}} \tag{4.3}$$

In which γ^{LW} and γ^{AB} are respectively the apolar and polar contribution to the surface tension, and $\gamma^{\oplus}$ and $\gamma^{\ominus}$ are respectively the electron-acceptor and electron-donor part of the polar surface tension.

The free energy of adhesion

The interaction between two materials 1 and 2 immersed in liquid 3 can be described by the Dupré-equation (Oss, 1993). This equation gives the work necessary for adhesion and is given by :

$$\begin{aligned} \Delta G_{132} \;=\; & 2[\sqrt{\gamma_1^{LW}\gamma_3^{LW}} + \sqrt{\gamma_2^{LW}\gamma_3^{LW}} - \sqrt{\gamma_1^{LW}\gamma_2^{LW}} - \gamma_3^{LW} \\ & + \sqrt{\gamma_3^{\oplus}}(\sqrt{\gamma_1^{\ominus}} + \sqrt{\gamma_2^{\ominus}} - \sqrt{\gamma_3^{\ominus}}) + \sqrt{\gamma_3^{\ominus}}(\sqrt{\gamma_1^{\oplus}} \\ & + \sqrt{\gamma_2^{\oplus}} - \sqrt{\gamma_3^{\oplus}}) - \sqrt{\gamma_1^{\oplus}\gamma_2^{\ominus}} - \sqrt{\gamma_1^{\ominus}\gamma_2^{\oplus}}] \cdot \Delta A \end{aligned} \tag{4.4}$$

Here is ΔG_{132} the free energy of adhesion of material 1 and 2 in 3, γ_i the surface tension of material i and ΔA is the interfacial area. The tendency of interaction between two materials 1 and 2 immersed in a certain medium 3 (e.g. water) is thus expressed in ΔG_{132}. If the value of the free energy of adhesion is positive, no interaction occurs between materials 1 and 2. If the value is negative, adhesion will take place. This criteria can be taken as a tool for adhesion of foulants onto surfaces, and plays an important role describing membrane fouling.

4.2.2 Characterisation of nonporous surfaces

Many techniques exist for characterisation of surfaces. Advanced and rather expensive techniques are X-ray photoelectron spectroscopy (XPS) or electron spectroscopy for chemical analysis (ESCA) (Bansal *et al.*, 1991; Cheryan and Merin, 1981; Flösch *et al.*, 1990; Kowalczynska *et al.*, 1993; Larsson *et al.*, 1981; Oldani, 1989), infrared spectroscopy (IR) (Flösch *et al.*, 1990; Jan *et al.*, 1996; Konar and Bhowmick, 1996; Rånby, 1996), atomic force microscopy (AFM) and scanning electron microscopy (SEM) (Bansal *et al.*, 1991; Kim and Fane, 1994; Kim *et al.*, 1992; Suwandi and Lefebre, 1990). These techniques can be used to determine the composition of the surface (XPS and IR) or to determine the surface roughness (AFM and SEM). Techniques to determine surface interaction forces are streaming potential measurements (or zeta potential measurements) (Causserand *et al.*, 1994; Grundke *et al.*, 1996; Jan *et al.*, 1996; Ohshima and Kondo, 1990; Oss, 1993) and contact angle measurements (Gekas, 1992; Gourley *et al.*, 1993; Lin, 1993; Morra, 1990; Oldani, 1989; Zhang, 1989; Zhang, 1990) for electrostatic and (a)polar interaction forces respectively. Finally, some fast and qualitative techniques to determine adhesion forces are peel-off (Rånby, 1996) and dye-adsorption tests (Jan *et al.*, 1996).

In this chapter only contact angle measurements are used to determine apolar and polar interaction forces of surfaces. It is an easy to use technique which quickly gives information about the surfaces. A drawback is that it can only be applied to relatively smooth, homogeneous surfaces without pores.

Contact angle measurements

Contact angle measurements can be carried out by the sessile drop technique (Gekas, 1992; Gourley *et al.*, 1993; Lin, 1993; Morra, 1990; Oldani, 1989; Zhang, 1989; Zhang, 1990). In performing contact angle measurements, a droplet is placed upon a flat homogeneous surface and the contact angle of the droplet with the surface is measured (see Figure 4.1). The shape of the droplet depends on the balance between the solid-liquid interfacial tension (γ_{SL}), the surface tension of the liquid (γ_L) and the solid (γ_S). This balance is given by the Young equation and is indicated in Figure 4.1. At equilibrium this balance is given by:

$$\gamma_S = \gamma_{SL} + \gamma_L \cdot \cos\theta \tag{4.5}$$

In which θ is a finite angle of contact between the liquid droplet and the solid surface, γ_S and γ_L the surface tensions of respectively the solid and the liquid and γ_{SL} the interfacial tension between the solid and the liquid. Hereby, it is assumed that the size of the droplet does not have any effect on the contact angle, by assuming no gravity effects on the droplets.

In this work only advancing contact angles are used, because all the investigated surfaces are expected to be smooth and homogeneous. The advancing contact angle (θ_a) is measured when a new phase advances over the surface, contrary to the receding contact angle (θ_r) which is found when a phase retreats. The difference between these two contact angles is known as contact angle hysteresis and will be neglected in this work.

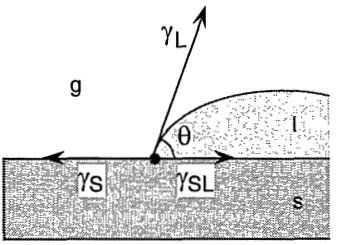

Figure 4.1: The sessile drop technique to determine contact angles (g = gas, l = liquid and s = solid)

Determination of the surface tension components

Contact angle measurements can be carried out to determine the surface tension components of an unknown surface (see §4.2.1). The surface tension components of both the surface and a liquid as a function of the contact angle are given by the Young-Dupré equation (Oss, 1993):

$$(1+\cos\theta)\gamma_L = 2(\sqrt{\gamma_S^{LW}\gamma_L^{LW}} + \sqrt{\gamma_S^{\oplus}\gamma_L^{\ominus}} + \sqrt{\gamma_S^{\ominus}\gamma_L^{\oplus}}) \tag{4.6}$$

This equation holds for materials which do not carry electrical charges and of which polar and apolar interaction forces dominate.

The three components of the surface tension of an unknown material can be found by performing contact angle measurements with three liquids with known surface tensions components. The apolar contribution of the surface tension, γ_S^{LW} of the solid surface can be determined by contact angle measurements with an apolar liquid. The two parts of the polar surface tension component γ_S^{AB} can be determined by contact angle measurements with two different polar liquids with a distinct difference in $\gamma^{\oplus}$ and $\gamma^{\ominus}$ values. A set of three equations with three unknowns is formed, which can easily be solved.

4.2.3 Characterisation of porous surfaces

Many techniques have been developed to characterise membranes and are usually divided in structure related and permeation related characterisation techniques (Mulder, 1991).

Structure related characterisation methods for porous surfaces are usually focused on determining the mean pore size and pore size distribution only. Another important factor is the surface porosity of a membrane (see also Chapter 2). For asymmetric membranes also the skin layer thickness is of importance. Factors which are related to the shape and geometry of the pores are often neglected leading to misinterpretations of the characterisation results.

Permeation related characterisation methods such as pure water flux measurements and solute rejection measurements determine the actual separation parameters of membranes, such as flux and retention. It is very difficult to relate permeation related charac-

terisation methods to structure related characterisation methods, because certain factors, such as concentration polarisation and fouling, obscure the separation parameters.

A review on different kinds of membrane characterisation techniques is given by Nakao (Nakao, 1994). In this work scanning electron microscopy (SEM), bubble-point, pure water and emulsion filtration experiments are used to characterise membranes. These methods will be discussed in section 4.3.2 in more detail.

4.3 Experimental part

4.3.1 Materials

Feed solution

An emulsion of 8 g Castor oil and 3.2 g surfactant (nonylphenolpolyethyleneoxide(9) from ICI) in 300 ml ultrapure water was prepared in a stirred vessel with baffles. The mean droplet size of the emulsion, obtained by a Microtrac X100 particle size analyser, was $d_{32} = 0.22\ \mu m$ (for more detail see Chapter 3). A six times diluted emulsion was used in the filtration and adsorption fouling experiments.

Polymer films

Polymer solutions were prepared from different polymers and solvents. Polymer materials were selected on the basis of the use as ultra- and microfiltration membrane materials in membrane filtration. The polymers that were used are cellulose acetate (CA) (BDH-chemicals), polyacrylonitrile (PAN) (Aldrich Chemical Comp, Inc.), polycarbonate (PC), (0.1 μm membranes, Nuclepore), polyetherimide (PEI) (Ultem 1000, General Electric), polyethersulfone (PES) (Victrex 4800, ICI), polypropylene (PP) (Carlon, Shell), polysulfone (PSf) (Udel P1800, Amoco), polytetrafluoroethylene (PTFE) (thread seal tape type R10 D1, Giveg) and polyvinylidenedifluoride (PVDF) (Solef 2008, Solvay). In Table 4.1 an overview is given of the different polymer solutions. The used solvents were acetone (Merck pro analysis $> 99.5\%$), dimethylformamide (DMF, Merck pro synthese $> 99\%$), chloroform (Merck pro analysis, $99\% - 99.4\%$) and n-methylpyrrolidone (NMP, Acros $> 99\%$).

The polymer solutions were cast onto glass plates with a casting knife of 0.15 mm and dried for about six hours in a nitrogen atmosphere to prevent water attraction from air. The PES in NMP films were dried overnight in a vacuum oven at 80°C to remove NMP from the film. Contact angle measurements were carried out onto the freshly prepared dry films.

Ultrapure water, glycerol (Merck pro analysis $> 99.5\%$) and α-bromonaphtalene (Merck pro synthese $> 98\%$) were used to determine respectively the two polar components $\gamma_s^{\oplus}$, $\gamma_s^{\ominus}$ and the apolar component γ_s^{LW} of the surface tension of the polymer surface. The known surface tension components of the three different liquids are listed in Table 4.2.

Table 4.1: The composition of the polymer solutions used for the preparation of polymer films

Polymer material	Amount [wt.%]	Solvent
CA	5	acetone
PAN	15	dimethylformamide
PC	15	chloroform
PEI	15	chloroform
PES	15	n-methylpyrrolidone
PP	pressed	[a]
PSf	15	chloroform
PTFE	tape	[a]
PVDF	15	dimethylformamide

[a] not relevant

Table 4.2: The surface tension components of the three liquids and several foulants [Oss, 1993]

	γ^{LW} $[mJ \cdot m^{-2}]$	$\gamma^{\oplus}$ $[mJ \cdot m^{-2}]$	$\gamma^{\ominus}$ $[mJ \cdot m^{-2}]$
Water	21.8	25.5	25.5
α-bromonaphthalene	44.4	≈ 0	≈ 0
Glycerol	34.0	3.9	57.4
PEO	43.0	0	64.0
Nonane	22.9	0	0

Ultrapure water was obtained from a MilliPore Q+ device, in which demineralised water was fed and purified. The electrical resistivity of the ultrapure water was 18.2 $M\Omega \cdot cm$ at 25 °C . The water was organic-free with a TOC < 10 ppb and was filtered through a 0.22 μm microfiltration membrane.

Membranes

In order to compare the calculated fouling tendency from contact angle measurements with filtration experiments, several ultrafiltration membranes were prepared from different polymeric materials. The same polymers were used as for the polymer films, except for PP and PTFE, from which no polymer solutions could be obtained at 25°C and for PEI from which no suitable membranes could be obtained. Ultrafiltration membranes were prepared by immersion precipitation. Polymer solutions in DMF were cast onto a glass plate and membranes were obtained by submersing the polymer solution on the glass plate into an ultrapure water bath of 20 – 25°C . The composition of the polymer solution was selected on the basis of trial and error to obtain membranes with an ultrapure water flux between $300 - 1000$ $kg \cdot m^{-2} \cdot h^{-1} \cdot bar^{-1}$. This is given in Table 4.3 together with the thickness of the casting knife. After membrane preparation, the membranes were put in an ultrapure water bath for about 12 hours to remove DMF from the pores. After this,

they were immediately used for the adsorption experiments with emulsions.

Table 4.3: The composition of the membrane solutions in DMF and the thickness of the casting knife used

Polymer	Conc. [*wt.* %]	Thickness casting knife [mm]
CA	14.0	0.15
PAN	13.0	0.15
PC [a]	-	-
PES	16.0	0.5
PSf [b]	15.0	0.15
PVDF	12.5	0.15

[a] commercial MF membranes have been used with a mean pore size of 0.1 μm
[b] NMP was used as a solvent

Different commercial membranes were used for membrane structure selection purposes. Polysulfone MF membrane ($0.1 - 2.0$ μm) and UF membranes (100 kDa) were kindly supplied by Dow Denmark Separation systems (DDS).

The chemical, thermal and mechanical stabilities of the polymers in this study were found in literature (Digest, 1991; Rubin, 1990). Chemical stabilities for various polymers with respect to concentrated and diluted acid and bases, salts and solvents were found in the International Plastic selector (Digest, 1991). An indication of the thermal stability can be obtained from the glass transition temperature, melting point and thermal deflection temperature of polymers (Rubin, 1990). The mechanical stability is expressed by the tensile modulus and the tensile strength (Kesting, 1985). The values given for chemical, thermal and mechanical properties were only valid for dense bulk polymers without any pores. The influence of a porous structure on these properties was not exactly known. Apart from this, the properties were only valid for dry-state polymers. Water can act as a plasticiser and soften the material. This will also affect the thermal and mechanical properties. These considerations are, however, beyond the scope of this work.

4.3.2 Set-up and methods

Contact angle measurements

Contact angle measurements were carried out on the dried films with a Krüss G1 contact angle meter, with three different liquids according to the concept of Van Oss. Contact angles were measured by a direct method, which was by reading the angle between the tangent of the contact point and the horizontal line of the solid surface using a protractor. For one type of polymer film, the average of the contact angles of three liquid droplets (two angles per droplet) on two different polymer film samples were taken. Contact angles were measured directly after applying the droplet onto the surface (within 1 minute) to prevent evaporation effects of the liquids.

Pore size determination

Pore size measurements were carried out with a commercial apparatus, the Coulter Porometer II (ASTM F316-80). Membranes were first wetted with a low surface tension liquid Coulter Porofil. The principle of this device is measuring the air flow through the liquid filled membrane during transmembrane pressure increase (Mulder, 1991). It is a simple technique to determine the mean pore diameter of a membrane sample and can be used only for the active or no dead-end pores in the membranes. The lower limit of the detectable pore size is 50 nm and is thus only applicable to microfiltration membranes. Another drawback is that this method depends on the pore length and the shape of the pore mouth (Zha, 1992).

Ultrafiltration membranes were characterised by the mwco given by the membrane manufacturer.

Scanning electron microscopy

SEM was used to investigate the pore structure of the commercial membranes. The principle of SEM is the irradiation of a surface with high-energy (primary) electron beams which generate low-energy (secondary) electrons from the surface layer. These secondary electrons determine mainly the image of the surface.

For SEM measurements dried membranes were covered with a gold-layer to avoid charging and eventually burning of the sample. This was done with a sputtering device of Balzer Union type SCD 040 at 0.1 $mbar$ in an Argon-atmosphere, using an electrical current of 15 mA. For the actual SEM-measurements the Jeol JSM 220 A scanning electron microscope device was used at a voltage of 20 kV. Since high energetic electrons were being used, the experiments were performed under vacuum.

Adsorption fouling measurements

Adsorption fouling measurements were carried out with the self prepared membranes for membrane material selection purposes. In these measurements it was assumed that membrane fouling was only due to adsorptive fouling. These experiments were carried out in an Amicon-type dead-end cell with a membrane at the bottom with an area of 38.5 cm^2. An indication of the membrane performance was obtained by the mass flux and is defined as:

$$J = \frac{1}{A_m}\frac{dm}{dt} \tag{4.7}$$

Here is J the permeate mass flux, A_m the membrane area, m the collected permeate mass and t the time. This permeate flux is a function of the transmembrane pressure. For ideally pure water, the flux is linear to the pressure. In practice, pure water contains contaminants (Fane and Fell, 1987; Jonsson *et al.*, 1996) resulting in a flux time dependence due to membrane fouling. In this work, a fixed filtration time of 2 hours was chosen in which a steady state flux was reached for most of the experiments.

First a pure water flux experiment was carried out for 2 hours at 2 bar transmembrane pressure to precondition the membranes and remove DMF from the pore structure. The

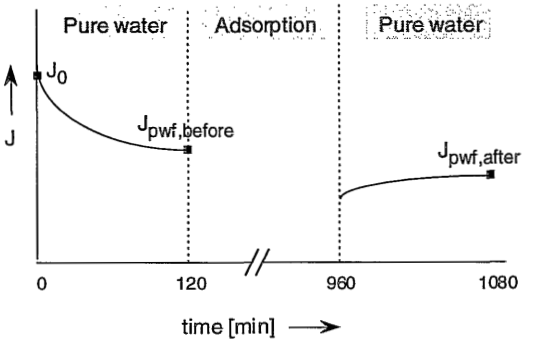

Figure 4.2: A schematic drawing of an example of an adsorption experiment

flux decline index (FDI) is now defined as the ratio of the first pure water flux after 2 hours and the initial pure water flux J_0 (see Figures 4.2 and 4.3):

$$FDI = \frac{J_{\text{pwf,before}}}{J_0} \tag{4.8}$$

After this, a so-called static adsorption experiment was carried out to achieve irreversible fouling. In this experiment the membrane was put into contact with the emulsion for 14 hours in the cell without any transmembrane pressure. After this, the feed solution was replaced by ultrapure water which was stirred for 5 *min.* at 1000 *rpm* with a Rushton turbine (the stirrer diameter $D = 20$ *mm*), assuming only to remove the reversible fouling. Finally, again a pure water flux experiment was carried out for 2 hours at 2 *bar*. An example of an adsorption experiment is given in Figure 4.2. The flux recovery is defined as the ratio of the pure water flux after and before the adsorption experiment and is a measure for the irreversible fouling.

$$FR = \frac{J_{\text{pwf,after}}}{J_{\text{pwf,before}}} \tag{4.9}$$

If the membrane is not fouled at all, $FR = 1$, otherwise $FR < 1$.

Emulsion filtration experiments

Filtration experiments with emulsion solutions were carried out with various commercial polysulfone membranes. This was done to determine the emulsion flux and retention behaviour of the different membranes for membrane structure selection. Pure water flux experiments were carried out for 2 hours at 2 *bar* transmembrane pressure before and after the emulsion filtration experiment. The actual emulsion filtration experiment was also carried out for 2 hours at 2 *bar* in a cross-flow set-up, which is described in more detail in Chapter 8. An example of such an experiment is given in Figure 4.3 in which all the parameters become clear. Again the flux decline index and the flux recovery can be calculated as was defined above.

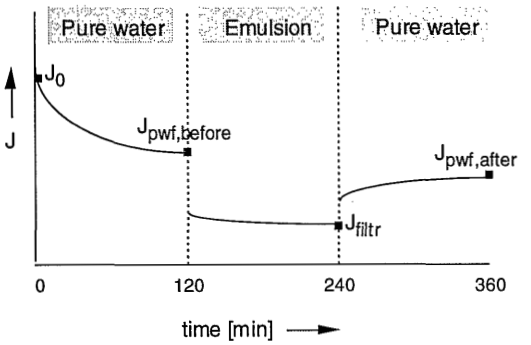

Figure 4.3: A schematic drawing of an example of a cross-flow filtration experiment

Retention was measured after 2 hours filtration by HPLC-analysis of the feed and permeate. The emulsion retention is defined as the ratio between the oil content in permeate and the feed solution:

$$R = 1 - \frac{c_{\text{permeate}}}{c_{\text{feed}}} \tag{4.10}$$

Here is R the retention, c_{feed} and c_{permeate} the emulsion concentration of the feed and permeate, respectively.

4.4 Results and discussion

4.4.1 Contact angles and calculated fouling tendencies

Contact angles of water, glycerol and α-bromonaphtalene onto the different polymer films are shown in Table 4.4. A change in contact angles in time because of surface rearrangements due to the change of surrounding phase (air is replaced by a liquid) as was reported in literature (Zhang, 1989; Zhang, 1990) has not been observed. From these measurements it can be seen that CA and PAN displayed the lowest contact angles with water, indicating that these are hydrophilic materials. Hydrophobic materials, such as PTFE, PP, PES and PVDF showed a contact angle with water which is larger than 90°. From Table 4.4 the polar and apolar components of the interfacial tension were calculated using the theory of Van Oss (see §4.2.1). These values are listed in Table 4.5 for the different surfaces. From this table it can be observed that the hydrophobic materials displayed a $\gamma^{\oplus}$-value of zero or a very low $\gamma^{\ominus}$-value, resulting in a low polar surface tension contribution.

The free energy of adhesion, which was calculated from equation 4.5, was used as a measure for the fouling tendency. To calculate this energy for fouling substances onto polymer surfaces in water, the three surface tension components of every substance (polymer, foulant and water) has to be known. The emulsion consisted of free surfactant

Table 4.4: Average values and standard deviations (of twelve experiments) of the measured contact angles of water, glycerol and α-bromonaphthalene

Polymers	θ_{water} [°]	$\theta_{glycerol}$ [°]	$\theta_{\alpha-bromonaphthalene}$ [°]
CA	59 ± 3	54 ± 3	26 ± 2
PAN	57 ± 3	49 ± 4	6 ± 1
PC	78 ± 1	66 ± 2	12 ± 1
PEI	79 ± 2	63 ± 2	8 ± 1
PES	92 ± 2	68 ± 5	13 ± 2
PP	94 ± 2	83 ± 3	42 ± 1
PSf	82 ± 2	67 ± 4	14 ± 7
PTFE	117 ± 2	112 ± 2	93 ± 2
PVDF	92 ± 2	104 ± 3	29 ± 2

Table 4.5: Calculated surface tension components of the different polymers

Polymers	γ_s^{LW} $[mJ \cdot m^{-2}]$	$\gamma_s^{\oplus}$ $[mJ \cdot m^{-2}]$	$\gamma_s^{\ominus}$ $[mJ \cdot m^{-2}]$
CA	40	0.5	19
PAN	44	0.6	19
PC	44	0.1	5.8
PEI	44	0.3	3.9
PES	43	0.5	0.1
PP	34	0	1.7
PSf	43	0.2	3.1
PTFE	10	0	0.9
PVDF	40	0	0.1

molecules, micelles and stabilised oil droplets. Both micelles and stabilised oil droplets were covered with surfactant molecules. Polyethyleneoxide (PEO) and nonane were taken as standard foulants because these compounds represent both ends of a nonylphenolpolyethyleneoxide surfactant molecule used in this study. Surface tension components for the polymers are tabulated in Table 4.5 and surface tension components for the foulants and water are tabulated in Table 4.2. The interfacial areas ΔA (see equation 4.5) of PEO and nonane during adsorption onto polymer surfaces, were 23.2 Å^2 and 33.7 Å^2 respectively (Oss, 1993). The calculated free energies of adhesion between the different polymers and the two foulant materials are plotted in Figure 4.4.

From this figure it can be seen that from all investigated polymers CA and PAN displayed the highest positive value of the free energy of adhesion for PEO and the lowest negative value of the free energy of adhesion for nonane in water. These materials are expected to have the lowest degree of irreversible fouling during membrane filtration of PEO and nonane. This contrary to PES and PVDF which have the highest negative value of the free energy of adhesion for PEO and nonane in water in Figure 4.4 and are expected to display the highest fouling tendencies. These conclusions can also be drawn

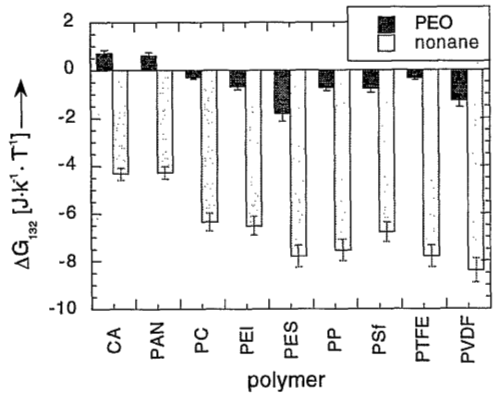

Figure 4.4: Calculated free energies of adhesion of PEO and nonane. Error bars are determined by calculation accounting the deviations in contact angles (see Table 4.4)

from only contact angle measurements with water and moreover are already known from literature (Fane and Fell, 1987; Hanemaaijer *et al.*, 1988). The advantage of the described approach of Van Oss, however, is that a difference in fouling tendency can be calculated for different foulants. Moreover, the concept can be used in different media besides water. From Figure 4.4 it can be seen for example that nonane is expected to foul more than PEO for every polymer.

For PEO no adhesion onto CA and PAN is expected, because of the positive sign of ΔG_{132}. All other materials display a negative free energy of adhesion, indicating a certain degree of adhesion. The free energies for nonane are more negative than the free energies for PEO for every polymer material, which indicates that surfactant adsorption takes place with the hydrophobic tail group on every investigated polymer material. This has also been found in literature (Welin-Klintström, 1993).

4.4.2 Adsorption fouling experiments

Emulsion adsorption fouling experiments with self prepared membranes were carried out to verify the calculated fouling tendencies (ΔG_{132}). Coulter porometer measurements were not possible for these membranes. Therefore, the pores were estimated to be smaller than 50 nm, indicating that the membranes were in the ultrafiltration range. In Table 4.6 the pure water flux and the flux recovery values are shown. From this table it can be found that all the pure water flux values fall within the range of $300 - 1000\ kg \cdot m^{-2} \cdot h^{-1} \cdot bar^{-1}$ except for the pure water flux of PC which was slightly higher, and the pure water flux of PVDF which was slightly lower. The PC membrane was not prepared by immersion precipitation, but is a commercial UF membrane, which might explain the higher $J_{\text{pwf,before}}$ value. The scattering in the pure water flux data was high, due to a rather uncontrolled membrane preparation (e.g. no temperature control).

The flux recovery values are also tabulated in Table 4.6 for the different polymer membranes. It can be seen that these values were highest again for CA and PAN, but were also, rather unexpectedly high for PVDF. PVDF was expected to display a large fouling due to adsorption because of its low ΔG_{132}-value. The high FR value for PVDF can be related to the low pure water flux values before adsorption compared to the other membranes. This can be the result of small pores, which led to a reduced internal adsorption. The FR value for PC was unexpectedly low, probably due to a large internal adsorption. Adsorption fouling experiments were susceptible to the surface area of the membranes, which varied for the different membranes. This makes it hard to interpret the results.

Table 4.6: Results of the adsorption fouling experiments with emulsions at 2 *bar*

Membrane	Emulsion	
	$J_{\text{pwf,before}}$ $[kg \cdot m^{-2} \cdot h^{-1} \cdot bar^{-1}]$	FR [-]
CA	558 ± 255	0.97 ± 0.10
PAN	499 ± 95	0.74 ± 0.11
PC	1095 ± 199	0.23 ± 0.09
PES[a]	472 ± 140	0.16 ± 0.07
PSf	407 ± 36	0.57 ± 0.15
PVDF[a]	294 ± 81	0.84 ± 0.18

[a] $0.25\ g \cdot \ell^{-1}$ nonionic surfactant added

The flux recovery value is a measure for the irreversible fouling and can be related to the calculated fouling tendencies in §4.4.1 expressed in the free energies of adhesion ΔG_{132} . These correlations are shown in Figures 4.5 and 4.6 for both PEO and nonane, respectively.

From Figures 4.5 and 4.6 it can be observed that a reasonable correlation exists between ΔG_{132} and FR for both PEO and nonane, despite the problem to interpret the FR measurements. In the right top corner of Figure 4.5 hydrophilic materials are located, while in the left bottom corner hydrophobic materials are located. Exceptions are again PVDF and PC, which contain a too high respectively too low FR value.

On the basis of the results presented so far, polysulfone was selected as the best material for further studies. It is a good chemical, thermal and mechanical stable material, contrary to CA and PAN, which also contains reasonable anti-fouling properties with respect to emulsions (indicated by ΔG_{132} and FR values).

4.4.3 Emulsion filtration experiments

SEM-pictures were made of the top layers of the four investigated membranes (see Figure 4.7). The MF membranes displayed a spongelike structure, while the UF membrane had a nodular structure on the skin side. The internal volume within these structures increased

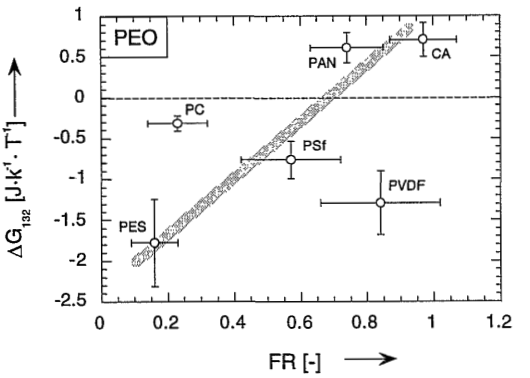

Figure 4.5: Correlation of $\Delta G_{132}(PEO)$ with FR from adsorption fouling experiments

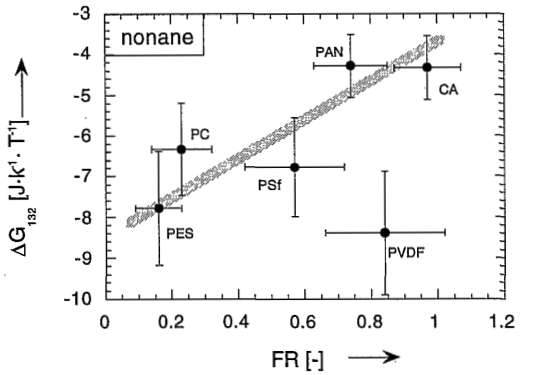

Figure 4.6: Correlation of $\Delta G_{132}(nonane)$ with FR from adsorption fouling experiments

with the mean pore diameter as was determined with the Coulter porometer, which can be seen in Figure 4.7 too.

From the cross-flow filtration experiments it was clear that the pure water fluxes were in the range of $100 - 200\ kg \cdot m^{-2} \cdot h^{-1}$ for each membrane, except for the 2.0 μm PSf membrane which had a pure water flux that was ten times higher. The emulsion fluxes were $40 \pm 10\ kg \cdot m^{-2} \cdot h^{-1}$ for all membranes, which indicated that mass transfer was limited by the emulsion feed solution, rather than by the membrane itself.

In Figure 4.8 the flux decline index, emulsion retention and flux recovery are given for the different membranes. The flux decline index is highest for the UF membrane and decreases with the mean pore diameter for the MF membranes. This phenomenon was

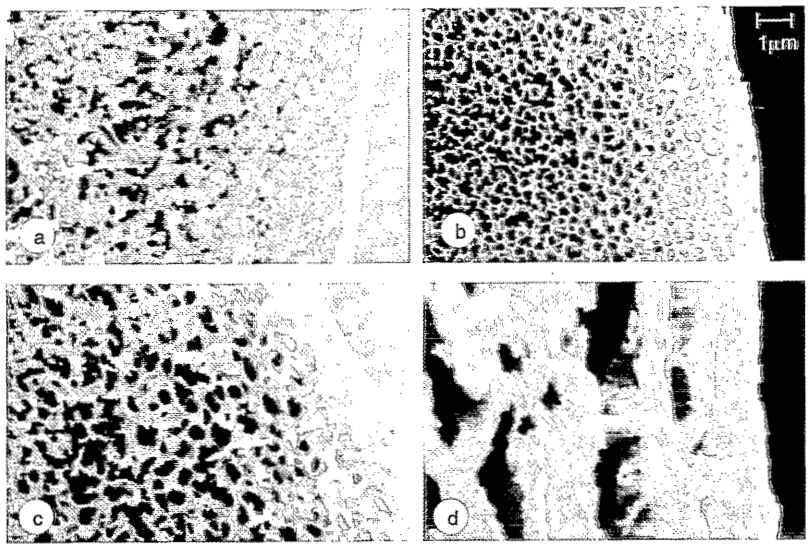

Figure 4.7: SEM-pictures of the top-layers of (a) 100 kDa UF membrane (GR40PP) with $r_p < 0.05$ μm and three MF membranes (b) $r_p = 0.18$ μm (GRM01PP), (c) $r_p = 0.33$ μm (GRM045PP) and (d) $r_p = 1.92$ μm (GRM20PP)

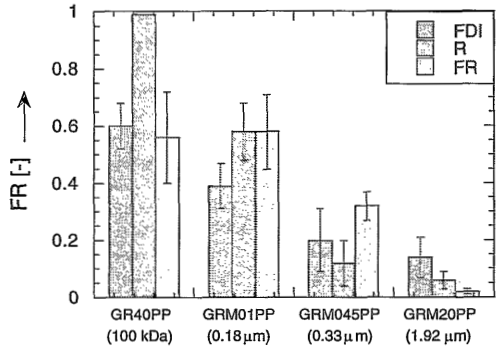

Figure 4.8: Flux decline index (FDI), emulsion retention after 2 hours (R) and flux recovery (FR) for the PSf UF and different MF membranes

also observed in literature (Gatenholm *et al.*, 1988) and can be explained by an increased reduction of the number of open pores by contaminants in water for MF membranes, resulting in a higher flux decline.

The emulsion retention is almost 100 % for the UF membrane and decreases with the

mean pore diameter for the MF membranes. This is explained by the ratio between the mean emulsion droplet diameter and the mean pore diameter. Emulsion droplets could not penetrate the UF membrane at all, which explained its high retention value. For the MF membranes the degree of retention depends on the mean pore diameter of the membrane. The GRM01PP PSf membrane had a mean pore diameter (0.36 μm) in the range of the mean emulsion droplet diameter (0.22 μm). Because of both a pore diameter and droplet diameter distribution, a certain extent of emulsion droplets was retained by the membrane which explained the intermediate retention value for this membrane. The other two membranes had a larger mean pore diameter, which explains the very low retention value.

The flux recovery for all the membranes was smaller than 1, which indicates the occurrence of irreversible fouling. This was more pronounced for the two MF membranes with the largest mean pore radii. This was due to the occurrence of internal membrane fouling. Both the UF membrane and the GRM01PP membrane had a flux recovery value of 0.55 ± 0.15.

On the basis of these measurements the GR40PP UF membrane is selected for further studies. This membrane almost fully retained the emulsion and had a high flux recovery value compared to the MF membranes.

4.5 Conclusions

The lowest fouling tendencies, calculated from a physico-chemical theory according to Van Oss, were found for CA and PAN and the highest fouling tendencies were found for PES and PVDF. For every investigated polymer the adsorptive fouling tendency for nonane was higher than for PEO. This indicates that surfactant adsorption takes place with the nonane tail group.

From adsorption fouling experiments on self prepared ultrafiltration membranes, PVDF, CA and PAN membranes were found to show the lowest adsorptive fouling (highest FR-value). These experiments depended, however, on the surface area and internal volume of the membranes, which could not be controlled accurately. The PVDF membrane had a very low surface area, which explained its high FR.

A reasonable correlation was found between the calculated fouling tendency and the FR-value. On the basis of both approaches and of considerations about the chemical and thermal stability of the polymers, PSf was selected as the optimal material in this work.

A membrane structure selection was carried out for the selected PSf material. An UF membrane (100 kDa) was selected for further studies because of the lowest pure water flux decline, highest emulsion retention and FR-value compared to MF membranes.

4.6 Acknowledgements

Ir S. Rekveld contributed to this work via many fruitful discussions about the Van Oss concept. The experimental work has been carried out by P. Wuis, L. Versteeg and B.

Folkers who carried out the contact angle measurements, the adsorption fouling experiments and the emulsion filtration experiments respectively. Their experimental work and their contribution to these topics are highly appreciated.

4.7 List of Symbols

Acronyms

Symbol	Quantity
CA	cellulose acetate
DMF	dimethylformamide
$ESCA$	electron spectroscopy for chemical analysis
FDI	flux decline index
FR	flux recovery
$HPLC$	high performance liquid chromatography
IR	infrared (spectroscopy)
NMP	n-methyl pyrrolidone
PAN	polyacrylonitrile
PC	polycarbonate
PEI	polyetherimide
PEO	polyethyleneoxide
PES	polyethersulfone
PP	polypropylene
PSf	polysulfone
$PTFE$	polytetrafluoroethylene
$PVDF$	polyvinylidenedifluoride
SEM	scanning electron microscopy
TOC	total organic carbon
XPS	X-ray photoelectron spectroscopy
$mwco$	molecular weight cut-off
AFM	atomic force microscopy

Symbols

Symbol	Quantity	Units
A_m	membrane area	$[m^2]$
J	membrane (permeate) flux	$[kg \cdot m^{-2} \cdot h^{-1}]$
R	retention	$[-]$
ΔA	interfacial area	$[m^2]$
ΔG	Free energy of adhesion	$[mN]$
ΔG_{132}	Free energy of adhesion between 1 and 2 in 3	$[J \cdot k^{-1} \cdot T^{-1}]$
ΔP	transmembrane pressure	$[bar]$
γ_{ij}	interfacial tension between i and j	$[mJ \cdot m^{-2}]$

γ_i	surface tension of i in vacuum	$[mJ \cdot m^{-2}]$
θ	contact angle	$[^o]$
m	(collected permeate) mass	$[kg]$
r_p	pore radius	$[m]$
t	time	$[s]$

Subscripts & superscripts

Symbol	Quantity
0	before filtration
AB	acid-base
BR	Brownian movements
EL	electrostatic
g	gas
l	liquid
LW	Lifshitz-Van der Waals
s	solid
$\ominus$	electron donor parameter part
$\oplus$	electron acceptor parameter part
a	advancing
max	maximum
pwf	pure water flux
r	receding

Chapter 5

Control of fouling by membrane modification

5.1 Introduction

Hydrophilic materials are known in membrane technology as membrane materials which have a low tendency to foul (Persson *et al.*, 1993). A drawback is their poor chemical and thermal instability at extreme pH-values and temperatures (Rubin, 1990). Cellulose acetate for example, degrades rapidly at high temperatures or at extreme pH values. It is for this reason that hydrophobic materials are usually selected for use as membrane material in several membrane applications despite of their relatively high fouling tendency (see Chapter 4 of this thesis).

A way to overcome this drawback is modification of the membrane surface which will give the chemically and thermally stable hydrophobic materials a hydrophilic surface. In this way, surface modified hydrophobic materials have the advantage of both a low fouling tendency and being chemically and thermally stable at extreme temperatures and pH values (Rubin, 1990).

In this chapter, polysulfone (PSf) material is used as standard material for surface modification studies. A reason for the selection of PSf is that it is stable at high pH values and high temperatures (see Chapter 4).

Several techniques are known in literature to modify both PSf membranes as well as PSf hard surfaces. In this work, modified surfaces are characterised by several surface techniques such as sessile drop contact angle measurements (only for hard surfaces), X-ray photoelectron spectroscopy (XPS), flux measurements (only for membranes) and scanning electron microscopy (SEM). With these different characterisation techniques the effect of each modification technique is compared to the unmodified material.

5.2 Theory

Generally, surface modification techniques can be subdivided in temporary (physical) and permanent (chemical) techniques. Permanent or chemical surface modification techniques

are used to modify a surface for longer times. In this work, only the latter techniques are used and will be discussed below.

Chemical modification is a collective term for many techniques that can be used to alter the surface properties of materials permanently, e.g. change in dyebility, weathering, wettability, microbiological attack, etc. In this work, chemical modification techniques are used to obtain non or less fouling surfaces, by making membrane surfaces more hydrophilic or by attaching negatively charged groups on the surfaces which repel negatively charged foulants.

Chemical modification is usually carried out with a reactive liquid or gas that is brought into contact with a certain surface. The degree of modification of the outer surface is regulated by the contact time of the reactive species with the surface and the temperature. Dependent on the modification agents and the type of substrate, sometimes an indepth modification can occur in which not only the surface is modified but also the bulk material to a certain extent, due to for example swelling of the surface.

In literature several chemical modification studies have been carried out to introduce carbonyl-, carboxylate acid-, sulfone-, hydroxy- (Larsson *et al.*, 1981; Stengaard, 1988), phosphate- (Dumon and Barrier, 1992), amine- (Müller and Krieger, 1981; Stengaard, 1988) and fluorine-groups to a surface. Two techniques are used in this work to modify PSf surfaces (both nonporous surfaces and membranes) to make them more foulant-repelling. These techniques are plasma modification and sulfonation and will be discussed below in more detail.

5.2.1 Plasma modification

Gas discharge or plasma techniques can be used to modify a surface for several different applications (e.g. adhesion, wettability improvement, etc.). It is a relatively simple and direct technique that has to be applied in the dry state (Terlingen, 1993). With plasma techniques only the outermost surface is modified. A drawback of this method is that the final composition of the surface is usually not precisely predictable.

A plasma consists of a (partially) ionised gas. A plasma is created by free electrons present in a gas which are accelerated by the electric field, which collide with the neutral gas molecules or atoms. This generates ions, new electrons, radicals and UV-radiation which makes a plasma a highly reactive environment in which many reactions occur (e.g. ionisation, dissociation, charge transfer, attachment and reattachment reactions). When this plasma is brought into contact with a surface, a bombardment takes place of the surface with ions, electrons, radicals and UV-radiation. Dependent on many parameters in the plasma process, such as type of gas, type of substrate, flow of the gas, pressure and plasma power, the surface can undergo etching, crosslinking, functionalisation, degradation, deposition or a combination of these effects.

To conclude it can be said that plasma modification is a suitable technique to functionalise (modify) surfaces at the outermost surface only. In practice, plasma modification is difficult to control and optimise because of the large variety of parameters during the process. Often the reproducibility is poor.

5.2.2 Sulfonation

Sulfonation results in a difference in the properties of the polymer material, because charges are introduced (Jitsuhara and Kimura, 1983; Nakao *et al.*, 1988) and the material is hydrophilised by sulfone-groups ($-SO_3^{\ominus}$).

A distinction must be made between bulk and surface sulfonation. In bulk sulfonation a polymer is dissolved in a suitable solvent and sulfonated completely, contrary to surface sulfonation in which only the surface of the polymer material is modified. The advantage of surface sulfonation is that the bulk properties of the polymer, such as the chemical and mechanical stability are unaffected. Only surface sulfonation will be studied in this work.

Surface sulfonation is carried out by submersion of a polymer material into a sulfonation agent. Several of these agents are known, such as sulfuric acid (concentrated and fuming), chlorosulfonic acid, fluorosulfonic acid, sulfurtrioxide and complexes (LeRoi Nelson, 1964). A problem is that these agents are very reactive and that the sulfonation reaction is hard to control. Noshay et al. (Noshay and Robeson, 1976) showed that mechanical properties for bulk sulfonated PSf, such as tensile modulus, tensile strength, elongation and pendulum impact decreased with an increasing degree of sulfonation. Ways to control these reactions are cooling, dissolving sulfonation agents in a suitable solvent and complexation.

Sulfonation by submersion into dissolved sulfonation agents is an effective procedure. Chlorosulfonic acid for example, is partially dissolved into aliphatic hydrocarbons, such as hexane. Polyphenyloxide (PPO) surfaces for example, were sulfonated with a chlorosulfonic acid/hexane mixture as a sulfonation agent (Lee *et al.*, 1976).

Complexes of sulfurtrioxide are used to reduce the reactivity of the sulfonation agents. Also it has been shown (Noshay and Robeson, 1976) that crosslinking reactions during sulfonation are minimised by sulfonation with complexes. A complex can be formed with various types of solvents, such as pyridine, triethyleneamine, trimethylamine and triethylenephosphate (TEP) (Gilbert, 1965). With an increasing stability of the complex, the reactivity decreased. The degree of sulfonation can be regulated by varying the composition of the sulfonation complex. It has been found for TEP/SO_3-complexes that the degree of sulfonation could be controlled up to about one sulfone group per repeating PSf unit (Noshay and Robeson, 1976). To control the reactivity of the complex, it has to be diluted with another solvent. This solvent must not affect the reactivity of the complex and must not dissolve the polymer surface. This might result into an emulsion when stirred, if the two solvents are not miscible. Modification with emulsions will lead to local surface sulfonation effects (see §5.4.3). The modification depth can be controlled by the type of solvent (Noshay and Robeson, 1976).

5.3 Experimental part

Several surface modification techniques were applied to both PSf membranes and PSf nonporous surfaces. Different characterisation techniques were used in order to evaluate

the modification procedure. The work that was carried out on surface modification can be subdivided into plasma modification and sulfonation of PSf surfaces.

5.3.1 Materials

Nonporous hard PSf surfaces were prepared by casting a 15 $wt.\%$ PSf in chloroform solution onto a glass plate with a casting knife of 0.15 mm. The film was first dried in a nitrogen atmosphere for six hours and afterwards dried overnight in a vacuum oven at 30°C . PSf (P1700) was obtained from Amoco.

The membranes that were used in the two studies were PSf UF membranes with a mwco of 50 kDa (GR51PP) and 100 kDa (GR40PP).

Drying of the membranes

After removal of the conservation liquid from the pore structure, membranes have to be dried before plasma modification or characterisation by SEM or XPS. Four types of drying procedures were studied; 1) direct drying in air, 2) drying in vacuum at 30°C , 3) drying in air after rinsing with water, ethanol and hexane 4) drying in vacuum at 30°C after rinsing with water, ethanol and hexane.

The effect of the drying procedure was examined by a pure water flux measurement after drying, which was compared to a wet membrane. The external pressure difference across the membrane was taken at 2 bar. The results of the pure water flux values of the wet and dried membranes are given in Table 5.1.

Table 5.1: pure water fluxes J in $kg \cdot m^{-2} \cdot h^{-1} \cdot bar^{-1}$ of GR51PP membranes after different drying steps

Drying step	J_{pwf} $[kg \cdot m^{-2} \cdot h^{-1} \cdot bar^{-1}]$
no drying	40
direct in air	0
direct in vacuum	0
via hexane in air	50
via hexane in vacuum	55

From Table 5.1 it can be seen that direct drying in air or in a vacuum oven resulted in a zero pure water flux value, probably due to collapse of the membrane structure. Replacing water by ethanol and hexane was necessary to retain the original flux values. The flux due to drying via ethanol and hexane, however, was slightly higher, probably due to pore opening. Replacing water by ethanol and hexane and drying in air was selected as standard procedure for pretreatment before XPS and SEM characterisation and for plasma modification studies.

5.3.2 Characterisation of the surfaces

Hard surface characterisation

Characterisation of hard surfaces was carried out with a X-ray photospectropy device (Kartos X-SAM 800). With this technique functional groups and individual atoms on surfaces can be determined quantitatively and qualitatively. Apart from this, unknown surfaces can be characterised by matching measured XPS-maps with known reference maps. The principle of XPS is the determination of bonding energy of inner or valence electrons within the surface material, by measuring the kinetic energy of emitted electrons. These electrons are emitted by irradiating a surface by photons with a known frequency. Samples were dried for at least 5 hours in ultrahigh vacuum (up to 10^{-9} torr) before characterisation and did not degrade as a result of the X-rays.

Hard surfaces were also characterised by sessile drop contact angle measurements to determine apolar and polar interaction forces of surfaces. It is a simple and fast technique which is used extensively for surface characterisation. A drawback of this technique is its susceptibility to surface roughness. Contact angles were measured using a Krüss G1 contact angle meter. Interpretation of contact angle measurements was carried out in this chapter by the three liquid concept as developed by Van Oss et al. (Oss, 1993; Oss, 1994). With this concept the free energy of adhesion could be calculated, which is a measure for the fouling tendency (see Chapter 4). The free energy of adhesion for the surfaces with a foulant was calculated for polyethyleneoxide (PEO) and nonane, which represent both ends of a nonylphenolpolyethyleneoxide surfactant molecule used in this study.

Membrane characterisation

XPS-measurements with dried membranes were carried out using the same device and sample preparation methods as for the hard surfaces.

SEM-pictures can be used to investigate any change in structure due to the modification process. SEM is discussed in more detail in Chapter 4 of this thesis. For SEM-measurements dried membranes were covered with a gold layer with a sputtering device of Balzer Union type SCD 040 at 0.1 $mbar$ in an Argon atmosphere, using an electrical current of 15 mA. For the actual SEM measurements a Jeol JSM 220 A scanning electron microscopy device was used at a voltage of 20 kV.

Flux and retention measurements were carried out (after modification) with a bovine serum albumin (BSA) solution in an unstirred dead-end cell. For this measurement, 2.5 $g \cdot \ell^{-1}$ BSA was dissolved in a Sørensen buffer (0.7025 $g \cdot \ell^{-1}$ KH_2PO_4 and 8.735 $g \cdot \ell^{-1}$ Na_2HPO_4 in ultrapure water obtained from a Milli-Q plus device) at $pH = 7.2$ and filtrated for two hours at a transmembrane pressure of 2 bar. Samples were taken after two hours of filtration and analysed by a UV/VIS spectrophotometer (Philips PU 8720 scanning spectrophotometer) from which the retention could be calculated. Before and after the BSA-filtration experiment pure water flux measurements were carried out at a transmembrane pressure of 2 bar with the buffer solution. Values for the fluxes were taken after two hours of filtration.

5.3.3 Plasma modification of PSf surfaces

Plasma modification of the PSf surfaces was carried out in a plasma reactor (electrotech plasmafab 508) with a jar-type reactor chamber. First the pressure in the reaction chamber was lowered down to about 10^{-2} *torr*, then the chamber was filled with NH_3-gas with a constant flow of 59 cm^3 $(STP) \cdot min^{-1}$. After this, the electrodes were turned on in the plasma chamber. The modification time was varied from 5, 30 and 60 *min.* at a plasma power of 100 W and plasma power was varied from 25, 50 and 100 W at a fixed modification time of 5 *min.*

5.3.4 Sulfonation of PSf surfaces

Sulfonation of PSf surfaces was carried out with the different sulfonation agents, sulfuric acid (concentrated and fuming H_2SO_4), chlorosulfonic acid ($ClSO_3H$) and triethylenephosphate (TEP/SO_3).

Treatment of PSf material with both concentrated and fuming acid at ambient temperatures led to a visual damage of the material and was not investigated further. An attempt was made to sulfonate with cooled concentrated sulfuric acid at 0°C .

Sulfonation with chlorosulfonic acid was carried out in a 1 ℓ beaker in which 40 *ml* chlorosulfonic acid was added to 800 *ml* hexane. Two separate phases were formed with chlorosulfonic acid on the bottom. By adding $ClSO_3H$ to hexane, the hexane turned yellow. After 5 minutes of stirring the solution was put at rest for at least 10 minutes to stabilise the phases. The $ClSO_3H$-layer on the bottom changed in colour in time, from light-brown to almost black within about one day. Modification parameters were time and temperature. Reactions at about 0°C were studied by cooling the beaker. Modification was carried out by simply putting the PSf surface samples in the chlorosulfonic saturated hexane phase. The samples were sulfonated both at the same time or after each other, which did not result in any difference in the measured contact angles. The reactivity of the chlorosulfonic acid solution was assumed to be constant within about an hour (Lee *et al.*, 1976).

A new method was used to prepare a TEP/SO_3 complex. This method is described in detail in Appendix A1. An amount of 85.5 g 1:2 TEP/SO_3 complex was put in 200 *ml* vigorously stirred cyclohexane on top of a fixed membrane, resulting in a modification with an unstable dispersion. This dispersion was diluted 20 times and 40 times with cyclohexane to control the reactivity.

The sulfonated surfaces were rinsed with sodiummethoxide ($NaOCH_3$) for TEP/SO_3-modified surfaces or with 20 *wt.*% sodiumhydroxide ($NaOH$) solution for $ClSO_3H$ and H_2SO_4 sulfonated surfaces, before the XPS-measurements.

5.4 Results and discussion

5.4.1 Unmodified PSf surfaces

XPS measurements were carried out for the nonporous homogeneous films (Amoco PSf) and for the two untreated ultrafiltration membranes (DDS GR51PP and GR40PP). Results of these measurements together with the theoretical values are shown in Table 5.2 in which the relative percentage of the peak areas for different atoms are shown, which represent the relative amount of atoms in the polymer. Also several ratios of these peak areas are shown in the last three rows of Table 5.2.

Table 5.2: Theoretical and experimental XPS-data for untreated PSf surfaces (both nonporous films and two types of membranes

	theoretical	PSf (Amoco)	PSf (GR40PP)	PSf (GR51PP)
C1s	84.4	80.3	79.0	82.0
O1s	12.5	15.6	15.6	14.9
N1s	0	1.4	3.9	1.2
S2p	3.1	2.6	1.0	1.9
S/O	0.25	0.167	0.065	0.131
O/C	0.148	0.194	0.197	0.181
S/C	0.037	0.032	0.013	0.024

From Table 5.2 it is clear that the peak areas and ratios of the areas of the C and O peaks for all surfaces have values that are close to the theoretical ones. A relatively large N peak was found for the GR40PP membrane. This may be due to additives which were used during the membrane formation process by the manufacturer (e.g. use of NMP), which can not explain the existence of a N peak for the non porous film. The sulfur peak was relatively low for the GR40PP membrane, maybe as a result of the high N peak. The S/O and S/C ratio was low for all the surfaces relative to the theoretical value, especially for the GR40PP membranes.

Despite of the small differences in relative peak areas, the three different surfaces were considered to be the same.

5.4.2 Plasma modification of PSf surfaces

XPS-measurements

The results of the XPS measurements of plasma modified PSf membranes are given in Table 5.3. Modification time was 60 minutes at a plasma power of 100 W.

The plasma modified membrane showed a decreased O and S peak and a large increased N peak in Table 5.3. A solid explanation for the decrease in the O and S peak could not be found. The XPS spectra of the modified membrane (not shown here) gave evidence of incorporation of primary amine groups at the surface. This explained the increase in the N peak in Table 5.3.

Table 5.3: Relative peak areas of a XPS-spectrum for an unmodified and for a modified GR51PP membrane. Modification time was 60 minutes at a plasma power of 100 W

	reference	modified
C1s	81.99	81.04
O1s	14.85	10.90
N1s	1.22	6.70
S2p	1.94	1.13
N/O	0.082	0.615
O/C	0.181	0.135
N/C	0.015	0.083

Sessile drop measurements

Contact angle measurements were carried out with water, glycerol and α-bromonaphtalene. The contact angle of water has been plotted versus modification time for different plasma powers (see Figure 5.1). With an increasing modification time the contact angle of water decreased for all plasma powers used in these tests. The effect of the plasma power was not completely clear from these measurements, because of the large experimental errors.

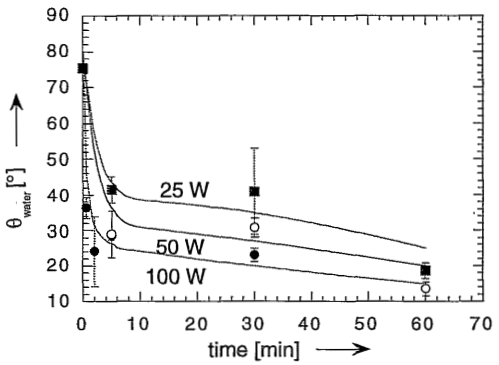

Figure 5.1: Contact angles of water θ_{water} versus plasma power and modification times

The three contact angles can be used to calculate the free energy of adhesion for both nonane and PEO, which is a measure for the fouling tendency (see Chapter 4). The free energy of adhesion was found to increase as a result of plasma modification in Figure 5.2.

From this figure it was clear that plasma modification with NH_3 resulted in a higher free energy of adhesion for both PEO and nonane. These modified surfaces were expected to have a lower fouling tendency. No effects of different plasma powers and modification times were observed. The free energy of adhesion reached a plateau value already after 30 seconds.

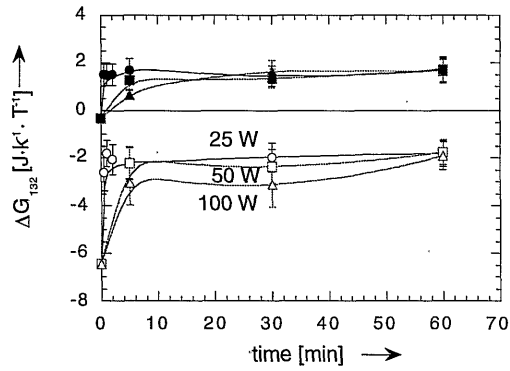

Figure 5.2: ΔG_{132}-values for NH_3-plasma modified surfaces with different modification times and plasma power. Open symbols represent the nonane part and closed symbols represent the PEO part of a nonionic surfactant molecule

Flux and retention measurements

Flux and retention measurements were carried out with a 2.5 $g \cdot \ell^{-1}$ buffered BSA solution with the plasma modified membranes modified with varying plasma powers (25, 50 and 100 W) at a fixed modification time of 5 min. NH_3 plasma modification did not result in any change in the pure water flux values before BSA-filtration which was found to be $J_{\text{pwf,before}} = 150 \pm 50\ kg \cdot m^{-2} \cdot h^{-1}$ at 2 bar (not shown here). Results for the BSA filtration flux, the retention and the flux recovery are shown in Figures 5.3 and 5.4.

Due to surface modification, the filtration flux increased and showed a maximum around 50 W plasma power. The retention of BSA, however, decreased as a result of plasma modification with NH_3-plasma, this contrary to the results found in literature (Wolff, 1988). These two phenomena indicated that the membrane structure was damaged (retention decreased from 60% to 5%). The cause of the damage may be the result of the modification process itself, because of etching off the top layer of the ultrafiltration membrane (see SEM-picture).

The flux recovery value in Figure 5.4 showed a slight increase with modification power, indicating a decrease in irreversible fouling tendency. This was probably the result of higher degree in hydrophilicity due to the modification, which was not observed by the sessile drop contact angle measurements.

SEM-measurements

To examine the damage of the membrane structure a SEM-picture was taken of the plasma modified GR51PP membrane, with a plasma power of 100 W for 60 min. The result showed that no damage can be visually observed in Figure 5.5.

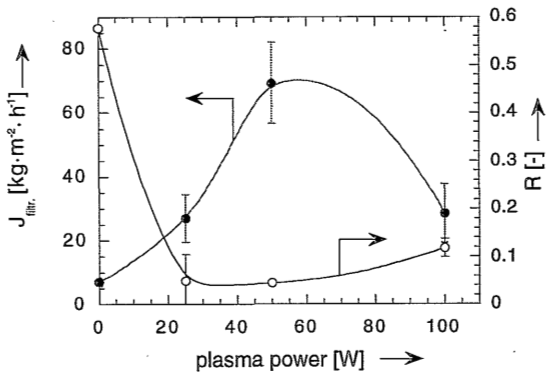

Figure 5.3: BSA filtration flux and retention versus the plasma power at constant modification of 5 minutes

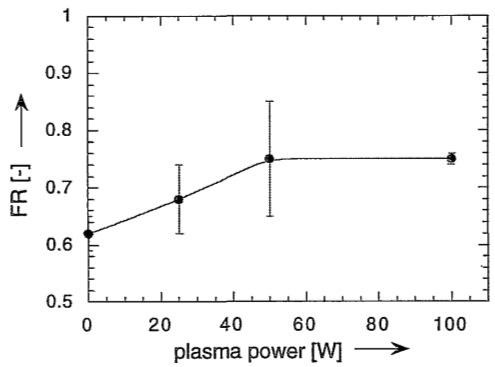

Figure 5.4: Flux recovery versus the plasma power at constant modification time of 5 minutes

5.4.3 Sulfonation of PSf surfaces

XPS-measurements

The results of the X-ray photoelectron spectroscopy measurements of the GR40PP membranes sulfonated for 30 seconds with $ClSO_3H$ at ambient temperatures and for 3 minutes with concentrated H_2SO_4 at 0°C are given in Table 5.4.

Comparison of the XPS-results of the $ClSO_3H$-sulfonated surfaces showed that both the S peak, the O peak and the Na peak increased significantly. This indicated an incorporation of $-SO_3^{\oplus}Na^{\ominus}$ groups onto the surfaces. Sulfonation with $ClSO_3H$ was

Figure 5.5: SEM-picture of a plasma modified membrane at 100 W and 60 *min*.

Table 5.4: Relative peak areas of a XPS-spectrum for an unmodified and for modified GR40PP membranes. Modification was carried out with $ClSO_3H$ (30 *sec* at ambient temperature) and with H_2SO_4 (3 *min* at 0°C)

Atoms	reference	$ClSO_3H$	H_2SO_4
C1s	79.0	70.0	78.7
O1s	15.6	18.3	15.2
N1s	3.9	4.7	3.5
S2p	1.0	2.0	1.1
Na1s	0.6	2.5	1.4
S/O	0.065	0.111	0.070
O/C	0.197	0.262	0.195
S/C	0.013	0.029	0.014

therefore useful for modification of PSf surfaces. This was confirmed by the peak ratios in Table 5.4.

From the table it was seen that sulfonation with concentrated H_2SO_4 at 0°C did not lead to a proper modification of the membrane surface; as was shown in the (almost) identical values for the different peaks and the peak-ratios. This modification technique was not investigated further.

Sessile drop measurements

Contact angles of water versus the sulfonation time for sulfonation with $ClSO_3H$ is shown in Figure 5.6. It was seen that the contact angle of water strongly declined within a few seconds sulfonation time.

In order to study the fouling tendency, ΔG_{132}-values were calculated and plotted versus time for PEO and nonane with sulfonated hard surfaces in Figure 5.7.

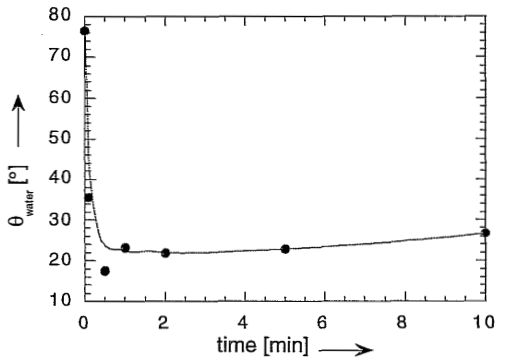

Figure 5.6: Contact angle of water on sulfonated surfaces versus time of sulfonation with $ClSO_3H$ (at 25°C)

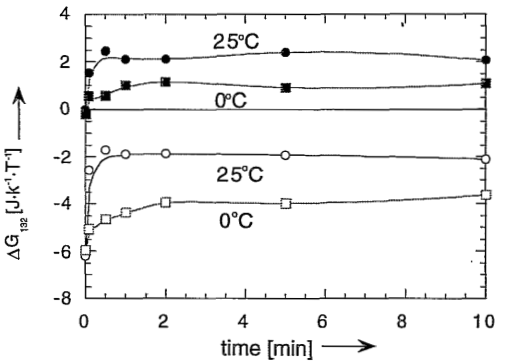

Figure 5.7: Free energies of adhesion of hexane on sulfonated surfaces versus time of sulfonation for $ClSO_3H$ at 25°C & 0°C . Open symbols represent the nonane part and closed symbols represent the PEO part of a nonionic surfactant molecule

In this figure it can be seen that that sulfonation with $ClSO_3H$ was effective in increasing ΔG_{132} for both PEO and nonane, indicating a decrease in fouling tendency. A plateau-value was reached within 20 seconds for ΔG_{132}.

Moderate $ClSO_3H$-sulfonation could be obtained by cooling the reactive mixture in an ice-bath, which also becomes clear from Figure 5.7. Again a plateau-value was reached within 20 seconds. This plateau-value was lower (ΔG_{132} (PEO at 0°C) $= 2\ J \cdot k^{-1} \cdot T^{-1}$) compared to no cooling (ΔG_{132} (PEO at room temperature) $= 1\ J \cdot k^{-1} \cdot T^{-1}$).

Flux and retention measurements

BSA-filtration experiments were carried out with TEP/SO_3-sulfonated PSf GR51PP membranes. In our case, visual damage of the membranes was observed of the membranes for 15 minutes of modification with the undiluted and the 20 times diluted TEP/SO_3-cyclohexane mixture (see also SEM-pictures). No visual damage could be observed for the 40 times diluted TEP/SO_3-cyclohexane mixture. Results of the flux and retention measurements with 30 minutes sulfonation of 40 times diluted TEP/SO_3 are given in Table 5.5.

Table 5.5: BSA flux and retention results at 2 *bar* of a TEP/SO_3 sulfonated GR51PP membrane

memb.	$J_{pwf,before}$ $[kg \cdot m^{-2} \cdot h^{-1}]$	J_{filtr} $[kg \cdot m^{-2} \cdot h^{-1}]$	FR [-]	R [-]
ref.	96 ± 30	5 ± 1	0.62 ± 0.03	0.60 ± 0.10
mod.	167 ± 10	8 ± 1	0.54 ± 0.02	0.40 ± 0.05

From the increase of both flux values and the decrease in retention due to sulfonation, it was concluded that the modified membrane was damaged by the TEP/SO_3-treatment. The flux recovery value decreased which can be attributed to an increase in irreversible fouling as a result of the increase in the pure water flux before filtration value.

SEM pictures

The GR51PP membrane was modified by an unstable TEP/SO_3 in cyclohexane emulsion. SEM was used to investigate if the surface was modified homogeneously. The results of the SEM-measurements of a 150 minutes sulfonated membrane surface with diluted TEP/SO_3-solution is given in Figure 5.8. From this picture light spots were visible on a darker shaded background, indicating that sulfonation with a TEP/SO_3 cyclohexane emulsion resulted in an inhomogeneous sulfonation.

A SEM-picture of a PSf membrane that is sulfonated with $ClSO_3H$ for 30 *sec* is shown in Figure 5.9. From this picture no damage to the membrane surface could be observed.

5.5 Conclusions

Direct drying of water rinsed membranes resulted in a collapse of the structure. This was prevented by first rinsing the water filled membranes with ethanol and hexane.

NH_3-plasma modification of PSf surfaces led to the formation of amine-groups at the surface, which resulted in an increase in hydrophilicity. It was shown, however, that the membrane structure of the ultrafiltration membranes was damaged by the modification process.

Modification of PSf surfaces with concentrated and fuming sulfuric acid at ambient temperatures led to a visual damage of the surfaces. Modification with cooled, concen-

Figure 5.8: SEM-picture of a 150 *min* sulfonated membrane with TEP/SO_3

Figure 5.9: SEM-picture of a 30 *sec* sulfonated membrane with $ClSO_3H$

trated sulfuric acid at 0°C did not result into modified PSf surfaces. Modification of PSf surfaces with a TEP/SO_3-complex resulted in damage of the surface even after 40 times dilution. Modification with $ClSO_3H$ resulted in an increase in hydrophilicity of PSf surfaces. The fouling tendency, decreased with modification time but reached a plateau after 120 seconds. No structural damage was observed with modification with $ClSO_3H$.

5.6 Acknowledgements

Thanks are due to R. Sander who carried out most of the work presented in this chapter, in order to fulfil the requirements for his M.Sc. thesis. Parts of the experimental work have been carried out as a practical trainee period of four monthes by P. Wuis and by

several chemical engineering students as a practical course during their study. The SEM-picture of the TEP/SO_3 modified PSf surface was obtained from P. v.d.Vlist and P. Nooteboom at the Unilever Research Laboratory Vlaardingen. All their help is highly appreciated.

5.7 List of Symbols

Acronyms

Symbol	Quantity
AFM	atomic force microscopy
BSA	bovine serum albumin
FR	flux recovery
PEO	polyethyleneoxide
PSf	polysulfone
SEM	scanning electron microscopy
STP	standard temperature and pressure
TEP	triethylenephosphate
UV	ultra violet
Vis	visual light
XPS	X-ray photoelectron spectroscopy
pwf	pure water flux

Symbols

Symbol	Quantity	Units
J	membrane (permeate) flux	$[kg \cdot m^{-2} \cdot h^{-1}]$
R	retention	$[-]$
ΔG_{132}	free energy of adhesion between 1 and 2 in 3	$[J \cdot k^{-1} \cdot T^{-1}]$
θ	contact angle	$[^o]$
t	time	$[s]$

Chapter 6

Membrane fouling by emulsions

6.1 Introduction

A well-known disadvantage of filtration processes is the decline of flux with time, which leads to a loss of performance of the process. The cause of this flux decline in time is the result of concentration polarisation and fouling during filtration (Berg and Smolders, 1990; Bhattacharjee *et al.*, 1994; Fane and Fell, 1987; Jonsson *et al.*, 1996). Concentration polarisation is the accumulation of feed solutes in front of the membrane due to a convective transport which leads to a reduction in the driving force because of an increase in the osmotic pressure of the feed solution or leads to the formation of a gel layer in front of the membrane (Berg and Smolders, 1990). Much research has been carried out to elucidate the mechanism of fouling. However, due to the complexity of the problem no general picture can be given. Several approaches exist to elucidate the membrane fouling mechanisms for simplified feed materials (Field *et al.*, 1995; Hermia, 1982; Jonsson *et al.*, 1996; Prránados *et al.*, 1996).

In this work a dilute oil-in-water emulsion has been chosen as foulant (see Chapter 3 of this thesis). The membranes that have been selected are polysulfone ultrafiltration membranes (see Chapter 4 of this thesis).

In literature the influence of several factors on the membrane flux has been investigated for emulsions, such as transmembrane pressure, temperature, cross-flow velocity and oil concentration (Bhattacharyya *et al.*, 1979; Lee *et al.*, 1984; Lipp *et al.*, 1988). The membrane flux behaviour is often described by empirical relations (Bhattacharyya *et al.*, 1979; Bodzek and Konieczny, 1994; Lee *et al.*, 1984; Lipp *et al.*, 1988; Matz and Meitlis, 1978; Vigo *et al.*, 1993). Little is known, however, about the exact mechanisms of emulsion fouling of membranes, such as pore narrowing, pore blocking and cake layer formation.

In this chapter an attempt has been made to elucidate the mechanism of membrane fouling with dead-end filtration experiments with emulsions and cryo-SEM pictures of fouled membranes. Also the flux decline during emulsion filtration is fitted with relations found in literature (Field *et al.*, 1995; Hermia, 1982; Jonsson *et al.*, 1996; Prránados *et al.*, 1996) to predict the fouling behaviour.

6.2 Theory

Fouling usually results in a continuous flux decline as a result of (ir)reversible deposition of retained particles or solutes on the membrane. This includes adsorption, pore narrowing (internal fouling), pore blocking and cake formation which represent the different fouling mechanisms (Mulder, 1996).

The type of fouling mechanism during membrane filtration depends on several parameters, such as the type, shape and diameter of the solutes (d_s) and the diameter of the membrane pores (d_p). If the diameter of the solutes are smaller than the diameter of the pores, the solutes are able to penetrate the internal membrane structure and cause internal fouling. If both solute and pore diameters are of the same size order and pore blocking can occur. If the diameter of the solutes are larger than the diameter of the pores, the solutes are unable to penetrate the internal membrane structure and a cake layer can be formed on top of the membrane. In Figure 6.1 the different fouling mechanisms are illustrated.

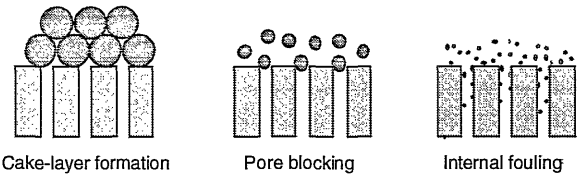

Figure 6.1: Schematic drawing of the different fouling mechanisms

If both microscopic parameters are known, an indication can be obtained of the expected type of fouling mechanism. There are however, several complications with this microscopic approach. Concentration polarisation occurs for $d_s \geq d_p$, which can affect the fouling mechanism. Apart from this, the parameters can change in time (e.g. d_s increases because of coalescence or clustering, d_p decreases because of pore narrowing), which affect the fouling mechanism. Also both d_s and d_p are usually distributed which can result in combinations of different fouling mechanisms. It is clear that the phenomenon of fouling is very complex and is very difficult to describe theoretically.

In literature macroscopic approaches are described to elucidate the fouling mechanism, such as flux and retention measurements. These measurements are the most common methods described in literature to investigate the membrane fouling mechanism (Lipp *et al.*, 1988). They are easy to apply and use the same solutes that cause membrane fouling. The disadvantage of these measurements is that it is a macroscopic approach to describe microscopic phenomena. In literature many theories are presented to bridge this gap (Bansal *et al.*, 1991; Belfort, 1989; Blatt *et al.*, 1970). The disadvantage of many of these theories is that they are focussed on only one fouling mechanism, such as internal fouling (Hanemaaijer *et al.*, 1989), pore narrowing (Zeman, 1983), pore blocking (Kawakatsu *et al.*, 1995; Le and Howell, 1984) and gel or cake layer formation (Bodzek and Konieczny, 1993; Kim *et al.*, 1992).

In a macroscopic approach developed by Hermia (Hermia, 1982), different fouling mechanisms are incorporated into a general formula in which the permeate flux time dependence is given (Jonsson *et al.*, 1996):

$$J = \frac{J_0}{(1+kt)^n} \tag{6.1}$$

In which J_0 is the initial permeate flux, t is the time, k is a characteristic system constant given by microscopic parameters (see Table 6.1) and n is a constant related to the type of fouling (see Table 6.1). For pore narrowing it is assumed that the pore volume decreases proportionally to the filtrate volume by particle deposits on the pore walls (Hermia, 1982). In this case $n = 2$ (see Table 6.1). For pore blocking it is assumed that the pore surface area decreases proportionally to the filtrate volume. In this case $n = 1$. For a formation of a gel or cake layer on top of the membrane $n = 0.5$.

Table 6.1: Overview of the parameters of different general formulae for the four different fouling mechanisms

Law	k	n
Pore narrowing [a]	$\frac{CJ_0}{L}$	2
Pore blocking [b]	σJ_0	1
Cake filtration [c]	$\frac{2r_cJ_0}{R_m} \cdot \left(\frac{\phi_b}{1-\phi_b \cdot m_r}\right)$	0.5

[a] In which, C is the volume of retained solid particles per unit permeate volume $[-]$ and L is the membrane thickness $[m]$

[b] In which, σ is the blocked area per unit permeate volume $[m^{-1}]$

[c] Here is r_c the specific resistance of the cake $[m^{-2}]$, ϕ_b the mass fraction in the bulk [-], m_r the mass ratio of wet to dry cake [-] and R_m is the hydraulic membrane resistance at $t = 0$ $[m^{-1}]$

Equation 6.1 can be used to fit a certain fouling mechanism to an actual filtration experiment. In practice, different fouling mechanisms may play a role during a filtration experiment at the same time and combined fouling mechanisms can occur at different time-scales. For example Pránados et al. (Pránados *et al.*, 1996) report a case in which pore blocking is followed by a cake layer formation.

Two approaches have been discussed in this section, a microscopic approach in which the fouling mechanism is related to microscopic membrane parameters (such as d_s and d_p) and a macroscopic approach in which the fouling mechanism is related to macroscopic parameters (such as flux and retention). Theoretically, the microscopic approach is preferred, but due to the complexity of fouling the macroscopic approach of Hermia has been used to gain insight into the fouling mechanism.

6.3 Experimental part

6.3.1 Materials

Polysulfone ultrafiltration membranes with a cut-off of 100 kDa were used, obtained from Dow Denmark Separation (DDS). Emulsions were used as a model for waste water

of domestic laundry machines. An emulsion of 6 g Castor oil (Merck chemicals) and 2.4 g surfactant (NP9 from ICI) in 300 ml ultrapure water was prepared by stirring in a baffled vessel and diluted 6 times afterwards. The mean droplet diameter is $d_{32} = 0.22$ μm (see Chapter 3 of this thesis for more details).

6.3.2 Characterisation methods

SEM and cryo-SEM

To investigate the membrane structures on a micro-scale, scanning electron microscopy pictures can be made. The disadvantage of SEM is that samples have to be dried, which can cause a change in the membrane and foulant structure. Therefore, cryo-SEM measurements were carried out at the Unilever research laboratory in Vlaardingen with which wet samples can be investigated. Fouled ultrafiltration membranes are investigated to study the structure of the emulsion fouling at the membrane. For cryo-SEM measurements, wet samples have been frozen in liquid nitrogen and have been put into the working-chamber of the cryo-SEM (Philips, 515 cryo-SEM). In this chamber, the samples have been etched at $-80°C$ for 15 minutes. After this, the samples have been covered by a gold-palladium layer and investigated by the cryo-SEM.

Dead-end set-up

A dead-end filtration set-up has been used to test the performance of the membranes and to investigate the mechanism of membrane fouling by emulsions. A schematic picture of the dead-end set-up is presented in Figure 6.2. A gas flask with air (1) is used to pressurise the feed tank (2). The important part of the set-up is the dead-end filtration cell (3) with the membrane to be investigated ($A_m = 38.5$ cm^2). The permeate stream is collected in a beaker (4), placed on a mass balance connected to a computer (5). Permeate data were collected in one minute intervals. For each experiment a new membrane has been used, and each experiment was carried out four times from which a standard deviation was calculated.

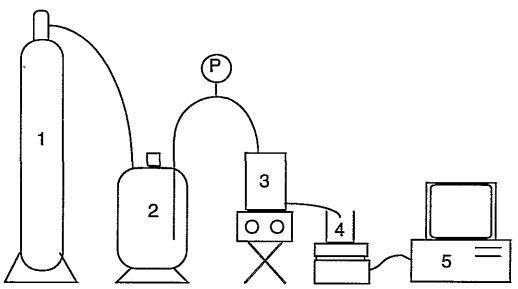

Figure 6.2: Schematic drawing of the dead-end set-up

6.3.3 Methods

Three types of experiments were carried out in this chapter. First, *pure water flux experiments* were carried out. Secondly, experiments were carried out with emulsions to gain more insight in the *fouling mechanism.* Cryo-SEM measurements were carried out and furthermore the flux versus time curve of emulsion filtration tests were fitted with equation 6.1. From the results of the measurements, the formation of a cake layer on top of the membrane was hypothesised and experiments were carried out to *test the proposed type of fouling.* These additional experiments consisted of measuring the compressibility of the cake layer, the irreversible fouling of the cake layer and the influence of surfactants on the cake layer. Surfactants were added to prevent or reduce compressibility and eventually coalescence of oil droplets in the cake layer which was expected when applying pressures on the hypothesised cake layer.

Pure water flux experiments

Pure water flux experiments were carried out for two hours at 2 bars to characterise every new membrane. During such experiments, the preservation liquid present in the membrane structure was removed. The flux value at two hours is taken as the value for the pure water flux before emulsion filtration $J_{\text{pwf,before}}$ (see Figure 6.3). It was checked that this time is sufficient to reach a steady state flux.

In an attempt to minimise the observed scattering of the flux data (Nilsson, 1989), new membranes were pretreated before the pure water flux experiment took place by filtration of a 1 $g \cdot \ell^{-1}$ NP9 surfactant solution for 10 minutes at five bar.

Emulsion filtration experiments

After the pure water flux experiment, the dead-end cell was filled with a dilute emulsion (0.42 $g \cdot \ell^{-1}$ Castor oil and 0.17 $g \cdot \ell^{-1}$ NP9) and the actual emulsion filtration experiment was carried out. Ultrapure water was used in the feed tank to pressurise the dead-end cell (unless stated otherwise). Different filtration times (0 – 300 minutes) and transmembrane pressures (0 – 5 bar) were used to filtrate the emulsion in the dead-end cell. The oil retention was expected to be high, which was confirmed by visual observation.

In order to test the hypothesis of cake layer compressibility during emulsion filtration, the emulsion filtration flux after two hours (J_{filtr}) was measured as a function of the transmembrane pressure.

After the emulsion filtration experiment the solution in the dead-end cell was stirred for five minutes at 1000 rpm with a Rushton impeller. The solution was replaced by (ultrapure) water to remove a concentrated viscous layer on top of the membrane. After this, again a pure water flux experiment was carried out for two hours at two bars to obtain an indication of the degree of irreversible fouling by calculating the flux recovery, defined as the ratio between the pure water flux after and before the emulsion filtration experiment (see Chapter 4). An example of the result of a standard filtration experiment is shown in Figure 6.3, in which the following three different zones can be distinguished,

the pure water flux before filtration, the filtration flux and the pure water flux after filtration.

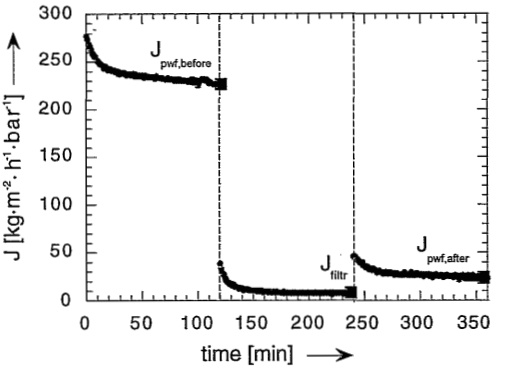

Figure 6.3: Standard filtration curve with a filtration time of two hours and a transmembrane pressure of two bars for both ultrapure water and emulsion

The influence of surfactants on the cake layer was investigated by the same emulsion filtration experiments as described above (variation of both time and transmembrane pressure). In these experiments, however, a surfactant solution of 0.17 $g \cdot \ell^{-1}$ NP9 in the feed tank had been used instead of ultrapure water to pressurise the dead-end cell.

6.4 Results and discussion

6.4.1 Pure water flux experiments

In Figure 6.4 it is shown that there exists a large scattering of pure water fluxes, which are divided into several classes. In this figure a large variation of pure water fluxes existed for the GR40PP membrane, ranging from $25 - 450\ kg \cdot m^{-2} \cdot h^{-1} \cdot bar^{-1}$. From statistical analysis of the plot, the mean pure water flux is $J_{\text{pwf,before}} = 186\ kg \cdot m^{-2} \cdot h^{-1} \cdot bar^{-1}$ with a standard deviation of $\sigma = 53\ kg \cdot m^{-2} \cdot h^{-1} \cdot bar^{-1}$. The large scattering in pure water flux might be due to variations in the membrane structure of the different membrane samples (Larsson and Wimmerstedt, 1993; Nilsson, 1989; Persson *et al.*, 1993). These differences in the membrane structure probably were the result of variations during the membrane preparation process.

The pure water flux scattering for pretreated membranes with surfactants are shown in Figure 6.5, from which an even larger scattering appeared than for the untreated membranes. By adding surfactants to water, the interfacial tension decreased which led to the opening of smaller pores in the membrane at a certain transmembrane pressure. The pure water flux was expected to increase by this mechanism. Another effect of adding

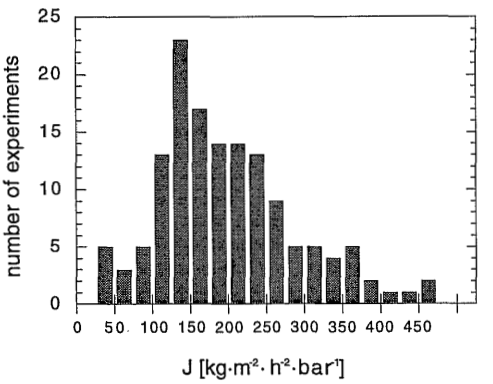

Figure 6.4: Pure water fluxes for 129 (new) GR40PP membranes measured after two hours ($150 - 500\ kg \cdot m^{-2} \cdot h^{-1} \cdot bar^{-1}$ according to manufacturer)

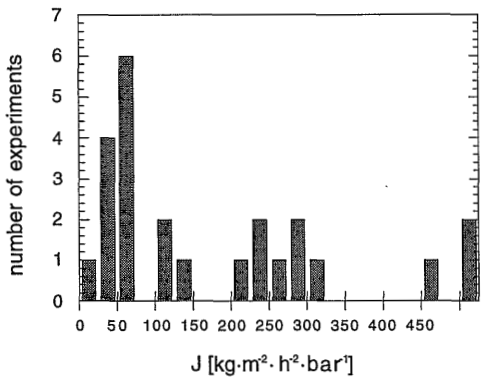

Figure 6.5: Pure water fluxes for 24 pretreated membranes with 1 $g \cdot \ell^{-1}$ NP9 surfactant solution; measured after two hours

surfactants to the system was adsorption into pores, which led to pore narrowing. By this mechanism, the pure water flux was expected to decrease. Both mechanisms depend on the pore radii of the membrane samples which varied strongly. This resulted in a pure water flux which could both increase or decrease. Pretreatment with surfactants was therefore not effective in reducing the scattering in pure water flux.

The flux behaviour in time of both untreated and pretreated membranes is shown in Figure 6.6. From this figure, an optimum at 90 minutes can be seen for the surfactant pretreated membrane, which occurred as a result of the balance between a flux increase

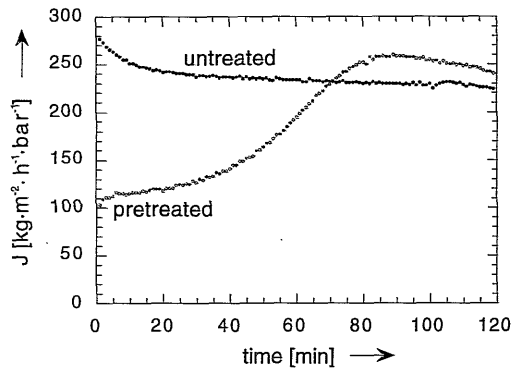

Figure 6.6: Pure water flux before emulsion filtration versus time for both pretreated and untreated membranes

due to removal of surfactants from the membrane structure (e.g. by pore opening) in time and a flux decrease due to fouling by inevitably present contaminants in the water. This optimum was found in all the pure water flux curves of the pretreated membrane, but the location of this optimum differed over the range of two hours, due to variations in the different membrane samples. No optimum could be seen for the untreated membrane in Figure 6.6.

6.4.2 Fouling behaviour

On the basis of a microscopic approach to membrane fouling by comparing the mean diameter of the droplets ($d_{32} = 0.22\ \mu m$) to the mean diameter of the pores ($< 0.10\ \mu m$), the emulsion droplets were not expected to penetrate the membrane structure during filtration. The formation of a cake layer on top of the membrane was likely, because of this size difference. It was expected that the cake layer consisted of separate droplets because the droplets were stable against coalescence. For emulsions at rest a long term stability was observed in Chapter 3 of this thesis.

Because of a droplet diameter distribution (see Chapter 3 of this thesis) and a pore diameter distribution it is possible that droplets existed of the same diameter as the membrane pores. In this case it was possible that other mechanisms such as pore blocking and internal membrane fouling could occur during filtration. From data analysis of the emulsion droplet distribution it was calculated that the number average value for the droplets was $d_{10} = 0.18\ \pm 0.06\ \mu m$. Because of the small amount of droplets smaller $< 0.10\ \mu m$ these mechanisms are not very likely.

The fouling mechanism will be investigated with cryo-SEM and with a fitting procedure, to investigate membrane fouling on a macroscopic scale.

Cryo-SEM

To verify the presence of a cake layer, cryo-SEM pictures were made of the fouled membranes. In Figure 6.7 a cross section of a fouled membrane sample is shown, in which a cake layer is visible with an estimated thickness of $35 - 50\ \mu m$. The cake layer thickness could also be calculated assuming a closest sphere packing of uniform incompressible emulsion droplets with a mean diameter of $d_{32} = 0.22\ \mu m$. The calculated cake layer thickness was 88 μm ($0.42\ g \cdot \ell^{-1}$ oil in a dead-end cell with a volume of 400 ml and a membrane area of 38.5 cm^2). The calculated cake layer thickness value was two times higher than the value from the cryo-SEM. This is probably due to the assumptions made to calculate the cake layers thickness.

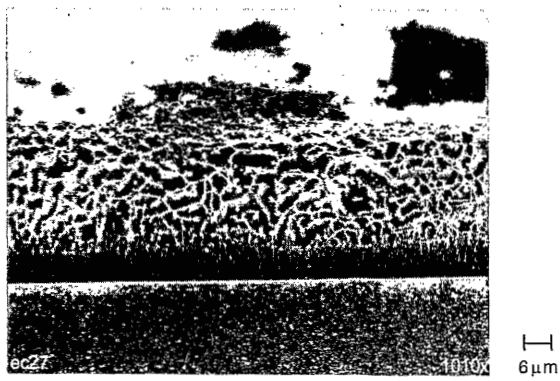

Figure 6.7: Cryo-SEM picture of a cross section of a fouled membrane sample

Because the resolution of the cryo-SEM picture in Figure 6.7 is $> 1\ \mu m$, no individual oil droplets could be observed in the cake layer on the face of the membrane, rather than ice-plated structures probably caused by freeze-drying of water which were present in the membrane sample. Other techniques are necessary to indicate the occurrence of droplet coalescence in the cake layer, if there is any.

Fitting procedure

The emulsion flux versus time behaviour during emulsion filtration is given in Figure 6.8 for an experiment of 300 minutes at two bar. In this plot it can be observed that the emulsion flux declined in time and that a plateau value of $6\ kg \cdot m^{-2} \cdot h^{-1} \cdot bar^{-1}$ was reached after approximately 100 minutes.

The emulsion flux versus time behaviour during emulsion filtration can be fitted to the equation 6.1 as was given by Jonsson et al. (Jonsson *et al.*, 1996). It was found that the average fit-constant was $n = 0.5 \pm 0.1$ for emulsion filtration experiments at 1, 2 and 3 bar, which corresponded to the cake filtration model (see Table 6.1). An example of such a fit is given in Figure 6.9 for the first 50 minutes of the experiment shown in Figure

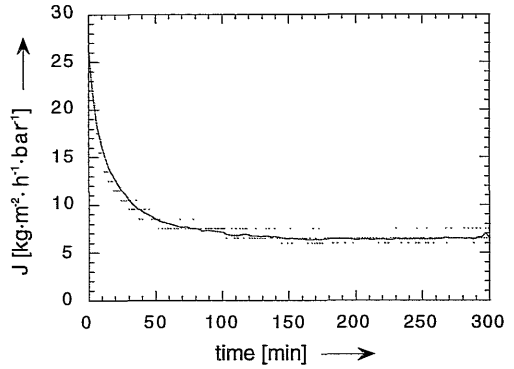

Figure 6.8: Flux versus time behaviour during emulsion filtration at two bar transmembrane pressure

6.8. No reasonable values for n were found for the emulsion filtration experiments with a transmembrane pressure higher than 3 bar.

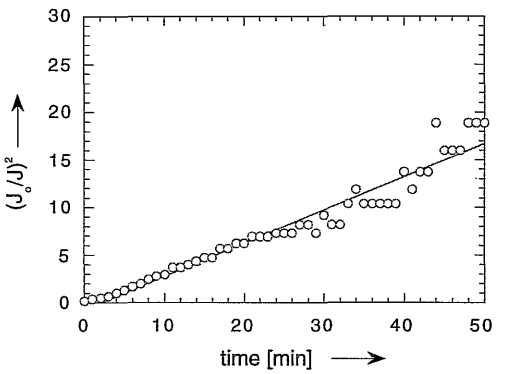

Figure 6.9: An example of a fit of the cake layer model for the first 50 minutes of Figure 6.8

The fit-constant n from the general equation 6.1 was also studied at different time intervals. At small time intervals of about 15 minutes good fits of the flux decline were obtained for $n \approx 1.0$, indicating that the pore blocking model applied (see Table 6.1). For larger time-intervals of about 100 minutes, fit-constants of $n \approx 0.5$ gave better fits, indicating that the cake layer formation model applied. Pránados (Pránados *et al.*, 1996) concluded for invertase proteins filtration with ceramic ultrafiltration membranes, that

the fouling mechanism changed from pore-blocking within the first minutes towards the formation of a cake layer on top of the membrane, on the basis of the described fit-procedure.

6.4.3 Testing of the proposed type of fouling

From the observations described above, it was concluded that the main membrane fouling mechanism during emulsion filtration was cake layer formation. The behaviour of this cake layer with respect to compressibility, irreversible fouling and adding surfactants was investigated in the following sections.

Compressibility of the cake layer

In order to investigate the influence of the compressibility of the cake layer, the influence of the transmembrane pressure on the emulsion filtration flux after two hours was studied. It was assumed that a complete cake layer had already been established after two hours of filtration. This can be argued by the fact that a steady state flux had been reached after about one hour (see Figure 6.3 and 6.8).

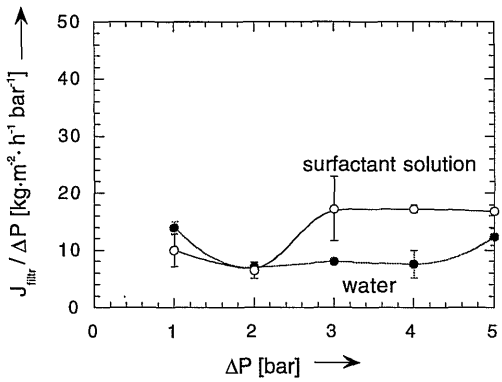

Figure 6.10: Emulsion filtration flux over pressure after two hours versus transmembrane pressure for both ultrapure water (black dots) and a 0.16 $g \cdot \ell^{-1}$ NP9 surfactant solution (white dots) to pressurise the dead-end cell

The emulsion filtration flux after two hours over the transmembrane pressure has been plotted against the transmembrane pressure in Figure 6.10. From this plot it can be seen that the flux over pressure was invariant of the transmembrane pressure (black dots in Figure 6.10), indicating an incompressible cake layer at pressures lower than five bar. From this result it could be concluded that the cake layer on top of the membrane did not change its structure at the investigated pressure range. Because of this incompressibility it was not likely that coalescence will occur.

Irreversible fouling by the cake layer

To investigate the degree of irreversible fouling caused by emulsion filtration the flux recovery value (FR) was studied as a function of the transmembrane pressure and time.

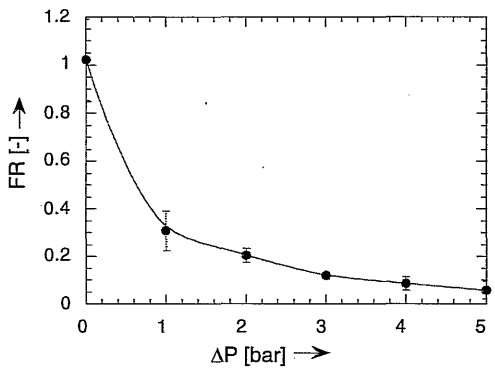

Figure 6.11: Flux recovery after two hours of emulsion filtration versus the transmembrane pressure

In Figure 6.11 the influence of the transmembrane pressure on the irreversible fouling is investigated. From this plot, it can be seen that the flux recovery value was lower than 1 for every transmembrane pressure > 0 *bar*, indicating that irreversible fouling occurred. This decrease in flux recovery can be explained by the presence of a cake layer which could not be completely removed by stirring and/or by pore blocking. A non removable cake layer could occur if the emulsion droplets at the membrane surface broke up and adsorbed at the membrane surface.

From Figure 6.11 it can also be seen that the degree of fouling increased for increasing transmembrane pressures. Apparently at higher pressures a cake layer was formed which was more difficult to remove by stirring than at lower pressures. It is possible that at higher pressures more emulsion droplets broke up and adsorbed at the membrane surface. Another explanation was that more pores are blocked at higher transmembrane pressures. This would result in a decrease in emulsion flux as a function of the pressure and was not observed in Figure 6.10 which makes this explanation less reasonable.

The time effect of the irreversible fouling is given in Figure 6.12 by the black dots. It can be seen that at times shorter than 30 minutes the flux recovery value was about 0.70, and at times larger than 60 minutes the flux recovery value was 0.15. At times shorter than 30 minutes fouling occurred, probably due to pore blocking. It is possible that at these short times, incomplete cake layers were formed which can be removed by stirring. At times higher than 60 minutes cake layers were present which can not be completely removed by stirring. At these times a steady state emulsion flux was reached as can be seen in Figure 6.8.

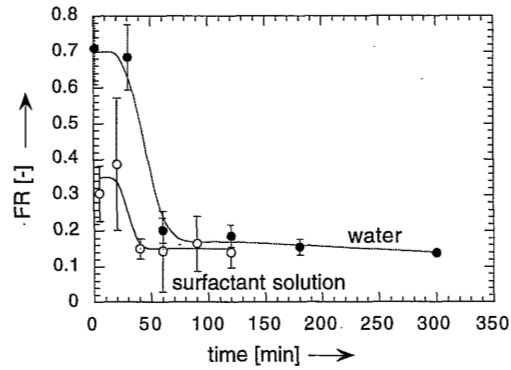

Figure 6.12: Flux recovery values at two bar versus the emulsion filtration time for water (black dots) and a 0.16 $g \cdot \ell^{-1}$ NP9 surfactant solution (white dots) to pressurise the dead-end cell

Influence of surfactants on the cake layer

In the experiments discussed so far, (ultrapure) water had been used to pressurise the dead-end cell filled with an emulsion. It was seen that irreversible fouling occurred when emulsion droplets at the membrane surface broke up and adsorbed at this surface. This breakup might be caused by a shortage of surfactants at the oil water interface of emulsion droplets. The fraction of free and clustered surfactants was very low (7 %) as had been measured with diffusion cell measurements (see Appendix B). In an attempt to prevent breakup of emulsion droplets due to a surfactant shortage, instead of (ultrapure) water, a 0.16 $g \cdot \ell^{-1}$ NP9 surfactant solution was used to pressurise the dead-end cell.

The degree of irreversible fouling as a function of the emulsion filtration time is plotted in Figure 6.12 (white dots). From this figure it can be seen that the flux recovery was about 0.35 for filtration times shorter than 20 minutes, and $FR = 0.15$ for filtration times higher than 40 minutes. The low flux recovery value at shorter filtration times for a surfactant feed solution was probably due to surfactant adsorption in the pores or an easier breakup of emulsion droplets at the membrane surface. At higher filtration times, the flux recovery values are comparable to the situation in which no surfactants was added.

The flux recovery versus the transmembrane pressure with the surfactant solution to pressurise the dead-end cell is comparable to Figure 6.11 and is not shown here. It can be concluded that adding surfactants to the feed vessel did not lead to a reduced irreversible fouling.

For the case of a surfactant solution used to pressurise the dead-end cell (white dots in Figure 6.10), it can be observed that the flux over pressure value showed a step wise increase above transmembrane pressures of two bar. A reasonable explanation for this

phenomenon can not be given. From this plot it is clear that the flux over pressure values above two bar were higher for surfactant solutions than for (ultrapure) water as feed material to pressurise the dead-end cell. Apparently the cake layer was more open when a surfactant solution was used, maybe because of a higher mutual repulsion of individual oil droplets in the cake layer.

6.5 Conclusions

The fouling mechanism during dead-end emulsion filtration was the formation of an irreversible gel or cake layer for commercial 100 kDa PSf UF membranes. The thickness of this gel or cake layer was $35 - 50$ μm for a fixed filtration time of two hours with a dilute emulsion feed solution (0.42 $g \cdot \ell^{-1}$ Castor oil and 0.17 $g \cdot \ell^{-1}$ NP9). This gel or cake layer of individual oil-droplets was formed on top of the membrane, after an initial phase of about 15 minutes of pore blocking.

These layers were found to be incompressible for pressures lower than five bar. The emulsion droplets in the cake layer did not coalesce in this pressure range.

At short emulsion filtration times (within 30 minutes) irreversible fouling was less pronounced. In these cases, cake layers could be removed easily by stirring. The observed flux decline at short times was ascribed to pore-blocking.

Adding surfactants to the feed vessel did not lead to a reduced irreversible fouling. For pressures above two bar, it did result in an increase in the emulsion filtration flux.

6.6 Acknowledgements

Thanks are due to P. Zandbergen (URL Vlaardingen) who kindly carried out the Cryo-SEM experiments. Most of the work presented in this chapter has been the topic of the M.Sc thesis of A. Moraal, who worked nine months on this topic to complete her chemical engineering study. Parts of the experimental work has been carried out by J.R. v.d. Zwan and H. Gruben in order to carry out their technical trainee period. Their work is highly appreciated.

6.7 List of Symbols

Acronyms

Symbol	Quantity
FR	flux recovery
SEM	scanning electron microscopy
$filtr$	emulsion filtration experiment
pwf	pure water flux

Symbols

Symbol	Quantity	Units
A_m	membrane area	$[m^2]$
C	volume of retained solid particles per unit permeate volume	$[-]$
J	membrane (permeate) flux	$[m \cdot s^{-1}]$ or $[kg \cdot m^{-2} \cdot h^{-1}]$
J_0	the initial emulsion filtration flux	$[m \cdot s^{-1}]$ or $[kg \cdot m^{-2} \cdot h^{-1}]$
L	membrane thickness	$[m]$
R_m	hydraulic membrane resistance at $t = 0\ s$	$[m^{-1}]$
ϕ_b	mass fraction in the bulk	$[-]$
σ	blocked pore area per unit permeate volume	$[m^{-1}]$
k	system constant in equation 6.1	$[s^{-1}]$
m_r	mass ratio of wet to dry cake	$[-]$
n	constant related to the type of fouling in equation 6.1	$[-]$
d_{32}	volume to area mean droplet diameter	$[\mu m]$
r_c	specific resistance of the cake	$[m^{-2}]$
d_p	membrane pore diameter	$[\mu m]$
d_s	diameter of the solutes	$[\mu m]$
t	time	$[s]$

Chapter 7

Use of prefilters to prevent fouling

7.1 Introduction

As was shown in the previous chapter, the mechanism of emulsion fouling is mainly determined by the formation of a cake layer on top of the membrane, leading to a decline in the water flux. Removal of this cake layer by stirring does not lead to a fully recovered pure membrane flux, due to adsorptive fouling. The magnitude of this inevitable decrease in flux recovery depends on the surface characteristics of the membrane material and has been described in Chapter 4 and 5.

A removable prefilter i.e. a prepared layer on top of a membrane, can be used for the purpose to prevent fouling of the membrane itself. In theory, when all foulants are attached to this prefilter (which can be removed completely) this would lead to a completely reversible process. Prefilters have been described in literature to obtain higher long time fluxes (Arora and Davis, 1994; Igawa *et al.*, 1977; Nakao *et al.*, 1986).

In this chapter membrane fouling prevention by the use of prefilters is described. Prefilters used for this purpose need to have certain properties, such as low solubility in the filtration medium (usually water), a high affinity for the foulant material, a high capacity to adsorb foulants and a low affinity for the membrane material. In this chapter several types and amounts of prefilter materials are studied.

7.2 Theory

7.2.1 The prefilter

In this work a prefilter is defined as a designedly prepared (cake) layer on top of a membrane. If during the filtration of particles (or solutes) a prefilter is formed on top of the membrane, the flux can be described by the resistance in series model. This flux is then expressed in terms of the driving force, i.e. the transmembrane pressure and the resistances against mass transfer as follows (Ho and Sirkar, 1992; Kawakatsu *et al.*, 1993):

$$J = \frac{\Delta P}{\eta R_{\text{tot}}} = \frac{\Delta P}{\eta \left(R_m + R_c + R_f\right)} \tag{7.1}$$

Here is ΔP the transmembrane pressure, η the viscosity of the medium (usually water) and R_{tot} the total resistance against mass transfer. This total resistance consists of the membrane resistance R_m, the resistance of the prefilter R_c and the resistance caused by fouling R_f as a result of pore blocking and internal fouling of the membrane and/or the prefilter. In the resistance in series model, all these contributions to the total resistance are assumed to be additive and independent of each other.

The membrane resistance can be found experimentally from a pure water flux experiment. In this case $R_{tot} = R_m$ in equation 7.1. In the case of prefilters, a layer is present on top of the membrane which adds an extra resistance to mass transfer and is given by:

$$R_c = r_c \delta_c \tag{7.2}$$

Here is r_c the specific resistance of the prefilter and δ_c the prefilter thickness. A direct and simple approach to estimate the specific prefilter resistance is the Carman-Kozeny equation, for rigid incompressible particles (Carman, 1938):

$$r_c = \frac{K \cdot (1-\epsilon)^2}{\epsilon^3} \left(\frac{S_p}{V_p}\right)^2 \tag{7.3}$$

Here is K a constant with the value of 5 (Ogden and Davis, 1990), ϵ the porosity or void fraction of the prefilter, S_p and V_p are the particle surface area and volume respectively. In the case of spherical particles with a particle diameter of d_p, $\frac{S_p}{V_p} = \frac{6}{d_p}$.

An experimental approach to determine the specific prefilter resistance during the formation of a prefilter on top of a membrane is given by the cake formation model (Belfort *et al.*, 1994; Berg, 1988):

$$\frac{t}{V} = \frac{\eta \cdot r_c \cdot \phi_b}{2\Delta P \cdot (\phi_c - \phi_b) \cdot A_m^2} V + \frac{\eta \cdot R_m}{\Delta P \cdot A_m} \tag{7.4}$$

Here is t the time, A_m the membrane area, V the volume of the permeate, ϕ_b the solids volume fraction in the bulk and ϕ_c the solids volume fraction of the prefilter, given by $(1-\epsilon)$. By plotting t/V as a function of V, specific resistance can be determined from the slope of such a plot. An example is given in Figure 7.1 for filtrating 2.5 g zeolite A24 through a 100 kDa PSf ultrafiltration membrane.

The prefilter thickness δ_c can be calculated from (Berg, 1988):

$$\delta_c = \frac{m_c}{\rho_c \cdot (1-\epsilon) \cdot A_m} \tag{7.5}$$

Here is m_c the dry mass of prefilter material and ρ_c is the density of the prefilter material.

To determine the specific resistance (both with equation 7.3 or experimentally with equation 7.4) and the prefilter thickness, the porosity of the prefilter has to be known. This porosity can be simply calculated if the prefilter consists of monodisperse spherical particles. This was done by Kawakatsu et al. (Kawakatsu *et al.*, 1995) for different kind of sphere packings. For a rhombohedral tetragonal sphere packing the volume porosity $\epsilon = 0.26$. For less simple prefilters, alternative techniques are required to determine the

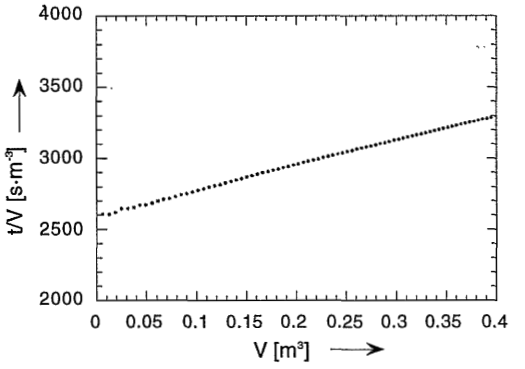

Figure 7.1: Experimental prefilter filtration curve of 2.5 *g* zeolite A24 on top of a PSf 100 kDa membrane

porosity of the prefilter. An experimental technique which will be used in this study is measuring the ratio between the dry mass and the wet mass for a fixed amount of prefilter material.

Until now, only incompressible prefilters have been discussed. For incompressible prefilters, the specific resistance is independent of the pressure. If prefilters are compressible, the prefilter resistance as a function of the pressure increases leading to a decrease in mass transfer, which is usually undesired (Kawakatsu *et al.*, 1993). Prefilter compressibility has been reviewed by Tiller (Tiller and Yeh, 1987) and is expressed in a change in the specific prefilter resistance as a function of the pressure given by:

$$r_c = r_{c,0} \cdot \Delta P^n \tag{7.6}$$

In which $r_{c,0}$ is the specific prefilter resistance at zero pressure and n is the compressibility index. If $n = 0$ no compression will occur, while for $n > 0$ the prefilter will show a certain compressibility.

In this chapter, different prefilters will be studied with respect to (specific) prefilter resistance, porosity and compressibility.

7.2.2 Prefilter fouling

In this study, the function of a prefilter on top of a membrane is to prevent fouling of the membrane itself. Fouling constituents, in this case emulsion droplets, encounter the prefilter and will have a certain interaction with the prefilter material. This interaction depends on different factors, such as the type of fouling constituents, type of prefilter material and the prefilter surface porosity.

Depending on this interaction and on the ratio between the particle diameter and the diameter of pores in the prefilter, three different prefilter fouling mechanisms can be

distinguished (Arora and Davis, 1994). These different mechanisms are surface filtration leading to rejection at the prefilter surface (mechanism 1 in Figure 7.2), adsorption throughout the entire prefilter depth (mechanism 2 in Figure 7.2) and membrane fouling due to internal pore deposition (mechanism 3 in Figure 7.2). These three mechanisms are schematically drawn in Figure 7.2.

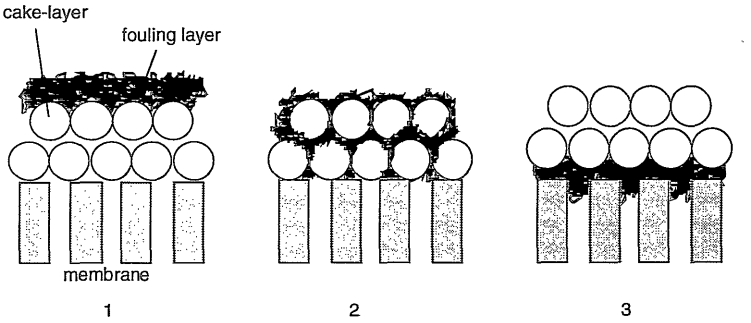

Figure 7.2: Schematic drawing of the three different prefilter fouling mechanisms. (1) rejection at prefilter surface, (2) adsorption within prefilter and (3) membrane fouling

Effective prefilters have to reject the fouling species at the prefilter surface or should have a sufficient capacity to adsorb the fouling species within the prefilter (e.g. prefilters with a sufficient thickness) in order to prevent fouling of the membrane surface. A simple model is discussed now to discriminate between the different prefilter fouling mechanisms. When a prefilter is assumed to consist of monodisperse spherical particles, the smallest pore diameter in a prefilter can be found from:

$$d_{cp} = (\frac{1}{3}\sqrt{3} - \frac{1}{2}) \cdot d_p \tag{7.7}$$

Here is d_{cp} is the diameter of the smallest pore in the prefilter and d_p is the diameter of the spherical particles in the prefilter (see Figure 7.3). If the diameter of the emulsion droplets is larger than d_{cp}, the emulsion droplets are rejected at the prefilter surface, neglecting the possibility of deformation of the emulsion droplets. In the case of emulsion droplets smaller than d_{cp}, internal prefilter fouling can occur.

In this chapter an attempt has been made to find out the prefilter fouling mechanism for different types and amounts of prefilters.

7.3 Experimental part

7.3.1 Materials

Membranes

Polysulfone ultrafiltration membranes with a molecular weight cut-off of 100 kDa were selected. Ultrafiltration membranes were selected to prevent internal fouling with the

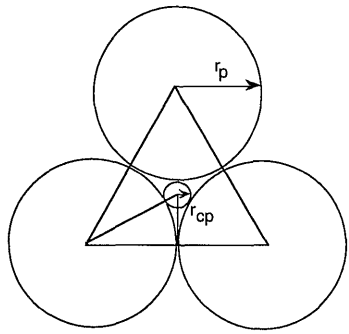

Figure 7.3: Construction of the smallest possible pore diameter d_{cp} in a prefilter of monodisperse spherical particles

prefilter material. The membranes were obtained from Dow Denmark separation (DDS) and referred to as GR40PP membranes. Membranes were conditioned by a pure water flux experiment at 2 *bar* for 2 hours unless stated otherwise.

Emulsion

Emulsions were used as a model for waste water from domestic laundry machines. An emulsion of 6.0 *g* Castor oil (Merck chemicals) and 2.4 *g* Synperonic NP9 (ICI) in 300 *ml* ultrapure water was prepared in a baffled vessel and diluted 6 times afterwards. The mean droplet diameter was $d_{32} = 0.22\ \mu m$ (see Chapter 3 of this thesis for further details).

Prefilters materials

Three different types of materials were used as prefilters on top of the ultrafiltration membranes : zeolites, calciumcarbonate and polystyrene-latex. All these materials were non soluble in water.

Zeolites were used in this study because it is present in washing powders. Two types of zeolites were studied: zeolite 4A (Merck chemicals) and zeolite A24 (obtained from Unilever). The structure is $Na_2O \cdot Al_2O_3 \cdot 2SiO_2$. Zeolite A24 is a new zeolite with a higher specific surface and a more efficient sodium-calcium ion exchange compared to zeolite 4A (Vogt, 1995).

Calciumcarbonate (Lamers & Pleuger) is also present in washing powders and therefore used in this study.

Polystyrene latex was used as dynamic membrane material because the mean particle diameter could be easily controlled with a very narrow particle diameter distribution.

A batch of polystyrene latex (PS A) was prepared according to the following procedure. Styrene (Aldrich) was purified by removing the polymerisation inhibitor by passage through a column with aluminumoxide (Merck chemicals) and seasand in the ratio of 1 : 1. An amount of 300 *ml* of this purified styrene was added to a well stirred, heated mixture at 70°C of 7.87 *g* Aerosol MA-80 (Cytech industry b.v.) and 0.61 *g* $NaHCO_3$ (Merck

chemicals) in 600 ml ultrapure water. The reactor was rinsed with nitrogen gas to avoid oxidation of the mixture. An amount of 0.49 g potassiumpersulfate ($K_2S_2O_8$ from Merck chemicals) in 50 ml water was added to this suspension to initiate an emulsion polymerisation reaction for 5.5 hours which led to the formation of a polystyrene latex (Goodwin *et al.*, 1974).

A second batch of polystyrene (PS B) was prepared according to the same procedure, using a mixture of 5.15 g Aerosol in 600 ml water and an initiator mixture of 0.32 g $K_2S_2O_8$ and 0.32 g $NaHCO_3$ in 50 ml water. The reaction was carried out for 20 hours.

7.3.2 Dead-end set-up

A dead-end filtration set-up was used to test the performance of the prefilters. This set-up was described in Chapter 6 of this thesis in detail. The membrane area for one cell was $A_m = 38.5\ cm^2$.

7.3.3 Characterisation methods

Particle size distribution

Particle diameters of the prefilter materials and the emulsion droplets were determined with a light scattering device (Microtrac X100; Leeds & Northrup). In this device a sample, while stirred, was investigated by a He-Ne laser-beam which was defracted by the particles in the sample. The intensity of the defracted outgoing beam was measured by several detectors which were present under different angles, each representing different area based diameters of the particles. The light scattering device returned a number based diameter distribution after data analysis, from which different mean particle diameters could be calculated from (Orr, 1983):

$$d_{nm} = \left(\frac{\sum \Delta n_i d_i^n}{\sum \Delta n_i d_i^m} \right)^{\frac{1}{n-m}} \tag{7.8}$$

Here is Δn_i the number of particles per diameter range, d_i is the number based diameter and n and m are constants related to the type of mean particle diameter. For example, the number, surface and volume mean particle diameter are given by respectively d_{10}, d_{20} and d_{30}. The most common expression for the mean particle diameter is, however given by the volume to surface mean diameter diameter d_{32}. This d_{32} is a quite useful diameter estimate, as it is directly related to the surface of the particles and because it is not very sensitive to the (often ill-known) number of extremely small particles present (Walstra, 1965). This d_{32} will be used from now on.

The following expression was defined for the particle diameter distribution and is given by the polydispersity number defined in this work as P_2:

$$P_2 = \frac{d_{21}}{d_{10}} \tag{7.9}$$

This polydispersity number is analogous to the polydispersity of the molecular weight distribution ratio M_w/M_n (Hiemenz, 1984). If this ratio is exactly 1, then the particles are completely monodisperse. Polydisperse particle samples have a polydispersity number value of $P_2 > 1$.

SEM

To investigate the prefilters on micro-scale, scanning electron microscopy pictures were made. Samples of the prefilters after filtration with only ultrapure water were prepared by drying them overnight (16 hours) in a vacuumoven at 30°C to remove the water. Experimentally, it was shown that this drying period was sufficient. To examine cross sections of the sample, it had to be exposed to liquid nitrogen and broken afterwards.

For SEM-measurements the samples were covered with a gold layer with a sputtering device (Balzer Union type SCD 040) at 0.1 *mbar* in an Argon-atmosphere, using an electrical current of 15 mA. The actual SEM-measurements were carried out in a scanning electron microscopy device (Jeol JSM 220 A) at a voltage of 20 kV.

Prefilter resistance, porosity and compressibility of the prefilter

The prefilter resistance was determined experimentally with the cake filtration model (equation 7.4) and calculated with the Carman-Kozeny equation 7.3. Experimental determination of r_c was done by dead-end filtration of a suspension of 2.5 g prefilter material in 400 ml water.

For both methods, the prefilter porosity was necessary, which was assumed to be $\epsilon = 0.26$ for prefilters consisting of spherical particles (for both the polystyrene latex prefilters). For the other prefilters a weight method was used to determine the porosity. This was carried out by determining the ratio between the weight of an overnight vacuum dried prefilter sample (see SEM sample preparation) and the weight of the same wet prefilter sample.

Compressibility of the prefilters was determined by measuring the pure water flux at different transmembrane pressures. If the prefilter was incompressible, a linear dependence existed between the water flux and the transmembrane pressure.

7.3.4 Fouling experiments with prefilters

In this study different types and amounts of prefilters were applied on top of a membrane to prevent or diminish fouling of the membrane. To study fouling phenomena, standard prefilter filtration experiments were carried out in a dead-end cell with emulsions as foulant. Such standard experiments consisted of several consecutive steps, described below and shown in Figure 7.4.

In the first step the membrane alone was preconditioned for 2 hours at 2 *bar* with ultrapure water as feed. After this step, a suspension of a certain amount of a given prefilter material in 400 ml ultrapure water was fed to the cell at 2 bar. Water permeated through the membrane, while the prefilter material was completely retained and

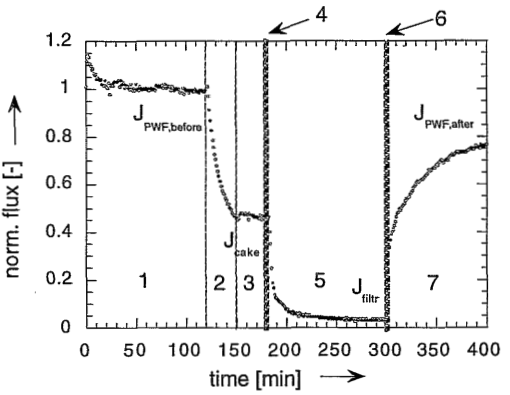

Figure 7.4: Different steps in a standard filtration experiment in which a prefilter is prepared (step 1-3), fouled (step 4-5) and recovered (step 6-7)

concentrated in front of the membrane, until a dry prefilter was established on top of the membrane. In this way a compact prefilter was formed (step 2). In the following step 3 the dead-end cell was completely filled with ultrapure water and the pure water flux was measured for 30 minutes in order to condition the prefilter. In the next step 4 a fixed amount of exactly 50 g emulsion was added to the cell, resulting in a castor oil and Synperonic NP9 concentration in the cell of 0.42 $g \cdot \ell^{-1}$ and 0.17 $g \cdot \ell^{-1}$ respectively. After this, the membrane flux was measured for a certain time at 2 *bar* in which water was used to pressurise the dead-end cell, in which the actual fouling step took place (step 5). Finally, the prefilter had been removed by a jet of ultrapure water (step 6) and a pure water flux experiment at 2 *bar* for 2 hours was carried out (step 7). A measure for the degree of fouling is the flux recovery as was defined in Chapter 6 as the ratio of the pure water flux after the experiments (step 7) and the pure water flux before applying the prefilter (step 1).

Several parameters were varied to investigate the behaviour of prefilters. During the filtration experiments described above, the type and amount ($0 - 2.5$ g) of the prefilter material and the filtration time (1–6 hours) during emulsion filtration were varied. Unless stated otherwise, prefilter filtration experiments were carried out with 2.5 g zeolite A24 material and the filtration time is 2 hours.

7.4 Results and discussion

7.4.1 Characterisation of the prefilter

Particle diameter distribution

Results of particle diameter distributions of the different prefilter samples are shown in Figure 7.5. The samples were stirred vigorously during measuring the particle diameter distribution to prevent settling of larger particles (see Table 7.1).

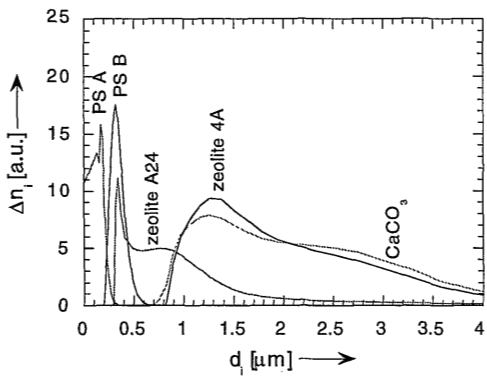

Figure 7.5: Particle diameter distributions of the different types of prefilter material

From this figure it can be seen that the two polystyrene particle samples had both the smallest mean particle diameter and the smallest particle diameter distribution. Zeolite 4A and $CaCO_3$ both had comparable mean particle diameters and particle diameter distributions, while zeolite A24 had an intermediate particle diameter and also a large particle diameter distribution.

An overview of the calculated mean particle diameters and the particle diameter distributions according to equations 7.8 and 7.9 respectively is given in Table 7.1, together with the pH of 5 $g \cdot \ell^{-1}$ prefilter material in ultrapure water and the density of the prefilter material. Also the properties of the emulsion are added in Table 7.1.

The same trends in mean particle diameters and particle diameter distributions discussed above are visible in Table 7.1 and as in Figure 7.5. These values will be used later for the calculation of the specific prefilter resistance. The pH-values of the suspensions were all about $pH = 10$, except for the PS-latices which did not display any decalcination action.

SEM

SEM pictures have been taken of the different types of prefilter materials and are shown in Figure 7.6 to give an impression of the shape of the prefilter particles.

Table 7.1: Some properties of the different prefilter suspensions

Material	pH [a] [-]	d_{32} [b] $[\mu m]$	P_2 [c] [-]	ρ $[kg \cdot m^{-3}]$
ultrapure water	6.5	-	-	1000
zeolite 4A	11.1	2.35	1.18	670
zeolite A24	10.8	1.75	1.56	670
$CaCO_3$	9.5	2.45	1.25	1100
PS-latex A	[d]	0.22	1.08	1110
PS-latex B	6.7	0.34	1.04	1110
Emulsion	4.8	0.22	1.16	≈ 1000

[a] suspension of 5 $g \cdot \ell^{-1}$ in ultrapure water
[b] calculated according to equation 7.8
[c] calculated according to equation 7.9
[d] not measured

The shape of the zeolite particles was irregular, $CaCO_3$ particles were cubic and the PS-latex particles were spherical. Furthermore it can be seen from the SEM-pictures that the zeolites and $CaCO_3$ prefilters showed a random ordering contrary to the PS-latex particles that showed rather uniform particles with a high degree of order.

Prefilter resistance, porosity and compressibility of the prefilter

Specific prefilter resistances were determined experimentally and calculated with help of the Carman-Kozeny equation (see equation 7.3). For both methods the prefilter porosity was necessary. In the case of the PS-latices, a closest sphere packing was assumed ($\epsilon = 0.26$). For other materials, the weight method was used as was described in §7.3.3. The measured prefilter porosity was 0.30 ± 0.02, 0.38 ± 0.05 and 0.40 ± 0.06 for zeolite 4A, zeolite A24 and $CaCO_3$ respectively. The porosities of these three prefilters were higher compared to the PS prefilter porosities. A closest sphere packing was not reached, probably because of the roughness and irregular shapes of these particles (see SEM-pictures).

Both experimentally determined and calculated values for the specific prefilter resistances of the different prefilters are given in Table 7.2. Experimental specific prefilter resistances were determined with the cake filtration model, for a filtration experiment with 2.5 g prefilter layer material suspended in 400 ml water at 2 bar. Calculated values of the specific prefilter resistances were determined with equation 7.3, assuming the prefilter to consist of spherical particles and using mean particle diameters and porosities of Table 7.1 and Table 7.2 respectively.

The difference between the specific resistances of PS A and PS B in Table 7.2 can be subscribed to the difference in mean particle diameters between the two prefilter materials. Furthermore a difference existed between the experimentally determined and calculated specific resistances. For the polystyrene latices the experimental specific resistance was about two times smaller than the calculated value. This is probably due to a more open

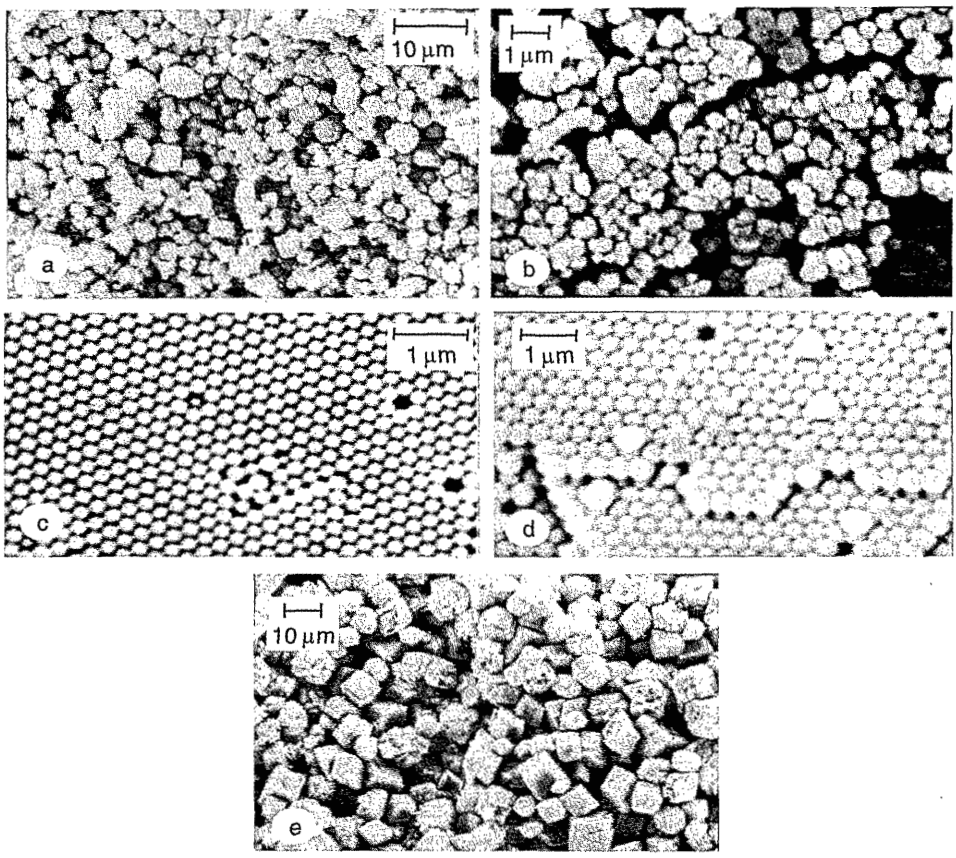

Figure 7.6: SEM pictures of the different types of prefilter materials; (a) zeolite 4A, (b) zeolite A24, (c) PS latex A, (d) PS latex B and (e) $CaCO_3$

structure in the actual prefilter compared to the assumed closest sphere packing in the Carman-Kozeny equation, because of clustering of particles or channels in the prefilter (Ogden and Davis, 1990).

Both PS-latices had a high resistance compared to the other three prefilters. This could be explained by the much higher porosity in the other prefilters compared to the PS-prefilters. No significant difference was found between the two different zeolite specific prefilter resistances. The larger mean particle diameter of the zeolite 4A particles was counterbalanced by a smaller prefilter porosity compared to the zeolite A24 prefilter. For the zeolite and $CaCO_3$ prefilters also a difference existed between the experimental and calculated specific resistance of roughly a factor 4. From these results it was concluded that the assumption of spherical particles in the Carman-Kozeny equation for these type of materials was not correct. In further discussion the experimentally obtained value will

Table 7.2: Experimentally determined and calculated specific prefilter resistances of the various prefilters

prefilter	ϵ [–]	$r_{c,exp}$ $\cdot 10^{-14}[m^{-2}]$	$r_{c,calc}$ $\cdot 10^{-14}[m^{-2}]$
PS A	0.26 [a]	610 ± 116	1159
PS B	0.26 [a]	247 ± 17	485
$CaCO_3$	0.40 ± 0.06	6.0 ± 2.4	1.69
zeolite A24	0.38 ± 0.05	15.6 ± 2.4	4.31
zeolite 4A	0.30 ± 0.02	22.2 ± 9.9	5.62

[a] theoretical value

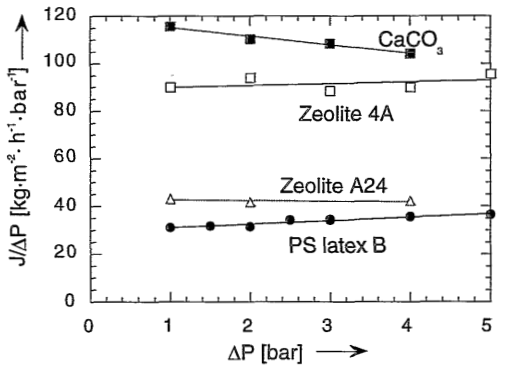

Figure 7.7: Compressibility curves showing the flux versus pressure differences across various prefilter materials

be used.

Compressibility curves are shown in fig 7.7 for the different types of prefilter material (except for PS-latex A which had not been measured). A horizontal line appeared for both zeolites and PS-latex B, indicating a non-compressible behaviour below 5 *bar*. A slightly decreasing $J/\Delta P$ versus ΔP behaviour has been found for $CaCO_3$, indicating a slightly compressible behaviour. This was probably due to the irregular structure of these particles and due to rearrangement of the prefilter packing when pressure increased. It was not expected that compressibility of the $CaCO_3$ prefilter arose from elasticity of the particles.

7.4.2 Fouling experiments with prefilters

Type of prefilter

First, experiments were carried out with different types of prefilter materials. Suspensions of 2.5 g prefilter material in 400 ml ultrapure water were used. The prefilter materials were zeolites (4A and A24), $CaCO_3$ and polystyrene latex A. In Figure 7.8 the flux recovery values are shown for the fouling experiments with emulsions with different prefilters (see §7.3.4 for more details about the procedure).

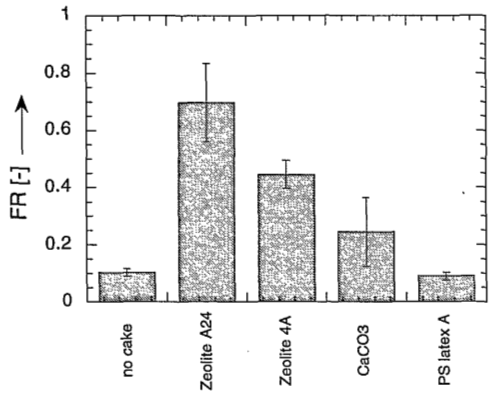

Figure 7.8: Flux recovery values for dynamic membrane fouling experiments for 2 hours with 2.5 g of different types of prefilter material in 400 ml ultrapure water

From Figure 7.8 it was clear that membrane fouling could be reduced by application of prefilters on top of the membranes. Flux recoveries could be increased from 0.10 without prefilters, to about 0.70 with zeolite A24 prefilters on top of the membranes. These flux values were however a function of the amount of prefilter material and filtration times, which were kept constant in these experiments. The amount of prefilter is 2.5 g and the filtration time is 2 hours. Variation of these parameters was investigated later. The reproducibility of these measurements was however poor, probably due to a variation in the prefilter structure.

Zeolite A24 was found to be the best prefilter material compared to the other investigated prefilter materials for a fixed amount of prefilter material and filtration time, probably because of the smaller mean particle diameter of this material. From equation 7.7 the diameter of the smallest pores in the prefilter could be calculated assuming monodisperse spherical particles. For the zeolite 4A and $CaCO_3$ prefilters $d_{cp} \approx 0.2\ \mu m$, which was about the diameter of the emulsion droplets. For non spherical particles this value of d_{cp} was different, depending on the shape of the particles. For these prefilters the flux recovery value in Figure 7.8 was low probably because emulsion droplets could easily penetrate the prefilter structure, resulting in fouling of the membrane itself (mechanism

2 and 3 in Figure 7.2). This could be hindered by prefilters consisting of smaller particles (e.g. zeolite A24). The low flux recovery value for the PS-latex A prefilter was due to the poor removability of this material from the membrane surface (step 6).

For prefilters other than PS-latices the situation was more complex as described above. In the simple model to investigate the prefilter fouling mechanism, no adsorption onto the prefilter material and deformation of the emulsion droplets were taken into account. Furthermore, because of the irregular structure of the particles (as was clear from the SEM-pictures) the pores in the prefilter might be smaller than can be calculated from equation 7.7, which is only applicable for spherical particles. Therefore the occurrence of prefilter penetration by emulsion droplets was not clear from these experiments.

Zeolite A24 will be used from now on in experiments, while other variables will be varied in an attempt to elucidate the prefilter fouling mechanism.

Amount of prefilter

The amount of zeolite A24 was varied in different experiments. The flux recovery values versus the prefilter thickness is given in Figure 7.9. The prefilter thickness was calculated from equation 7.5 using the porosity in Table 7.2.

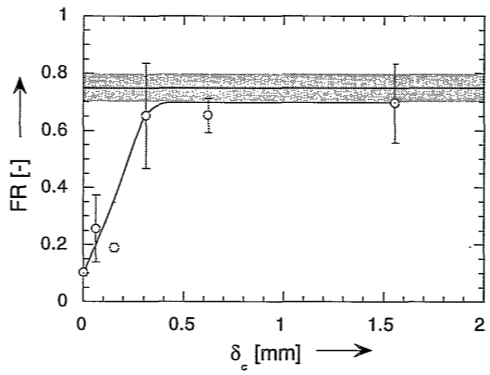

Figure 7.9: Flux recovery values for fouling experiments for 2 hours versus the thickness of zeolite A24 prefilter. The grey area represents the flux recovery value for an experiment without emulsion filtration

A critical prefilter thickness of 0.3 *mm* zeolite A24 can be found from this figure, for filtration times of 2 hours. Experiments with less than 0.3 *mm* zeolite A24 on top of the membrane had a flux recovery value of about 0.20. This could be explained by the emulsion breaking through prefilter material. For thicker prefilter layers, the flux recovery value was about 0.70. No variation had been observed in flux recovery values with a prefilter thickness above 0.3 *mm*.

The flux recovery value of a reference experiment without emulsion filtration was 0.75 ± 0.03, indicating an irreversible flux decline by the prefilter material zeolite A24 itself. This value closely resembled the flux recovery value when emulsion filtration was carried out with prefilters thicker than 0.3 *mm*.

At this point, it was concluded that the prefilter functions as a depth filter to prevent emulsion droplets to reach the membrane. The critical thickness was just enough to prevent membrane fouling (mechanism 2 and 3 in Figure 7.2).

Emulsion filtration time

To test the hypothesis of the prefilter as a depth filter to reject emulsion droplets, the flux recovery was measured as a function of the emulsion filtration time with a fixed amount of emulsion (see §7.3.4 for more details about the procedure).

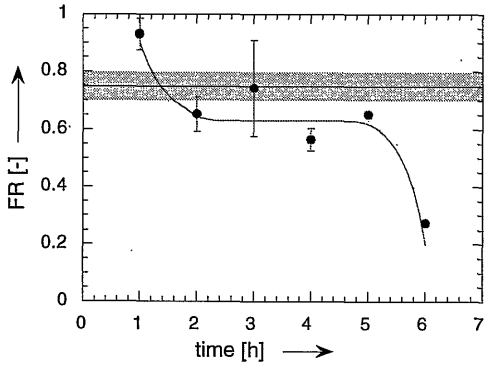

Figure 7.10: Flux recovery values for prefilter fouling experiments for different emulsion filtration times with a prefilter thickness of 0.6 *mm*. The grey area represents fouling by the prefilter itself.

From Figure 7.10 it can be seen that flux recovery values around 0.70 were maintained for emulsion filtration times up to 5 hours. For an emulsion filtration time of 6 hours, the flux recovery value decreased to 0.20. This phenomenon supported the assumption that the prefilter acted as a depth filter. For 0.6 *mm* zeolite A24 it took about 6 hours for the emulsion solution to penetrate the prefilter. The penetration velocity could be calculated and was about $30 - 40\ nm \cdot s^{-1}$ and depended strongly on the adsorption of emulsion onto the prefilter material.

The critical thickness of zeolite A24 was 0.3 *mm* as was seen in Figure 7.9 could be explained as the amount which was just enough to prevent emulsion droplets to reach the membrane surface in 2 hours of emulsion filtration.

7.5 Conclusions

Several different types of prefilters (zeolites, calcium carbonate and polystyrene latices) prevented membrane fouling with emulsions. For a fixed prefilter thickness of 1.5 mm, zeolite A24 was most effective in preventing fouling, by preventing emulsion droplets to reach the membrane surface. For the same prefilter thickness, calciumcarbonate and zeolite 4A resulted in more loose prefilters, which resulted in membrane fouling by emulsions. PSPS-latex prefilters were hard to remove from the membrane surface and resulted in membrane fouling by these prefilters.

A critical zeolite A24 thickness of at least 0.3 mm at a filtration time of 2 hours was necessary to prevent membrane fouling. Too thin prefilters resulted in membrane fouling, because of emulsion breaking through the prefilter, which acted as a depth filter.

A time effect existed for emulsion droplets to leak through a prefilter with a fixed thickness. For a prefilter of 0.6 mm, the membrane got fouled after 6 hours. This was explained by the depth filter mechanism.

In general, membrane fouling can be reduced by the use of a prefilter on top of the membrane with a sufficient thickness.

7.6 Acknowledgements

Thanks are due to dr. F.F. Stengaard from Dow Denmark Separation who kindly supplied the membrane samples. Most of the work presented in this chapter has been the topic of the M.Sc thesis of P. Haverkort, who worked nine months on this topic to complete his chemical engineering study. Parts of the experimental work have been carried out by J. Mulder in order to carry out his technical trainee period. Last but not least, several chemical engineering students participated in this research by performing several dynamic prefilter filtration experiments. Their work is highly appreciated.

7.7 List of Symbols

Acronyms

Symbol	Quantity
FR	flux recovery
pwf	pure water flux

Symbols

Symbol	Quantity	Units
A_m	membrane area	$[m^2]$
FR	flux recovery ($= \frac{J_{\text{pwf,before}}}{J_{\text{pwf,after}}}$)	$[-]$
J	membrane (permeate) flux	$[kg \cdot m^{-2} \cdot h^{-1}]$

K	constant in equation 7.3	$[-]$
M_n	number average molecular weight	$[g \cdot mol^{-1}]$
M_w	weight average molecular weight	$[g \cdot mol^{-1}]$
P_2	polydispersity number	$[-]$
R_c	prefilter resistance	$[m^{-1}]$
R_f	fouling resistance due to pore blocking	$[m^{-1}]$
R_m	membrane resistance	$[m^{-1}]$
R_{tot}	total resistance against mass transfer	$[m^{-1}]$
S_p	particle surface area	$[m^2]$
V	permeate volume	$[m^3]$
V_p	particle volume	$[m^3]$
ΔP	transmembrane pressure	$[bar]$
Δn_i	number of droplets within a class	$[a.u.]$
δ_c	prefilter thickness	$[m]$
ϵ	volume porosity or void fraction of the prefilter	$[-]$
η	viscosity of the feed solution	$[Pa \cdot s]$
ϕ_b	solids volume fraction in the bulk	$[-]$
ϕ_c	solids volume fraction in the prefilter	$[-]$
ρ_c	density of the prefilter	$[kg \cdot m^{-3}]$
d_{cp}	diameter of the smallest pore in the prefilter	$[m]$
d_i	number based droplet diameter of i	$[m]$
d_{nm}	mean droplet diameter according to formula 7.8	$[m]$
d_p	particle diameter	$[m]$
m_c	mass of (dry) prefilter	$[kg]$
n	compressibility index	$[-]$
$r_{c,0}$	specific prefilter resistance at zero pressure	$[m^{-2}]$
r_c	specific prefilter resistance	$[m^{-2}]$
t	time	$[s]$

Chapter 8

Critical membrane pressures during ultra- and microfiltration in cross-flow filtration

8.1 Introduction

Until now, only dead-end filtration has been described. This chapter will focus on cross-flow filtration, which is a continuous process, in which steady state fluxes are achieved, contrary to dead-end filtration. Existing work is usually focused at minimising the problem of concentration polarisation by optimising module design, process conditions and membrane type and material (Belfort *et al.*, 1994). When the membrane wall is susceptible for adsorption of particles of the feed stream, the increase of concentration near the membrane wall lead to membrane fouling, which is an irreversible process.

In this chapter fouling and cake layer formation is minimised or even avoided by operating the cross-flow filtration process at low transmembrane pressures. The highest value of the transmembrane pressure at which cake formation due to precipitation of material can still be avoided is defined as the critical transmembrane pressure. The current research is focused on the dependence of this critical transmembrane pressure on membrane related factors such as membrane material and mean pore sizes.

8.2 Theory

8.2.1 Definitions of terms

The system that will be discussed consists of a mixture of well defined particles in a liquid approaching a porous clean membrane. During pressure driven cross-flow filtration there are two phenomena effecting the transport of these particles:

- convection tends to drag particles towards the membrane surface and pores, along with solvent. This is proportional to the local transmembrane solvent flux

- a back transport tends to move particles away from the membrane surface, for example due to Fickian diffusion (Field, 1993; Sridhar, 1991), charge effects (Lojkine *et al.*, 1992), lateral migration (Romero and Davis, 1988) or shear enhanced transport (Davis and Leighton, 1987)

There are two ways to reduce deposition of particles; enhancing back transport (e.g. by increasing the cross-flow velocity or temperature) or reducing the convective flux, by operating at low transmembrane pressures (or, more correctly, at low transmembrane solvent fluxes).

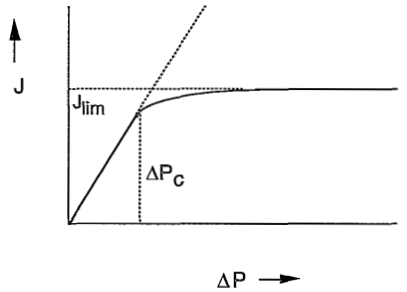

Figure 8.1: The limiting flux and the critical transmembrane pressure

If a transmembrane flux in filtration of a liquid mixture is considered as a function of the hydraulic pressure, two regimes can be distinguished, i.e. a non fouling regime where the permeate flux is linearly dependent on the transmembrane pressure and a fouling regime in which the flux is independent of the hydraulic pressure. The pressure at which deviation of Darcy's law occurs will be defined as the critical transmembrane pressure (ΔP_c). This is schematically depicted in Figure 8.1. A non fouling region is defined as the region at which no fouling occurs ($\Delta P < \Delta P_c$). At pressures larger than ΔP_c, a limiting flux J_{lim} is reached eventually if the resistance of the fouling layer is larger than the membrane resistance, which is usually the case in practical situations (Field, 1993; Sridhar, 1991). With these two parameters (J_{lim} and ΔP_c) the flux pressure behaviour can be described. The non fouling region, however, can be described by only ΔP_c. This critical transmembrane pressure depends on feed solution factors (chemical nature, concentration and size of particles, pH, ionic strength, etc.), membrane related factors (mean pore size, porosity, membrane roughness, type of material, etc.) and process related factors (turbulence, temperature, cross-flow velocity, etc.).

8.2.2 Description of non fouling

Many models are known which describe the flux dependence on the transmembrane pressure (see also Chapter 2 for more details) (Lojkine *et al.*, 1992). A rather new concentration polarisation based model which is successfully applied in literature is a model developed by Romero and Davis (Romero and Davis, 1988). It is based upon a local film

model which was defined by Davis (Davis and Leighton, 1987) and extended along the axial coordinate of a cross-flow module under steady-state operation.

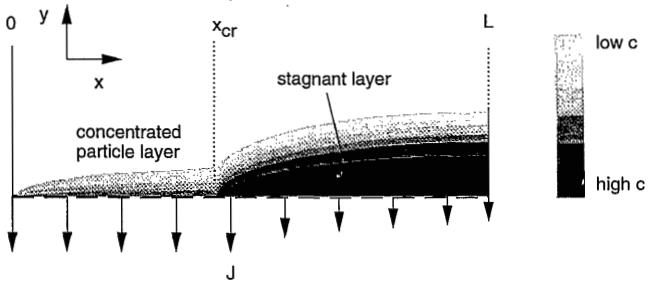

Figure 8.2: Schematic drawing of a concentrated particle layer and a stagnant layer in a cross-flow channel (Romero & Davis, 1988).

In Figure 8.2 a suspension containing particles is transported through a channel having microporous membrane walls. Purified fluid passes through the membranes as permeate, whereas the retained particles form a thin cake or fouling layer adjacent to the membrane surface. This fouling layer, which is analogous to the gel layer for ultrafiltration of macromolecules, reduces the permeate flux. Fortunately, the action of the bulk flow of suspension tangent to the membrane surface limits the accumulation of the immobile cake layer. Romero & Davis (Romero and Davis, 1988) found that there is a region near the entrance of the filter where the shear flow is able to sweep the particles downstream, so that the membrane surface remains clean. Beyond a critical distance, x_{cr}, from the filter entrance, however, the shear flow is not able to sweep downstream all of the deposited particles, and so the stagnant cake or fouling layer forms on the membrane surface $x > x_{cr}$. They also showed that axial convection of particles may not be neglected, which balanced at steady state the total rate of deposition of particles into the boundary layer due to the permeate flow everywhere upstream of the given location. It is this particle deposition which causes the boundary layer to thicken, and the permeate flux to decrease with distance from the filter entrance.

The critical distance is given by (Romero and Davis, 1988):

$$x_{cr} = \frac{\tau_0^3 r_p^4 \hat{Q}_{cr}}{\mu_0^3 J_{\text{pwf}}^3 \phi_0} \tag{8.1}$$

In which τ_0 is the shear stress at the wall without particles, r_p the particle radius, μ_0 the viscosity of the medium (water), J_{pwf} the pure water flux and ϕ_0 the bulk particle volume fraction. $\hat{Q}_{cr}$ is a dimensionless excess particle flux which is a material constant of the feed medium (Romero and Davis, 1988). According to this equation the critical distance, which expresses the length of the clean part in a membrane module, increases with the shear stress and the particle radius. At high shear stress and for larger particles, particles are swept away from the surface and backflux mechanisms are more effective.

At higher bulk concentrations or pure water fluxes, this critical distance decreases, as a result of a higher degree of accumulation near the membrane surface. The pure water flux can be described by:

$$J_{\text{pwf}} = \frac{\Delta P}{\mu_0 R_m} \tag{8.2}$$

In which ΔP is the transmembrane pressure and R_m the membrane resistance.

If in Figure 8.2 the critical distance is exactly equal to the entire feed channel length, no stagnant layer is formed in the entire channel and only a concentrated particle layer is present. It is assumed in this work that this situation does not lead to membrane fouling and refers to the case that $\Delta P = \Delta P_c$. If this is used, and equation 8.1 and 8.2 are combined the following expression can be found for ΔP_c:

$$\Delta P_c = R_m \cdot \left(\frac{\tau_0^3 r_p^4 \hat{Q}_{cr}}{L \phi_0} \right)^{\frac{1}{3}} \tag{8.3}$$

According to this equation the critical transmembrane pressure depends linearly on the membrane resistance if feed solution and cross-flow velocity are kept constant.

8.3 Experimental part

8.3.1 Set-up

In the set-up described in Figure 8.3 two rotary gear pumps (Verder 2036, GmbH, Germany) were used, which respectively regulated the cross flow velocity (1) and the transmembrane pressure (2) independent of each other. The cross-flow velocity was kept constant at $v = 0.1\ m \cdot s^{-1}$ ($Re = 300$). A membrane module (3) was placed in this loop and had a rectangular feed channel with a length, width and height of $L = 140\ mm$, $W = 20\ mm$ and $H = 1.6\ mm$ respectively. The membrane area was $A_m = 20\ cm^2$. Permeate was collected in a beaker on a mass balance (4; Mettler, PM4000), which was connected to a computer (5) for data acquisition. An outlet was present in the closed-loop which was necessary to remove air-bubbles in the loop during filling (6). When the permeate vessel was full, it was added again to the feed vessel. In this way the concentration in the closed loop was kept constant.

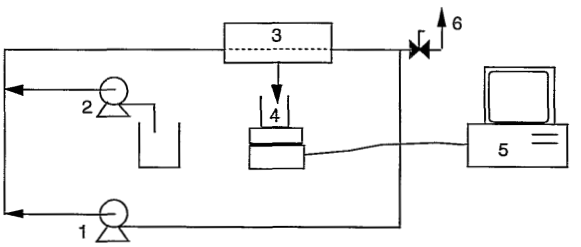

Figure 8.3: Experimental cross-flow set-up

8.3.2 Materials

Different commercial PSf and PVDF membranes were obtained from Dow Denmark Separation (DDS). Ultra- and microfiltration membranes were used for filtration experiments and are shown in Table 8.1. Pore sizes of microfiltration membranes were determined by a Coulter Porometer II (ASTM F316-80). Pore sizes of ultrafiltration membranes were estimated using the Hagen-Poiseuille equation (Jonsson, 1975) for the pure water flux results. A porosity value of 0.3 % and a top-layer thickness of $0.2\mu m$ were chosen similar to Cuperus and Smolders (Cuperus and Smolders, 1990) for a DDS GR61PP PSf membrane (see Table 8.1).

Table 8.1: Measured pore sizes with Coulter porometer (MF membranes) and calculated pore sizes with Hagen-Poiseuille equation (UF membranes)

Membrane	Material	d_p
GRM0.45PP	PSf	0.33 μm [a]
GRM0.2PP	PSf	0.20 μm [a]
GRM0.1PP	PSf	0.18 μm [a]
GR40PP	PSf	3.3 nm
GR51PP	PSf	2.5 nm
FSM0.1PP	PVDF	0.17 μm [a]
FS40PP	PVDF	4.2 nm
FS50PP	PVDF	3.0 nm
FS61PP	PVDF	2.2 nm
FS81PP	PVDF	2.0 nm

[a] determined with Coulter porometer

The same emulsion was used as has been described in Chapter 3 with $d_{32} = 0.22\ \mu m$.

8.3.3 Method

In order to characterise the membranes before and after fouling, pure water fluxes were determined at a transmembrane pressure of 1 *bar* for two hours, before and after the emulsion filtration experiments. Emulsion filtration experiments were performed at different pressures. At a pressure of 0.1 *bar* the average permeate flux was measured for 15 minutes. This procedure was repeated for each pressure increase of approx. 0.1 *bar* until 1 *bar* was reached. The flux recovery value was calculated as the ratio of the pure water flux after and before the emulsion filtration experiment.

8.4 Results and discussion

8.4.1 Critical transmembrane pressures of commercial membranes

A typical result of an emulsion filtration experiment is depicted in Figure 8.4 for a PSf membrane with a mean pore diameter of 0.1 μm.

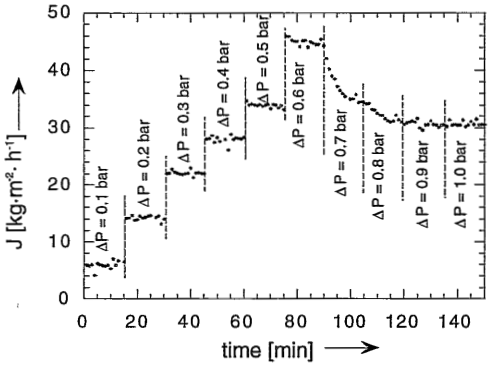

Figure 8.4: Experimental fluxes versus time at various pressures for a 0.1 μm PSf membrane

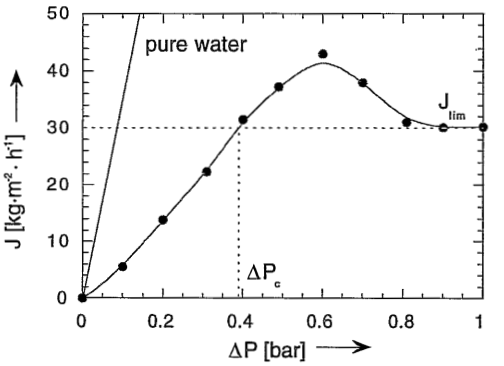

Figure 8.5: Experimental emulsion filtration and pure water flux versus pressure curve for a 0.1 μm PSf membrane (average values obtained from Figure 8.4

Figure 8.5 is obtained from Figure 8.4 by taking average values for the flux at constant transmembrane pressures. From Figure 8.5 two characteristic parameters could be

obtained, i.e. the critical transmembrane pressure ΔP_c and the limiting flux J_{lim}. In this figure, ΔP_c was constructed from the intercept between the horizontal line at the J_{lim}-plateau and the linear flux pressure curve in the non fouling regime. Below the critical pressure no flux decline was observed in time for 15 minutes, as can be seen in Figure 8.4.

As soon as the transmembrane pressure exceeds ΔP_c, the flux was instationary. Coming from a lower transmembrane pressure, the flux will start at a value higher than J_{lim} and slowly decreased towards J_{lim}. This behaviour may become evident in an apparent maximum in flux at transmembrane pressures slightly higher than ΔP_c, when the fluxes were only measured during a fixed time interval. In Figure 8.5 the membrane flux exceeded the limiting flux between $\Delta P = 0.4 - 0.7$ *bar* as a result from taking an average value of the decreasing flux in a time interval of 15 minutes. At higher transmembrane pressures (> 0.7 *bar*) the limiting flux plateau was reached. If longer measuring times were applied the 'bump' in Figure 8.5 is expected to disappear, because of the decline in the average flux in time.

Table 8.2: Results of emulsion filtration experiments of different commercial DDS membranes (PSf and PVDF)(mean average values of three experiments)

Membrane	$J_{\text{pwf,before}}$ $[kg \cdot m^{-2}h^{-1}]$	R_m $\cdot 10^{-12}[m^{-1}]$	J_{lim} $[kg \cdot m^{-2}h^{-1}]$	ΔP_c $[bar]$	$\frac{J_{\text{lim}}}{\Delta P_c \cdot J_{\text{pwf,before}}}$ $[-]$	FR $[-]$
GRM0.45PP	2000	0.2	16	0.09	0.09	0.11
GRM0.2PP	475	0.8	25	0.35	0.15	0.21
GRM0.1PP	355	1.0	30	0.36	0.22	0.42
GR40PP	204	1.5	21	0.47	0.25	0.20
GR51PP	160	2.3	29	0.55	0.36	0.37
FSM0.1PP	1200	0.3	11	< 0.1	< 0.09	0.20
FS40PP	600	0.6	10	< 0.1	< 0.17	0.10
FS50PP	300	1.2	10	0.15	0.22	0.13
FS61PP	165	2.2	$20 - 15$	0.30	$0.41 - 0.38$	0.33
FS81PP	130	2.8	[a]	0.40	[a]	0.25

[a] no plateau found

The results of all emulsion filtration experiments are shown in Table 8.2 and are the mean values of four experiments for each membrane. For the FS81PP membrane no plateau value for J_{lim} could be observed. In this case the membrane resistance was apparently no longer negligible compared to the resistance of the fouling layer (Field, 1993).

From Figure 8.6 it can be seen that the critical transmembrane pressure linearly increased with the membrane resistance R_m for both PSf and PVDF membranes, which was also found in equation 8.3. From these findings it could be found that ΔP_c was inversely proportional to the pure water flux before filtration (see Table 8.2) and inversely proportional to the membrane pore diameter (see Table 8.1).

Furthermore, from Figure 8.6 it can be seen that a difference existed between the

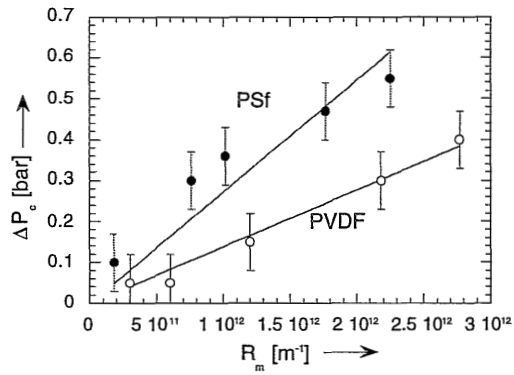

Figure 8.6: Critical transmembrane pressure versus the membrane resistance. The solid lines are linear fits according to equation 8.3

ΔP_c versus R_m relation for PSf and PVDF membranes. This was remarkable because according to equation 8.3, ΔP_c only varied with R_m while keeping feed properties and cross-flow velocity constant. The situation was more complex than only on the basis of the non fouling model as was discussed in §8.2. If the cross-flow model was operating under conditions that no stagnant cake was formed (i.e. $\Delta P < \Delta P_c$), other fouling mechanisms such as pore plugging or adsorption can occur. This can also be seen in Figure 8.5, in which the pure water flux curve did not coincide with the emulsion filtration flux curve before the limiting flux was reached. This deviation can be calculated from $\frac{J_{\text{lim}}}{\Delta P_c \cdot J_{\text{pwf,before}}}$ and is shown in Table 8.2. From this table it can be seen that the deviation increased with the pure water flux as a result of the occurrence of internal fouling (e.g. pore narrowing and adsorption).

In Table 8.2 flux recoveries (i.e. the ratio of the pure water flux before and after filtration, see §8.3.3) are given for different membranes. The flux recovery is a measure for the amount of irreversible fouling and it depends on the history of fouling, which differed for each membrane and FR-values should be used with care. From Table 8.2 it can be seen that FR-values were lower for PVDF membranes than for PSf membranes. This indicated that fouling was more severe for PVDF membranes than for PSf membranes as was seen above. This was usually ascribed to the relative hydrophobicity of PVDF compared to PSf (Hanemaaijer *et al.*, 1988). Also it can be seen that the FR-value increased with a decrease in pure water flux before filtration (Hanemaaijer *et al.*, 1989; Howell and Nyström, 1993).

An additional experiment was carried out to verify flux recovery values after emulsion filtration at transmembrane pressures under and above ΔP_c. In Figure 8.7 two emulsion filtration experiments have been plotted for one hour at $\Delta P = 0.3$ *bar* and $\Delta P = 1.0$ *bar* for a GR40PP PSf membrane ($\Delta P_c = 0.42$ *bar*). Before, between and after the experiments a pure water flux was measured for one hour at 1 *bar*. From this figure

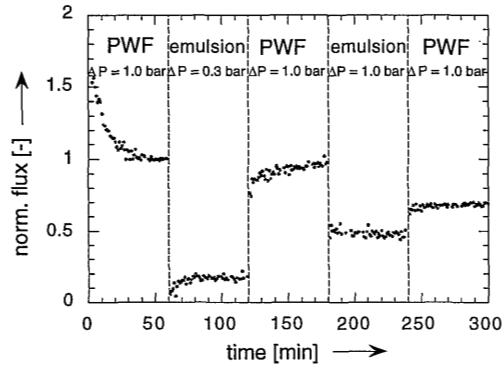

Figure 8.7: Flux decline before and after ΔP_c for a PSf GR40PP

it can be seen the pure water flux fully recovered after a filtration experiment at a transmembrane pressure smaller than ΔP_c. No fouling was observed for $\Delta P < \Delta P_c$ and the adsorption and pore plugging effects described above could not be observed from this experiment with a PSf membrane. If the transmembrane pressure exceeded ΔP_c, a decrease in the pure water flux was observed (see Figure 8.7) as a result of irreversible fouling due to cake formation.

8.5 Conclusions

Operation below a critical transmembrane pressure during cross-flow filtration prevents gel or cake layer formation. In this case no flux decline during cross-flow filtration was observed for PSf and PVDF membranes. These critical pressures were linearly dependent on the membrane resistance as was found both theoretically and experimentally. Critical transmembrane pressures were higher for PSf membranes compared to PVDF membranes due to membrane solute interaction effects.

Fouling due to pore plugging and adsorption was not prevented below critical transmembrane pressures. These phenomena were more pronounced for microfiltration membranes than for ultrafiltration membranes. Also a higher irreversible fouling was found for PVDF than for PSf membranes.

In general, operation below the critical transmembrane pressure of a membrane will lead to a longer membrane lifetime, owing to a reduction in membrane fouling.

8.6 Acknowledgements

The author is grateful for the membrane samples kindly supplied by dr. F.F. Stengaard from Dow Denmark Separation. Many fruitful discussions with dr. R.M. Boom (URL)

are highly appreciated, without which this work was not possible. Last but not least, several chemical engineering students participated in this research by performing several cross-flow experiments. A.J.L. Kassies participated to carry out his technical trainee period.

8.7 List of Symbols

Acronyms

Symbol	Quantity
PSf	polysulfone
$PVDF$	polyvinylidene fluoride
pwf	pure water flux

Symbols

Symbol	Quantity	Units
A_m	membrane area	$[m^2]$
FR	flux recovery ($= \frac{J_{\text{pwf,before}}}{J_{\text{pwf,after}}}$)	$[-]$
H	height of feed channel	$[m]$
J	membrane (permeate) flux	$[kg \cdot m^{-2} \cdot h^{-1}]$
J_{lim}	limiting flux	$[kg \cdot m^{-2} \cdot h^{-1}]$
L	length of feed channel	$[m]$
R_m	membrane resistance	$[m^{-1}]$
Re	Reynolds number ($= \frac{\rho \cdot v \cdot d_h}{\mu_0}$)	$[-]$
W	width of feed channel	$[m]$
ΔP	transmembrane pressure	$[bar]$
ΔP_c	critical transmembrane pressure	$[bar]$
$\hat{Q}_{cr}$	dimensionless excess particle flux (Bowen, 1994; Henry *et al.*, 1977)	$[-]$
μ_0	viscosity of the feed solution	$[Pa \cdot s]$
ϕ_0	bulk particle volume fraction	$[-]$
τ_0	shear stress at the wall without particles	$[Pa]$
d_h	hydraulic diameter ($= \frac{2W \cdot H}{W+H}$)	$[m]$
d_p	pore diameter	$[m]$
r_p	particle radius	$[m]$
t	time	$[s]$
v	cross-flow velocity	$[m \cdot s^{-1}]$
x_{cr}	length of the concentrated particle layer (non fouling) region	$[m]$

Chapter 9

Use of electric forces in cross-flow ultrafiltration

9.1 Introduction

During cross-flow filtration steady state fluxes can be obtained, because of an existing balance between friction forces towards the membrane surface and diffusional forces from the surface. When charged particles are present in the feed stream, an electric field perpendicular to the membrane surface can influence this balance. This process is called (cross-flow) electro-filtration (CFEF). In this process, particles are swept away from the surface because of electrophoretic migration due to the electric force (Bowen, 1994; Henry *et al.*, 1977) and because of shear forces (see Chapter 8). Electro-osmosis of solvent can occur as well, when the pores of the membrane and/or the cake layer are charged (Rios *et al.*, 1988; Singh, 1989). In this chapter the use of an electric field is studied in order to minimise membrane fouling and to increase the membrane performance.

9.2 Theory

Deposition of particles on membrane surfaces can be minimised by using electric forces when the particles are charged. This results in thinner cake layers or more loose structures of these cake layers (Tarleton, 1988; Wakeman and Sabri, 1995). It is even possible that the formation of cake layers is completely prevented (Yukawa *et al.*, 1983). Therefore it will be of interest to have more insight in the application of electric forces to prevent or reduce membrane fouling and increase steady state fluxes during cross-flow membrane filtration.

The effects of CFEF depend on many factors, such as the magnitude of the electric field, concentration of the feed solution, electrode arrangements and material, zeta potential of the membrane surface and particles, size and charge of the feed particles. It is found that CFEF find application in filtration of suspensions with a low conductivity in the continuous phase (Henry *et al.*, 1977). In this work, emulsions are used with a conductivity of 1 $\mu S \cdot m^{-1}$.

In an attempt to describe the electro-filtration process, many models are known in literature that can roughly be divided into resistance in series approaches (Brors and Kroner, 1993; Henry *et al.*, 1977; Nadh Jagannadh and Muralidhara, 1996) and film model approaches (Guizard *et al.*, 1989; Henry *et al.*, 1977; Kroner, 1993; Rios *et al.*, 1988; Yukawa *et al.*, 1983). Because of the more fundamental character, the film model approach is preferred. A mass balance of the particles in the concentration polarisation layer in front of the membrane is (Rios *et al.*, 1988; Yukawa *et al.*, 1983):

$$J \cdot c_0 = J \cdot c + D \cdot \frac{dc}{dx} - k_e \cdot \Delta E \cdot (c - c_0) \tag{9.1}$$

Here is J the steady state flux, c and c_0 are the solute concentrations at a point in the boundary layer and in the bulk, D the solute diffusivity, ΔE the electric field strength and k_e the electrophoretic permeability. This k_e can be determined by a J versus ΔE plot (Blokhra and Prakash, 1992; Rios *et al.*, 1988; Singh and Shahi, 1991; Yukawa *et al.*, 1983). By integration of the mass balance over the following boundary conditions :

$$\begin{aligned} c &= c_b \quad \text{at} \quad x = \delta_m \\ c &= c_m \quad \text{at} \quad x = 0 \end{aligned}$$

the following extended film model is obtained:

$$J = k_m \cdot \ln\left(\frac{c_g - c_0}{c_m - c_0}\right) + k_e \cdot \Delta E \tag{9.2}$$

Here is $k_m = \frac{D}{\delta_m}$ the mass transfer coefficient, δ_m the thickness of the boundary layer and c_g the gel layer concentration. For electric fields directed to sweep charged particles from the membrane surface, it is clear from this equation that the flux increases when increasing ΔE, keeping all other variables constant (e.g. cross-flow velocity, temperature, transmembrane pressure etc.).

Electro-filtration has been investigated by variation of cross-flow velocity (Henry *et al.*, 1977; Yukawa *et al.*, 1983), concentration of the feed solution (Rios *et al.*, 1988; Robinson *et al.*, 1993) and transmembrane pressure (Brors and Kroner, 1993; Robinson *et al.*, 1993). The influence of these parameters on the CFEF process is the same as in a normal CF process. The influence of a pulsed electric force has been studied and compared with a fixed electric force over the membrane. The effect of pulsing was not clear. Some authors found an improvement of the overall filtration process (Bowen, 1994; Brors and Kroner, 1993), others found no difference (Robinson *et al.*, 1993) or even a worse performance (Wakeman and Sabri, 1995). The variation of membrane structure, which is the topic of this work, could not be found in literature. In this chapter both charged and uncharged membrane are investigated. The surface charge can occur at the membrane interface and can influence the fouling behaviour. Also on colloidal particles, such as emulsion droplets or other foulants a charge is likely to occur. Measurement of these charges can give more insight in membrane fouling phenomena. The charge of emulsions and membrane surfaces were determined by electrophoresis and streaming potential measurements respectively.

9.3 Experimental part

9.3.1 Materials

The emulsion described in Chapter 3 was used. The mean droplet diameter was $d_{32} = 0.22\ \mu m$ and the conductivity was $\lambda_0 = 1\ \mu S \cdot m^{-1}$.

Two commercial ultrafiltration membranes were used both with a molecular weight cut-off of 100 kDa. The difference between these two membranes was the presence of a modification (sulfonation) (IRIS 100, Rhône Poulenc) and the absence of such a modification (GR40PP, DDS).

9.3.2 Set-up

The same cross-flow set-up was used in this study as described in Chapter 8, except for the membrane module that was used (see Figure 9.1). The membrane module consists of a rectangular channel with a length of $L = 154\ mm$, width of $W = 25\ mm$ and height of $H = 1.6\ mm$. The membrane area was 20 cm^2. On both sides of the membrane electrodes were present. The anode ($\oplus$), at the skin side of the membrane, was made of platinum plated stainless steel and the cathode ($\ominus$) was made of nickel. The distance between the two electrodes was 2 mm. A power supply device (Delta elektronika, power supply ES 030-5, 180 W) was used to apply an electric field across the membrane of $0 - 15\ kV \cdot m^{-1}$.

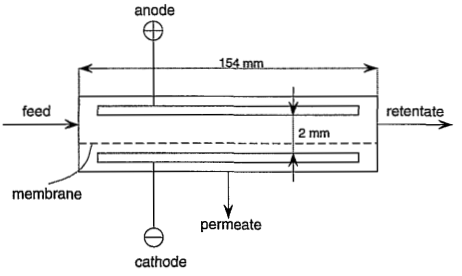

Figure 9.1: A schematic drawing of the membrane module used for the electro-filtration experiments

9.3.3 Characterisation methods

Determination of the particle charge

An indication of the particle charge of the emulsion droplets was obtained by a Malvern Zetasizer IIc device, which measured the electrophoretic velocity of emulsion droplets. This electrophoretic migration was related to the zeta potential ζ by the so-called Smoluchowski equation (Overbeek, 1952):

$$u_e = \frac{\zeta \epsilon}{\eta_c} \cdot \Delta E \tag{9.3}$$

Here is u_e the electrophoretic migration, ϵ the dielectric constant and ΔE the electric field strength. It is assumed in this equation that the double layer thickness is small compared to the radius of the curvature of the particle.

Because zeta potentials could only be determined in an electrolyte solution, measurements were carried out with different KCl (Merck pro analysis) concentrations of $10^{-4} - 10^{-2}$ M. Temperature was constant at $20 - 23°C$ and pH of the electrolyte solution was 6.0 ± 0.5.

Streaming potential measurements

In order to investigate the outer surface charges of membranes, streaming potential measurements were carried out by the same method and set-up as was described by Peeters (Peeters, 1997).

Different electrolyte concentrations of 10^{-5} to 10^{-1} M KCl (Merck pro analysis) were used. The bulk conductivity was measured with a conductivity meter (Microprocessor conductivity meter LF537, WTW) and for each concentration a new membrane was used. The temperature was constant at $20 - 23°C$ and the pH of the electrolyte solution was 6.0 ± 0.5.

9.3.4 Electro-filtration experiments

First reference experiments were carried out without an electric field. These experiments were carried out by cross-flow filtration of the emulsion for two hours at 1 bar with a cross-flow velocity of 0.1 $m \cdot s^{-1}$. Before and after this experiment, pure water flux experiments were carried out for two hours at 1 bar. Replacing the feed by emulsion or water, respectively before and after the emulsion filtration experiment, was carried out after 5 minutes rinsing the channel at a cross-flow velocity of again 0.1 $m \cdot s^{-1}$ and a transmembrane pressure smaller than 0.2 *bar*.

The actual electro-filtration experiments could be divided into three parts. First the influence of an electric field of 5 $kV \cdot m^{-1}$ on the pure water flux was studied for both membranes. Secondly, the influence of an electric field of 15 $kV \cdot m^{-1}$ on the emulsion filtration flux for 8 hours was studied. Finally the flux was measured as a function of a decreasing electric field from 15 $kV \cdot m^{-1}$ down to 0 $kV \cdot m^{-1}$, with steps of 2.5 $kV \cdot m^{-1}$. Also the reversibility was checked by measuring the flux at an increasing electric field from 0 $kV \cdot m^{-1}$ to 15 $kV \cdot m^{-1}$ with steps of 2.5 $kV \cdot m^{-1}$.

9.4 Results and discussion

9.4.1 Characterisation methods

Determination of the particle charge

Zeta potential measurements were carried out for the emulsion in the presence of different amounts of KCl. The results are plotted in Figure 9.2, in which a slightly negative zeta

potential can be observed with a large scattering for every point in Figure 9.2 due to experimental errors. The negative charge of the emulsion droplets was expected (Elimelech *et al.*, 1994; Henry *et al.*, 1977; Nadh Jagannadh and Muralidhara, 1996; Tarleton, 1988) and can be explained by the presence of fatty acids at the emulsion droplet interface. Because of this small charge value, emulsion droplets were not expected to migrate strongly in an electric field.

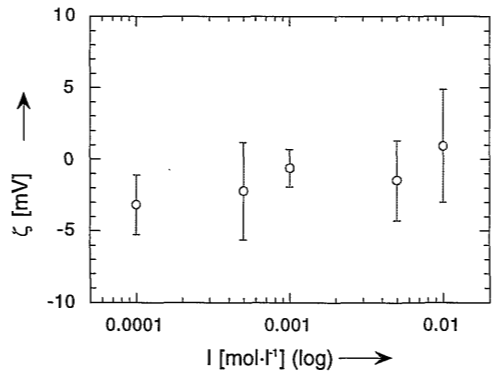

Figure 9.2: The measured zeta potential of emulsions determined with the Malvern Zetasizer IIc as a function of the KCl concentration

Streaming potential measurements

In Figure 9.3 the results are shown of the streaming potential measurements of the membrane wall, in which the zeta potential is plotted as a function of the KCl concentration. For the IRIS membranes it was found that the zeta potential increased as a function of the KCl concentration. According to the manufacturer, IRIS membranes were made of sulfonated PSf, which is charged in aqueous media, because of dissociation of sulfone groups (Elimelech *et al.*, 1994). Adding electrolytes resulted in a decrease in the zeta potential which is observed in Figure 9.3. This was due to a suppression of the double layer, which resulted in a shift of the shear plane (Lyklema, 1991). The zeta potential values found for the IRIS membrane were in reasonable accordance to literature data. At pH = 6, Causseraud et al. found a $\zeta = -20\ mV$ ($I = 0.001\ M$ KCl) for the type of IRIS membranes (Causserand *et al.*, 1994), compared to $\zeta = -44\ mV$ ($I = 0.001\ M$ KCl) in this work.

The DDS membrane was invariant to the KCl concentration. These membranes were prepared from untreated polysulfone on which no dissociatable sulfone groups were present at the surface. The charge of these membranes might be due to preferential adsorption, resulting in a negative zeta potential. At pH = 6.0, Kim et al. found

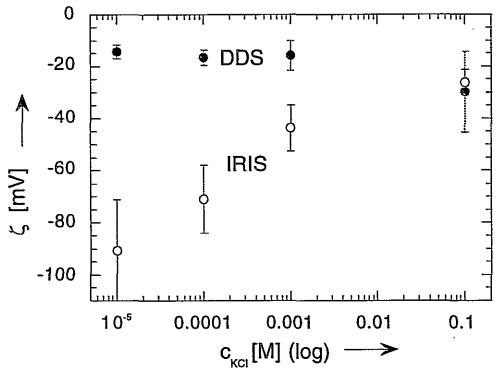

Figure 9.3: Zeta potentials by streaming potential measurements of DDS and IRIS PSf 100 kDa ultrafiltration membranes as a function of the KCl concentration

$\zeta = -18\ mV$ ($I = 0.001\ M$ KCl) for PSf 100 kDa MilliPore membranes (Kim *et al.*, 1996), which was in accordance with our work ($\zeta = -16\ mV$ at $I = 0.001\ M$ KCl).

9.4.2 Electro-filtration experiments

Reference measurement

In Table 9.1, the results are shown of the reference experiments without an electric field (see §9.3.4 for more details about the procedure). A large scattering in the pure water flux was observed for both membranes as was seen before in Chapter 6. The pure water flux was higher for the IRIS membranes, which resulted in a lower value of the emulsion filtration flux, due to higher concentration polarisation and fouling compared to DDS membranes. Fouling was more pronounced for the IRIS membranes which can be seen from the flux recovery values in Table 9.1. This was not expected on the basis of the higher zeta potential of IRIS compared to DDS which would result in a higher repulsion of negatively charged emulsion droplets by the IRIS membranes leading to less fouling. The opposite effect was observed and can only be explained by a difference in surface structure between the two membranes. Possibly IRIS membranes contained more larger pores than DDS, which can be blocked easier, leading to a larger fouling of IRIS membranes.

In the case of IRIS membranes a lower pure water flux value was found after emulsion filtration compared to the emulsion flux value. This can be explained by coalescence of an irreversible fouling cake (which was not removed by rinsing).

The influence of an electric field on the pure water flux

In Figure 9.4 the effect is shown of applying an electric field of $\Delta E = 5\ kV \cdot m^{-1}$ on the pure water flux. The direction of the electric field was such, that negatively charged

Table 9.1: Fluxes and FR for the different sulfonated and unsulfonated membranes

Membrane	$J_{pwf,before}$ $[kg \cdot m^{-2}h^{-1}]$	J_{filtr} $[kg \cdot m^{-2}h^{-1}]$	$J_{pwf,after}$ $[kg \cdot m^{-2}h^{-1}]$	FR [-]	ζ [a] $[mV]$
DDS	179 ± 74	54 ± 8	97 ± 42	56 ± 16	-16
IRIS	356 ± 144	34 ± 10	21 ± 11	8 ± 5	-44

[a] at $I = 0.001$ $MKCl$ and $pH = 6$

particles migrated away from the membrane surface (see 9.1). From this figure it is clear that higher steady state fluxes could be obtained when an electric field was applied. This can not be interpreted as electro osmotic transport as was done by Jain et al. (Jain and Srivastava, 1996). The observed effect of the electric field can be contributed to charged contaminants in water which were prevented to reach the membrane at $\Delta E = 5\ kV \cdot m^{-1}$.

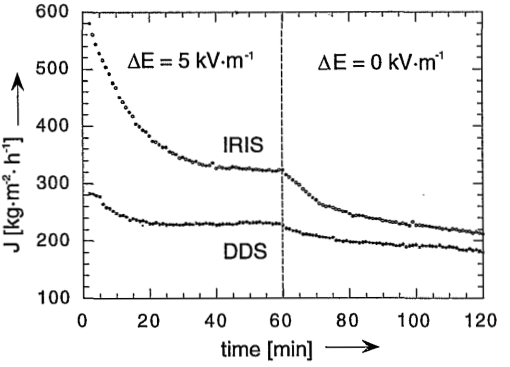

Figure 9.4: The effect of applying an electric field of $\Delta E = 5\ kV \cdot m^{-1}$ on the pure water flux

The influence of an electric field on the emulsion filtration flux

In Figures 9.5 and 9.6 the effect is shown of applying an electric field of $\Delta E = 15\ kV \cdot m^{-1}$ on the emulsion filtration flux for 8 hours, for DDS and IRIS membranes. For both membranes a higher steady state emulsion filtration flux was obtained when an electric field was applied compared to these values without an electric field (Figures 9.5). The flux improvement might be ascribed to a migration of particles from the forming cake layer during emulsion filtration (Wakeman and Sabri, 1995). This phenomenon should led to a reduction in cake layer thickness. From equation 9.3 the migration velocity can be calculated and was about 4 $\mu m \cdot s^{-1}$ for the emulsions. This means that emulsion droplets needed $7 - 8$ minutes to travel from the anode to the cathode in the membrane channel. From the cross-flow velocity it can be calculated that emulsions move through

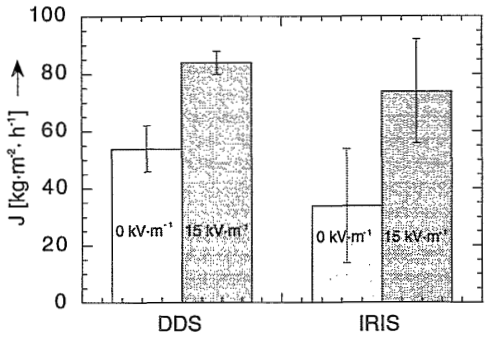

Figure 9.5: The influence of an electric field of $\Delta E = 15\ kV \cdot m^{-1}$ on the emulsion filtration flux after 8 hours of a DSS and IRIS PSf 100 kDa membrane. The error bars are the standard deviation of five experiments.

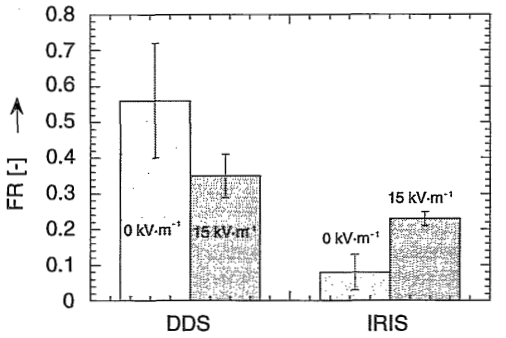

Figure 9.6: The influence of an electric field of $\Delta E = 15\ kV \cdot m^{-1}$ on the flux recovery with a DSS and IRIS PSf 100 kDa membrane after 8 hours emulsion filtration. The error bars are the standard deviation of five experiments.

the channel within about 2 seconds. This calculation indicates that the migration effect is very small. It might, however, play a role in the concentrated particles layer near the membrane surface resulting in a higher flux.

In Figure 9.6 the flux recovery is shown for filtration experiments using electric fields of $\Delta E = 0\ kV \cdot m^{-1}$ and $\Delta E = 15\ kV \cdot m^{-1}$ for both IRIS and DDS membranes. For filtration experiments with electric fields of $\Delta E = 15\ kV \cdot m^{-1}$, the flux recovery values

for both membranes were smaller than 0.35, indicating the occurrence of irreversible fouling despite of applying an electric field. The degree of irreversible fouling increased for DDS membranes and decreased for IRIS membranes when an electric field was applied compared to the reference values. A solid explanation for the observed phenomenon could not be found.

The hysteresis effect

In Figure 9.7 the effect of applying different electric field strengths on the emulsion filtration flux as a function of time is plotted. First emulsion filtration was performed at 1 bar in the presence of an electric field of $\Delta E = 15\ kV \cdot m^{-1}$ across the membrane. Permeation flux was monitored continuously. After 1 hour the electric field was decreased to $\Delta E = 12.5\ kV \cdot m^{-1}$, while keeping all other parameters constant. These steps were repeated until no electric field was applied. In the following steps the electric field was increased with increments of $\Delta E = 2.5\ kV \cdot m^{-1}$ until $\Delta E = 15\ kV \cdot m^{-1}$ was reached again.

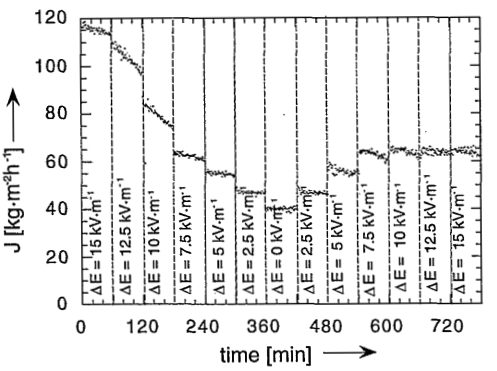

Figure 9.7: Stepwise decrease and increase of ΔE during emulsion filtration with a DDS membrane

In Figure 9.7 the emulsion filtration flux as a function of time is present. At the start of the experiments no steady state fluxes were obtained in 1 hour with $\Delta E > 10\ kV \cdot m^{-1}$. At fields between $\Delta E = 10\ kV \cdot m^{-1} - 0\ kV \cdot m^{-1}$ steady state fluxes could be obtained.

In Figure 9.8 the steady state fluxes obtained from the results presented in the previous figure are plotted as a function of the applied electric field. In cases where no steady state was reached, the fluxes after 1 hour were used. The arrows represent the direction of the electric field increase or decrease. The start and the end of the experiment are indicated in the figure as well.

From this figure it is clear that fluxes did increase as a function of the applied electric field. It is also clear from this figure, that a hysteresis effect occurred at $\Delta E > 7.5\ kV \cdot$

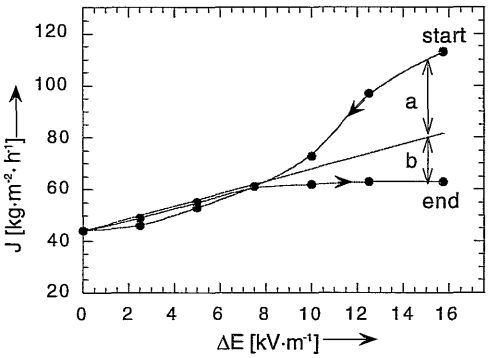

Figure 9.8: Emulsion flux versus the electric field strength of a DDS PSf membrane of 100 kDa. The straight line represents a linear extrapolation of J versus ΔE for a decreasing $\Delta E < 7.5\ kV \cdot m^{-1}$.

m^{-1}. By extrapolating the flux versus electric field behaviour at $\Delta E < 7.5\ kV \cdot m^{-1}$, a straight line was obtained (Blokhra and Prakash, 1992; Jain and Srivastava, 1996; Singh and Shahi, 1991). The deviation of this straight line at the beginning of the experiment (part a in Figure 9.8) was the result of the unsteady state behaviour, due to preconditioning of the membrane. The deviation of the straight line at the end of the experiment (part b in Figure 9.8) was the result of the occurrence of irreversible fouling. The slope of the straight line was given by $k_e = 6.7\ \pm 2.8\ cm^2 \cdot s^{-1} \cdot V^{-1}$. This value represented the electrophoretic permeability given in equation 9.2.

In Figure 9.9 the results of a similar experiment is shown for an IRIS membrane in which again the hysteresis effect is more clearly visible. Similar to the DDS membrane, the IRIS membrane was irreversibly fouled. By increasing the electric field, none of this fouling was reversed, contrary to the DDS membrane. No effect of the lower zeta-potential of IRIS could be observed in these measurements, as was concluded before in Figure 9.9. For this membrane also unsteady state fluxes were observed and again a straight line was drawn from flux values for $\Delta E < 10\ kV \cdot m^{-1}$, with a slope of $k_e = 7.8\ \pm 5.0\ cm^2 \cdot s^{-1} \cdot V^{-1}$.

9.5 Conclusions

Pure water fluxes were enhanced by an electric field for both IRIS and DDS 100 kDa UF PSf membranes due to prevention of contaminants in water from the membrane surface. A constant directly applied electric field also enhanced the emulsion filtration flux for both membranes due to migration of particles from the surface, but did not prevent irreversible fouling for both membranes. Part of this fouling was reversible for DDS membranes, contrary to fouling of the IRIS membranes which could not be reversed by

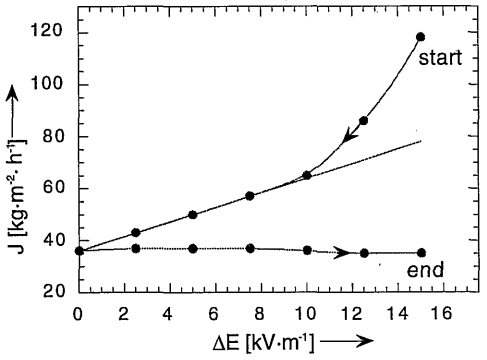

Figure 9.9: Emulsion flux versus the electric field strength of an IRIS PSf membrane of 100 kDa. The straight line represents a linear extrapolation of J versus ΔE for a decreasing $\Delta E < 7.5\ kV \cdot m^{-1}$.

an electric field.

In general, electrofiltration is useful to enhance the flux, but does not prevent irreversible fouling during emulsion filtration. An economical evaluation is necessary to study the use of electric forces to increase the membrane performance.

9.6 Acknowledgements

Dr. F.F. Stengaard (Dow Denmark Separation Systems) is acknowledged for the free membrane samples. Caroline Bruinsma is kindly acknowledged for the experimental work that has been carried out in this chapter to fulfil the requirements for her M.Sc. thesis. Thomas Raming of the inorganic material science group (UT) is thanked for his help on measuring the zeta potentials of the emulsion with the Malvern zetasizer.

9.7 List of Symbols

Acronyms

Symbol	Quantity
$CFEF$	cross-flow electro-filtration
MF	microfiltration
PSf	polysulfone
UF	ultrafiltration
pwf	pure water flux
$mwco$	molecular weight cut-off

Symbols

Symbol	Quantity	Units
A_m	membrane area	$[m^2]$
D	diffusion coefficient	$[m^2 \cdot s]$
FR	flux recovery ($= \frac{J_{\text{pwf,before}}}{J_{\text{pwf,after}}}$)	$[-]$
H	height of feed channel	$[m]$
I	ionic strength	$[g \cdot mol^{-1}]$
J	emulsion filtration flux	$[kg \cdot m^{-2} \cdot h^{-1}]$
L	length of feed channel	$[m]$
W	width of feed channel	$[m]$
ΔE	electric field strength	$[V \cdot m^{-1}]$
ΔP	applied pressure difference	$[bar]$
δ_m	thickness of the boundary layer	$[m]$
ϵ	dielectric constant ($= \frac{\epsilon_0 \epsilon_r}{4\pi}$)	$[F \cdot m^{-1}]$
ϵ_0	dielectric constant of vacuum	$[F \cdot m^{-1}]$
ϵ_r	relative dielectric constant	$[-]$
η_c	viscosity of the continuous phase	$[Pa \cdot s]$
λ_0	conductivity of the electrolyte solution	$[S \cdot m^{-1}]$
ψ^0	potential of the particle surface	$[V]$
ψ^δ	potential at the Stern plane	$[V]$
ζ	zeta potential	$[V]$
c	solute concentration in boundary layer	$[kg \cdot m^{-1}]$
c_0	bulk solute concentration	$[kg \cdot m^{-1}]$
c_g	gel layer concentration	$[kg \cdot m^{-1}]$
d_{32}	mean droplet diameter of emulsion droplet	$[\mu m]$
d_p	particle diameter	$[m]$
k_e	electrophoretic permeability	$[cm^2 \cdot s^{-1} \cdot V^{-1}]$
k_m	mass transport coefficient	$[m \cdot s^{-1}]$
t	time	$[s]$
u_e	electrophoretic velocity	$[m \cdot s^{-1}]$
v	cross-flow velocity	$[m \cdot s^{-1}]$
x	distance from the particle surface	$[m]$

Bibliography

Aimar, P. and R. Field, *Limiting flux in membrane separations : a model based on the viscosity dependency of the mass transfer coefficient.* Chem. Eng. Sci., 1991. **47**(3): p. 569-586.

Aimar, P., M. Meireles, P. Bacchin, and V. Sanchez. *Fouling and concentration polarisation in ultrafiltration and microfiltration.* in *ASI Nato meeting.* 1993. Curia, Portugal:

Altena, F. W., B. Belfort, J. Otis, F. Fiessinger, J. M. Rovel, and J. Nicoletti, *Particle motion in a laminar slit flow : a fundamental fouling study.* Desalination, 1983. **47**: p. 221-232.

Arnold, C. and R. A. Assink, *Development of sulfonated polysulfone membranes for redox flow batteries.* J. Membrane Sci., 1988. **38**: p. 71-83.

Arora, N. and R. H. Davis, *Yeast cake layers as secondary membranes in dead-end microfiltration of bovine serum albumin.* J. Membrane Sci., 1994. **92**: p. 247-256.

Baker, R. J., A. G. Fane, C. J. D. Fell, and B. H. Yoo, *Factors affecting flux in crossflow filtration.* Desalination, 1985. **53**: p. 81-93.

Bansal, A., R. R. Biederman, Y. H. Ma, and W. M. Clark, *Protein adsorption and fouling of ceramic membranes as measured by scanning electron microscopy with digital x-ray mapping.* Chem. Eng. Commun., 1991. **108**: p. 365-379.

Bauser, H., H. Chmiel, N. Stroh, and E. Walitza, *Interfacial effects with microfiltration membranes.* J. Membr. Sci., 1982. **11**(3): p. 321-32.

Becher, P., *Techniques of emulsification*, in *Emulsions: Theory and practice*, P. Becher, Editor. 1957, Reinhold publishing corporation: New York. p. 209-243.

Becher, P., *Emulsification*, in *Nonionic surfactants*, M. J. Schick, Editor. 1966, Marcel Dekker, Inc: New Jersey. p. 604-626.

Belfort, G., *Fluid mechanics in membrane filtration: recent developments.* J. Membr. Sci., 1989. **40**(2): p. 123-47.

Belfort, G., R. H. Davis, and A. L. Zydney, *The behaviour of suspensions and macromolecular solutions in crossflow microfiltration.* J. Membrane Sci., 1994. **96**: p. 1-58.

Berg, G. B. v. d. and C. A. Smolders, *Flux decline in ultrafiltration processes.* Desalination, 1990. **77**: p. 101-133.

Berg, v. d., G.B., *Concentration polarisation in ultrafiltration. Models and experiments*, PhD dissertation, University of Twente, 1988.

Bhattacharjee, C., P.K. Bhattacharya, *Flux decline analysis in ultrafiltration of kraft black liquor.* J. Membrane Sci., 1993. **82**: p. 1-14.

Bhattacharjee, S., A. Sharma, and P. K. Bhattacharya, *Surface interactions in osmotic pressure controlled flux decline during ultrafiltration.* Langmuir, 1994. **10**: p. 4710-4720.

Bhattacharyya, D., A. B. Jumawan, R. B. Grieves, and L. R. Harris, *Ultrafiltration characteristics of oil-detergent-water systems: membrane fouling mechanisms.* Sep. Sci. Technol., 1979. **14**(6): p. 529-49.

Blatt, W. F., A. Davis, A. S. Michaels, and L. Nelsen, *Solute polarization and cake formation in membrane ultrafiltration: causes, consequences and control techniques*, in *Membrane science and technology*, J. E. Flinn, Editor. 1970, Plenum Press: New York. p. 47-97.

Blokhra, R. L. and C. Prakash, *Electro-kinetic transport coefficients of aqueous binary mixtures through titanum oxide porous plug.* J. Membrane Sci., 1992. **70**: p. 1-7.

Bodzek, M. and K. Konieczny, *Characterisation of gel layer formed during ultrafiltration of latex emulsion waste waters.* Desalination, 1993. **94**: p. 81-100.

Bodzek, M. and K. Konieczny, *Modelling of the ultrafiltration of electrophoretic emulsion paint.* Desalination, 1994. **94**: p. 261-272.

Bowen, W. R., *Electro-osmotic membrane backwashing.* Ind. Eng. Chem. Res., 1994. **33**: p. 1245-1249.

Bowen, W. R. and F. Jenner, *Dynamic ultrafiltration model for charged colloidal dispersions: A wigner-seitz cell approach.* Chem. Eng. Sci., 1995. **50**(11): p. 1707-1736.

Bowen, W. R. and F. Jenner, *Theoretical descriptions of membrane filtration of colloids and fine particles : an assessment and review.* Adv. Colloids Interf. Sci., 1995. **56**: p. 141-200.

Brekel, v. d., L.D.M., *Hydrodynamics and mass transfer in domestic drum-type fabric washing machines*, PhD dissertation, University of Delft, 1987.

Brors, A. and K. H. Kroner, *Querstrom-Elektrofiltration mikrobieller Suspensionen.* Filtr. u. Sep., 1993. **7**(4): p. 189-192.

Bruin, S., A. Kikkert, J.A.G. Weldring, and J. Hiddink, *Overview of concentration polarization in ultrafiltration.* Desalination, 1980. **35**: p. 223-242.

Cain, C. W., *Filtration theory.* 2nd ed. Handbook of separation techniques for chemical engineers, ed. P. A. Schweitzer. 1988, McGraw-Hill.

Carman, P. C., *Fundamental principles of industrial filtration.* Trans. Inst. Chem. Eng., 1938. **16**: p. 168.

Causserand, C., M. Nyström, and P. Aimar, *Study of streaming potentials of clean and fouled ultrafiltration membranes.* J. Membrane Sci., 1994. **88**: p. 211-222.

Cheryan, M. and U. Merin. *The effect of protein-mineral-membrane interactions on the fouling of ultrafiltration membranes.* in *Fundam. Appl. Surf. Phenom. Assoc. Fouling Clean. Food Process., Proc. Int. Workshop.* 1981. Tylösand:

Chudacek, M. W. and A. G. Fane, *The dynamics of polarisation in unstirred and stirred ultrafiltration.* J. Membrane Sci., 1984. **21**: p. 145-160.

Coulson, J. M. and J. F. Richardson, *Liquid mixing,* in *Chemical engineering.* 1996, Butterworth & Heinemann: Oxford.

Cuperus, F. P. and C. A. Smolders, *A new method to determine the skin thickness of anisotropic ultrafiltration membranes using colloidal gold particles.* J. Colloid Interf. Sci., 1990. **135**: p. 486-498.

Davis, R. H. and D. T. Leighton, *Shear-induced transport of a particle layer along a porous wall.* Chem. Eng. Sci., 1987. **42**(2): p. 275-281.

Dickinson, E., *Emulsion and droplet size control,* in *Controlled particle, droplet and bubble formation,* D. J. Wedlock, Editor. 1994, Butterworth & Heinemann: Oxford. p. 191-216.

Digest, D. A. T. A., *chemical and environmental resistance,* in *International Plastic selector.* 1991,

Donaldson, R., *Dynamics of emulsification,* in *Mixing in the process industries,* N. Harnby, M. F. Edwards, andA. W. Nienow, Editors. 1995, Butterworth: London.

Doshi, M. R., *Limiting flux in the ultrafiltration of macromolecular solutions,* in *Reverse osmosis and ultrafiltration.* 1985,

Doulia, D., V. Gekas, and G. T. a. g. a. rdh, *Interaction behaviour in ultrafiltration of nonionic surfactants. Part 1. Flux behaviour..* J. Membrane Sci., 1992. **69**: p. 251-258.

Dumon, S. and H. Barrier, *Ultrafiltration of protein solutions on ZrO2 membranes. The influence of surface chemistry and solution chemistry on adsorption.* J. Membrane Sci., 1992. **74**: p. 289-302.

Eckstein, E. C., D. G. Bailey, and A. H. Shapiro, *Self-diffusion of particles in shear flow of a suspension.* J. Fluid Mech., 1977. **79**(1): p. 191-208.

Elimelech, M., W. H. Chen, and J. J. Waypa, *Measuring the zeta (electrokinetic) potential of reverse osmosis membranes by a streaming potential analyzer.* Desalination, 1994. **95**: p. 269-286.

Everett, D. H., *Manual of symbols and terminology for physicochemical quantities and units.* Pure Appl. Chem., 1972. **31**: p. 577-638.

Fane, A. G., *Ultrafiltration of suspensions.* J. Membrane Sci., 1984. **20**: p. 249-259.

Fane, A. G., K.J. Kim, C.J.D. Fell, A.B. Suki. *Characterization of ultrafiltration membranes : Flux and surface properties.* in *Workshop on characterization of UF membranes ;.* 1987. Orenas Slott, Sweden:

Fane, A. G. *Developing the potential of membrane processes for a cleaner environment.* in *Euromembrane '95.* 1995. Bath: European Society for Membrane Science and Technology.

Fane, A. G. and C. J. D. Fell, *A review of fouling and fouling control in ultrafiltration.* Desalination, 1987. **62**: p. 117-136.

Field, R. W., *Transport processes in membrane systems*, in *Membranes in bioprocessing : Theory & Practice*, V. S. J.A. Howell, R.W. Field, Editor. 1993, Blackie academic & prof.: Glasgow.

Field, R. W. and P. Aimar, *Ideal limiting fluxes in ultrafiltration: comparison of various theoretical relationships.* J. membrane Sci., 1993. **80**: p. 107-115.

Field, R. W., D. Wu, J. A. Howell, and B. B. Gupta, *Critical flux concept for microfiltration fouling.* J. Membrane Sci., 1995. **100**: p. 259-272.

Flösch, D., G. Clarotti, K. E. Geckeler, H. D. Lehmann, and W. Göpel. *Characterization of hydrophilic and hydrophobic surfaces of fluorocarbon membranes by ESCA, FTIR and SIMS.* in *ICOM.* 1990. Chicago:

Fontyn, M., *A membrane-foulant interaction study*, PhD dissertation, Agricultural university of Wageningen, 1991.

Futselaar, H., *The transverse flow membrane module*, PhD dissertation, University of Twente, 1993.

Gatenholm, P., S. Paterson, A. G. Fane, and C. J. D. Fell, *Performance of synthetic membranes during cell harvesting of E. Coli.* Proc. Biochem., 1988. **23**: p. 79-81.

Gekas, V., K.M. Persson, M. Wahlgren, B. Sivik, *Contact angles of ultrafiltration membranes and their possible correlation to membrane performance.* J. Membrane Sci., 1992. **72**: p. 293-302.

Gekas, V. and B. Hallström, *Mass transfer in the membrane concentration polarization layer under turbulent cross flow I. Critical literature review and adaptation of existing Sherwood correlations to membrane operations.* J. membrane Sci., 1987. **30**: p. 153-170.

Gilbert, E. E., *The reagents*, in *Sulfonation and related reactions.* 1965, Interscience publishers (John Wiley and Sons Inc.): New York. p. 1-30.

Goldsmith, R. L., *Macromolecular ultrafiltration with microporous membranes.* Ind. Eng. Chem. Fundam., 1971. **10**(1): p. 113-120.

Goodwin, J. W., J. Hearn, C. C. Ho, and R. H. Ottewil, *Studies on the preparation and characterisation of monodisperse polystyrene latices. III Preparation without added surface active agents.* Colloid & polymer Sci., 1974. **252**: p. 464-471.

Gourley, L., M. Britten, S. F. Gauthier, and Y. Pouliot, *Use of contact angle measurements for the characterisation of asdorptive fouling on UF membranes by peptide mixtures*, to appear, 1993.

Gourley, L., M. Britten, S. F. Gauthier, and Y. Pouliot, *Characterization of adsorptive fouling on ultrafiltration membranes by peptides mixtures using contact angle measurements.* J. Membrane Sci., 1994. **97**: p. 283-289.

Green, G. and G. Belfort, *Fouling of ultrafiltration membranes : Lateral migration and trhe particle trajectory model.* Desalination, 1980. **35**: p. 129-147.

Grieves, R. B., D. Bhattacharyya, W. G. Schomp, and J. L. Bewley, *Membrane ultrafiltration of a nonionic surfactant.* AIChE J., 1973. **19**(4): p. 766-774.

Griffin, W. C., *Emulsions*, in *Encyclopedia of chemical technology.* 1979, John Wiley & sons: p. 900-930.

Grundke, K., H.-J. Jacobasch, F. SImon, and S. Schneider, *Physico-chemical properties of surface-modified polymers*, in *Polymer surface modification : relevance to adhesion*, K. L. Mittal, Editor. 1996, VSP: Utrecht. p. 431-454.

Guizard, C., F. Legault, N. Idressi, A. Larbot, L. Cot, and C. Gavach, *Electronically conductive mineral membranes designed for electro-ultrafiltration.* J. Membrane Sci., 1989. **41**: p. 127-142.

Hanemaaijer, J. H., T. Robbertsen, d. B. T. Van, and J. W. Gunnink, *Fouling of ultrafiltration membranes. The role of protein adsorption and salt precipitation.* J. Membr. Sci., 1989. **40**(2): p. 199-217.

Hanemaaijer, J. H., T. Robbertsen, d. B. T. Van, C. Olieman, P. Both, and D. G. Schmidt, *Characterization of clean and fouled ultrafiltration membranes.* Desalination, 1988. **68**(2-3): p. 93-108.

Henry, J. D., L. F. Lawler, and C. H. A. Kuo, *A solid/liquid separation process based on cross flow and electrofiltration.* AIChE J., 1977. **23**(6): p. 851-859.

Hermia, J., *Constant pressure blocking filtration law: Application to power law nonnewtonian fluids.* Trans. I. Chem. Eng., 1982. **60**: p. 183-187.

Heusch, R., *Emulsions*, in *Ullmann's encyclopedia of industrial chemistry*, W. Gerhartz, Editor. 1987, VCH Verlagsgesellschaft mbH: Weinheim. p. 297-339.

Hiemenz, P. C., *Polymer chemistry.* 1st ed. 1984, New York: Marcel Dekker. 738.

Ho, W. S. W. and K. K. Sirkar, *Membrane handbook.* 1st ed. 1992, New York: Van Nostrand Reinhold.

Howell, J. A. and M. Nyström, *Fouling phenomena*, in *Membranes in bioprocessing : Theory & Practice*, V. S. J.A. Howell, R.W. Field, Editor. 1993, Blackie academic & prof.: Glasgow. p. 203-241.

Howell, J. A. and O. Velicangil, *Theoretical considerations of membrane fouling and its treatment with immobilized enzymes for protein ultrafiltration.* J. Appl. Pol. Sci., 1982. **27**: p. 21-32.

Igawa, M., M. Seno, H. Takahashi, and T. Yamabe, *Reverse osmosis by dynamic membranes.* Desalination, 1977. **22**: p. 281-289.

Jain, A. K. and R. K. Srivastava, *Ab-initio studies on electroosmotic separation: separation of 1,4-dioxane in water solution.* J. Membrane Sci., 1996. **112**: p. 41-46.

Jakobi, G. and A. Löhr, *Detergents and textile washing. Principles and practice.* 1987, Düsseldorf: VCH Verlagsgesellschaft mbH. 241.

Jan, D., J. S. Jeon, and S. Raghavan, *Surface modification of PVDF membrane by grafting of a vinylphosponium compound*, in *Polymer surface modification : relevance to adhesion*, K. L. Mittal, Editor. 1996, VSP: Utrecht. p. 337-348.

Jitsuhara, I. and S. Kimura, *Structure and properties of charged ultrafiltration membranes made of sulfonated polysulfone.* J. Chem. Eng. Jap., 1983. **16**(5): p. 389-393.

Johnson, B. C., I. Yilgör, C. Tran, M. Iqbat, J. P. Wightman, D. R. Lloyd, and J. E. McGrath, *Synthesis and characterisation of sulfonated poly(arylene ether sulfones).* J. Polymer Sci., 1984. **22**: p. 721-737.

Jonsson, G., C.E. Boesen, *Water and solute transport through cellulosic acetate reverse osmosis membranes.* Desalination, 1975. **17**: p. 145-165.

Jonsson, G., *Boundary layer phenomena during ultrafiltration of dextran and whey proteins solution.* Desalination, 1984. **51**: p. 61-77.

Jonsson, G., C.E. Boesen, *Polarization phenomena in membrane processes*, in *Synthetic membrane processes*, A. press, Editor. 1984, Academic press: New York. p. 552.

Jonsson, G., *Molecular weight cut-off curves for ultrafiltration membranes of varying pore sizes.* Desalination, 1985. **53**: p. 3-10.

Jonsson, G., *Transport phenomena in ultrafiltration: membrane selectivity and boundary layer phenomena.* Pure & Appl. Chem., 1986. **58**(12): p. 1647-1656.

Jonsson, G., P. Prádanos, and A. Hernández. *Fouling mechanisms in microporous membranes.* in *Membrane Proc. & Appl., Europ. Soc. Membrane Sci. & Techn.*. 1993. Vallodilid:

Jonsson, G., P. Prádanos, and A. Hernández, *Fouling phenomena in microporous membranes. Flux decline kinetics and structural modifications.* J. Membrane Sci., 1996. **112**: p. 171-183.

Judsen King, C., *Separation processes.* 1971, New York: McGraw Hill.

Jönsson, A.-S. and B. Jönnson, *The influence of nonionic andionic surfactants on hydrophobic and hydrophilic ultrafiltration membranes.* J. Membrane Sci., 1991. **56**: p. 49-76.

Kawakatsu, T., M. Nakajima, S. Nakao, and S. Kimura, *Three-dimensional simulation of random packing and pore blocking phenomena during microfiltration.* Desalination, 1995. **101**: p. 203-209.

Kawakatsu, T., S. Nakao, and S. Kimura, *Effects of size and compressibility of suspended particles and surface pore size of membrane on flux in crossflow filtration.* J. Membrane Sci., 1993. **81**: p. 173-190.

Kesting, R. E., *Synthetic polymeric membranes: A structural perspective.* 2nd ed. Vol. 1. 1985, New York: John Wiley & Sons. 348.

Kim, K. J. and A. G. Fane, *Low voltage scanning electron microscopy in membrane research.* J. Membrane Sci., 1994. **88**: p. 103-114.

Kim, K. J., A. G. Fane, and C. J. D. Fell, *The effect of Langmuir-Blodgett layer pretreatment on the performance of ultrafiltration membranes.* J. Membr. Sci., 1989. **43**(2-3): p. 187-204.

Kim, K. J., A. G. Fane, C. J. D. Fell, and D. C. Joy, *Fouling mechanisms of membranes during protein ultrafiltration.* J. Membr. Sci., 1992. **68**(1-2): p. 79-91.

Kim, K. J., A. G. Fane, M. Nyström, A. Pihlajamaki, W. R. Bowen, and H. Mukthar, *Evaluation of electroosmosis and streaming potential for measurement of electric charges of polymeric membranes.* J. Membrane Sci., 1996. **116**: p. 149-159.

Kirk-Othmer, *Surfactants and detersive systems*, in *Encyclopedia of chemical technology*, M. Grayson, Editor. 1979, John Wiley & Sons: New York. p. 393.

Kolmogorov, A. N., *The break-up of droplets in a turbulent stream.* Dok. Akad. Nauk., 1949. **66**(5): p. 825-828.

Konar, J. and A. K. Bhowmick, *Surface properties of polyethylene grafted with triallyl cyanurate in the presence of an electron beam*, in *Polymer surface modification : relevance to adhesion*, K. L. Mittal, Editor. 1996, VSP: Utrecht. p. 327-336.

Koops, G. H., *Nomenclature and symbols in membrane science and technology.* 1st ed. 1995, Den Haag: CIP-data Koninklijke bibliotheek. 78.

Kowalczynska, H. M., P. Mrozek, and J. Kaminski, *Surface sulfonation of styrene.methacrylate copolymers studied by x-ray photoelectron spectroscopy.* J. Colloid Interfac. Sci., 1993. **160**: p. 317-323.

Krijgsman, J., *Vloeistof-vastestofscheiding in de biotechnologie*, in *NPT Procestechnologie*1994, p. 11-19.

Kroner, K. H. *Cross-flow filtration of biological suspensions.* in *Membrane processing in separation and purification.* 1993. Curia, Portugal: Kluwer Acedemic Publishers.

Kumar, S., R. Kumar, and K. S. Gandhi, *A simplified procedure for predicting dmax in stirred vessels.* Chemical engineering science, 1993. **48**(17): p. 3092-3096.

Larsson, A. C. and R. Wimmerstedt, *Solvent fluxes measured on a membrane module.* J. membrane Sci., 1993. **84**: p. 139-150.

Larsson, N., A. Biverstedt, and J.-C. Ericsson. *Chemical modification of polymer surfaces.* in *Fundamentals and applications of surface phenomena associated with fouling and cleaning in food processing.* 1981. Tylösand:

Le, M. S. and K. L. Gollan, *Fouling of microporous membranes in biological applications.* J. Membrane Sci., 1989. **40**: p. 231-242.

Le, M. S. and J. A. Howell, *Alternative model for ultrafiltration.* Chem. Eng. Res. Dev., 1984. **62**: p. 373-380.

Lee, S., Y. Aurelle, and H. Roques, *Concentration polarization, membrane fouling and cleaning in ultrafiltration of soluble oil.* J. Membr. Sci., 1984. **19**(1): p. 23-38.

Lee, S. Y., S. Corbino, and G. B. Wood, *Antistatic polyphenylene oxide by surface sulfonation.* Polym. Eng. Sci., 1976. **16**(6): p. 389-393.

Leonard, E. F. and C. S. Vassilieff, *The deposition of rejected matter in membrane separation processes.* Chem. Eng. Commun., 1984. **30**: p. 209-217.

LeRoi Nelson, K., *Chapter XLII Sulphonation*, in *Friedel crafts and related reactions, III acylation and related reactions*, G. A. Olah, Editor. 1964, Interscience publishers: New York.

Lin, F. Y. H., A.W. Neumann, *Effect of surface roughness on the dependence of contact angles on drop size.* J. colloid & Interf. Sci., 1993. **159**: p. 86-95.

Lipp, P., C. H. Lee, A. G. Fane, and C. J. D. Fell, *A fundamental study of the ultrafiltration of oil-water emulsions.* J. Membr. Sci., 1988. **36**: p. 161-177.

Lojkine, M. H., R. W. Field, and J. A. Howell, *Crossflow microfiltration of cell suspensions: a review of models with emphasis on particle size effects.* TransIChemE, 1992. **70**(c): p. 149-164.

Lopez-Leiva, M. and E. Matthiasson. *Solute adsorption as a source of fouling in ultrafiltration.* in *Fundamentals and applications of surface phenomena associated with fouling and cleaning in food processing.* 1981. Tylösand:

Luckham, P. F., *Measurements of the interaction between adsorbed polymer layers: the steric effect.* Adv. Colloid Interf. Sci., 1991. **34**: p. 191-215.

Lund, D. B. and C. Sandu. *State-of-the-art of fouling : heat transfer surfaces.* in *Fundamentals and applications of surface phenomena associated with fouling and cleaning in food processing.* 1981. Tylösand:

Lyklema, J., *Fundamentals of interface and colloid science. Volume I : fundamentals.* 1 ed. Fundamentals of interface and colloid science, ed. J. Lyklema. Vol. 1. 1991, London: Academic press.

Marshall, A. D., P. A. Munro, and G. T. a. g. a. rdh, *The effect of protein fouling in microfiltration and ultrafiltration on permeate flux, protein retention and selectivity. A literature review.* Desalination, 1993. **91**: p. 65-108.

Matthiason, E. and B. Sivik, *Concentration polarization and fouling.* Desalination, 1980. **35**: p. 59-103.

Matthiasson, E., *The role of macromolecular adsorption in fouling of ultrafiltration membranes.* J. Membr. Sci., 1983. **16**: p. 23-36.

Matz, R. and Y. Meitlis, *Design and operating parameters for tubular ultrafiltration membrane modules.* Desalination, 1978. **24**: p. 281-294.

McDonough, R. M., A. G. Fane, and C. J. D. Fell, *Charge effects in the crossflow filtration of colloids and particulates.* J. Membrane Sci., 1989. **43**: p. 69-85.

McDonough, R. M., T. Gruber, N. Stroh, H. Bauser, E. Walitza, H. Chmiel, and H. Strathmann, *Criteria for fouling layer disengagement during filtration of feeds containing a wide range of solutes.* J. Membrane Sci., 1992. **73**: p. 181-189.

Meireles, M., P. Aimar, and V. Sanchez, *Effects of protein fouling on the apparent pore size distribution of sieving membranes.* J. Membrane Sci., 1991. **56**: p. 13-28.

Michaels, A. S., *New separation technique for the CPI.* Chem. Eng. Progress, 1968. **64**(12): p. 31-43.

Morra, M., E. Occhiello, F. Garbassi, *Knowledge about polymer surfaces from contact angle measurements.* J. Colloids Interf. Sci., 1990. **173**: p. 79-115.

Mulder, M., *Basic principles of membrane technology.* 1st ed. 1991, Dordrecht: Kluwer academic publishers. 363.

Mulder, M., *Basic principles of membrane technology.* 2nd ed. 1996, Enschede: Kluwer Academic publishers. 564.

Müller, F. J. and W. Krieger. *Reduction of membrane fouling in reverse osmosis by means of surface modification of the membranes.* in *Fundamentals and applications of surface phenomena associated with fouling and cleaning in food processing.* 1981. Tylösand:

Nadh Jagannadh, S. and H. S. Muralidhara, *Electrokinetics methods to control membrane fouling.* Ind. Eng. Chem. Res., 1996. **35**: p. 1133-1140.

Nakao, S., T. Nomura, S. Kimura, and A. Watanabe, *Formation and characteristics of inorganic dynamic membranes for ultrafiltration.* J. Chem. Eng. Jap., 1986. **19**(3): p. 221-226.

Nakao, S., H. Osada, H. Kurata, T. Tsuru, and S. Kimura, *Separation of proteins by charged ultrafiltration membranes.* Desalination, 1988. **70**: p. 191-205.

Nakao, S.-I., *Determination of pore size distribution 3. Filtration membranes.* J. Membrane Sci., 1994. **96**: p. 131-165.

Napper, D. H., *Steric stabilisation.* J. Colloid Interf. Sci., 1977. **58**(2): p. 390-407.

Nilsson, J.-L., *A study of ultrafiltration membrane fouling,* PhD, University of Lund, 1989.

Noshay, A. and L. M. Robeson, *Sulfonated polysulfone.* J. Applied Polym. Sci., 1976. **20**: p. 1885-1903.

Nyström, M., *Fouling of unmodified and modified polysulfone ultrafiltration membrane by ovalbumin.* J. Membrane Sci., 1989. **44**: p. 183-196.

Nyström, M., *Flux enhancement,* in *Membranes in bioprocessing : Theory & Practice,* V. S. J.A. Howell, R.W. Field, Editor. 1993, Blackie academic & prof.: Glasgow.

Oers, v., C.W., *Solute rejection in multicomponent systems during ultrafiltration*, PhD dissertation, University of Eindhoven, 1994.

Ogden, G. E. and R. H. Davis, *Experimental determination of the permeability and relative viscosity for fine latexes and yeast suspensions.* Chem. eng. comm., 1990. **91**: p. 11-28.

Ohshima, H. and T. Kondo, *Electrokinetic flow between two parallel plates with surface charge layers : electro-osmosis and streaming potential.* J. Colloid Interf. Sci., 1990. **135**(2): p. 443-448.

Oldani, M., G. Schock, *Characterization of UF membranes by infrared spectroscopy, ESCA and contact angle measurements.* J. Membrane Sci., 1989. **43**: p. 243-258.

Ophoff, J., G. S. Vos, I. G. Racz, and T. Reith. *Systematic approach of membrane module design based on hydrodynamics. The helically twisted tubular membrane module.* in *1996 international congress on membranes and membrane processes.* 1996. Yokohama:

Orr, C., *Emulsion droplet size data*, in *Encyclopedia of emulsion technology*, P. Becher, Editor. 1983, p. 369-404.

Oss, v., C.J., *Acid-base interfacial interactions in aqueous media.* Colloids & Surfaces A: physicochemical and engineering aspects, 1993. **78**: p. 1-49.

Oss, v., C.J., *Interfacial forces in aqueous media.* 1st ed. Vol. 1. 1994, New York: Marcel Dekker, inc. 440.

Oss, v., C.J., *Repulsive forces in aqueous solubility, micelle stability, microemulsion formation, and phase separation*, in *Encyclopedia of emulsion technology*, P. Becher, Editor. 1996, Marcel Dekker, inc.: New York. p. 357.

Overbeek, J. T. G., *Electrokinetic phenomena*, in *Colloid science*, H. R. Kruyt, Editor. 1952, Elsevier publishing company: New York. p. 194-226.

Paul, H., *Membrantrennung und Eindampfung, eine Wirtschaftliche und Umweltfreundliche Verfahrenskombination zur Aufarbeitung von ölhartige Industriewaschwassern*, PhD dissertation, Universtity of Aachen, 1984.

Peeters, J. M. M., *Characterization of nanofiltration membranes*, PhD dissertation, University of Twente, 1997.

Persson, K., C. Andersson, and V. Gekas. *Non deterministic models of the hydraulic permeability of fouled and unfouled UF membranes.* in *Membr. Proc. & Appl., Europ. Soc. Membr., Sci & Techn..* 1993. Vallodilid:

Persson, K. M., G. Träg årdh, and P. Dejmek, *Fouling behaviour of silica on four different microfiltration membranes.* J. membrane Sci., 1993. **76**: p. 51-60.

Porter, M. C., *Concentration polarization with membrane ultrafiltration.* Ind. Eng. Chem. Prod. Res. Develop., 1972. **11**(3): p. 234-248.

Pránados, P., A. Hernández, J. I. Calvo, and F. Tejerina, *Mechanisms of protein fouling in cross-flow UF through an asymmetric inorganic membrane.* J. Membrane Sci., 1996. **114**: p. 115-126.

Reihanian, H., C. R. Robertson, and A. S. Michaels, *Mechanisms of polarization and fouling of ultrafiltration membranes by proteins.* J. Membr. Sci., 1983. **16**: p. 237-258.

Rios, G. M., H. Rakotoarisoa, and B. Tarodo de la Fuente, *Basic transport mechanisms of ultrafiltration in the presence of an elctric field.* J. Membrane Sci., 1988. **38**: p. 147-159.

Robinson, C. W., M. H. Siegel, A. Condemine, C. Fee, T. Z. Fahidy, and B. R. Glick, *Pulsed-electric field crossflow ultrafiltration of bovine serum albumin.* J. Membrane Sci., 1993. **80**: p. 209-220.

Rogers, A. N., *Economics of the application of membrane processes. Part 2: Waste water treatment*, in *Synthetic membrane processes*, A. press, Editor. 1984, Academic press: New York. p. 552.

Romero, C. A. and R. H. Davis, *Global model of crossflow microfiltration based on hydrodynamic particle diffusion.* J. Membrane Sci., 1988. **39**: p. 157-185.

Rubin, I. I., *Handbook of plastic materials & technology.* 1990, New York: John Wiley & Sons, Inc. 1744.

Rånby, B., *'Surface photografting' onto polymers - a new method for adhesion control*, in *Polymer surface modification : relevance to adhesion*, K. L. Mittal, Editor. 1996, VSP: Utrecht. p. 303-318.

Scamehorn, J. F., S. D. Christian, and R. T. Ellington, *Use of micellar-enhanced ultrafiltration to remove multivalent metal ions from aqueous streams.* 1st ed. Surfactant-based separation processes, eds. M. J. Schick and F. M. Fowkes. Vol. 33. 1989, New York: Marcel dekker, inc. 339.

Shuval, H. I., *Water renovation and reuse.* 1st ed. Water pollution series, eds. K. S. Spiegler and J. Bregman. Vol. 3. 1977, New York: Academic press.

Singh, K. and V. K. Shahi, *Permeation studies on supported lecithin liquid membranes.* J. Membrane Sci., 1991. **59**: p. 27-38.

Singh, R., *Surface properties in membrane filtration.* Chem. Eng. Prog., 1989. **85**(6): p. 59-64.

Song, L. and M. Elimelech, *Theory of concentration polarisation in cross-flow filtration.* J. Chem. Soc. Faraday Trans., 1995. **91**(19): p. 3389-3398.

Sridhar, S., P.K. Bhattacharya, *Limiting flux phenomena in ultrafiltration of kraft black liqour.* J. Membrane Sci., 1991. **57**: p. 187-206.

Stengaard, F. F., *Characteristics and performance of new types of ultrafiltration membranes with chemically modified surfaces.* Desalination, 1988. **70**: p. 207-224.

Stengaard, F. F., *Preparation of asymmetric microfiltration membranes and modification of their properties by chemical treatment.* J. Membr. Sci., 1988. **36**: p. 257-275.

Strathmann, H., *Trennung von molekilaren Mischungen mit Hilfe synthetischer Membranen.* 1st ed. Wissenschaftlichen forschungsberichte, Vol. 2. 1979, Darmstadt: Dr. Dietrich Steinkopff Verlag. 206.

Suwandi, M. S. and M. S. Lefebre. *A new self assembly organic-inorganic composite membrane.* in *ICOM.* 1990. Chicago:

Tadros, T. F., *Emulsion stability,* in *Encyclopedia of emulsion technology,* P. Becher, Editor. 1983, p. 369-404.

Tarleton, E. S., *How electric and ultrasonic fields assist membrane filtration.* Filtr. Sep., 1988. **25**(6): p. 402-406.

Terlingen, J. G. A., *Introduction of functional groups at polymer surfaces by glow discharge techniques,* PhD dissertation, University of Twente, 1993.

Tiller, F. M. and C. S. Yeh, *Compressibility of particulte structures in relation to thickening, filtration and expression - a review.* Sep. Sci. Techn., 1987. **22**(2 & 3): p. 1037-1063.

Trettin, D. R. and M. R. Doshi, *Ultrafiltration in an unstirred batch cell.* Ind. Eng. Chem. Fundam., 1980. **19**: p. 189-194.

Vigo, F., C. Uliana, and D. Cicalese, *Ultrafiltration treatment of waste waters containing creosote oil.* La Chimica e L'indistria, 1984. **66**(9): p. 515-518.

Vigo, F., C. Uliana, E. Ravina, A. Lucifredi, and M. Gandoglia, *The vibrating ultrafiltration module. Performance in the 50-1000 Hz frequency range.* Sep. Sci. Techn., 1993. **28**(4): p. 1063-1076.

Vogt, E., *Nieuwe zeoliet overspoelt wasmiddelmarkt.* Chem. Mag., 1995. 4: p. 10-11.

Wahlgren, M., T. Arnebrant, *Adsorption of β-Lactoglobulin onto silica, methylated silica and polysulfone.* J. Colloids & Interf. Sci., 1989. **136**(1): p. 259-265.

Wakeman, R. J. and M. N. Sabri, *Utilizing pulsed electric fields in crossflow microfiltration ot titania suspensions.* Trans. I. Chem. E., 1995. **73**(A): p. 455-463.

Walstra, P., *Light scattering by milk fat globules.* Neth. Milk & dairy J., 1965. **19**: p. 93-109.

Walstra, P., *Formation of emulsions,* in *Encyclopedia of emulsion technology,* P. Becher, Editor. 1983, p. 57-127.

Walstra, P., *principles of emulsion formation.* Chem. Eng. Sci., 1993. **48**(2): p. 333-349.

Walstra, P., *Emulsion stability,* in *Encyclopedia of emulsion technology,* P. Becher, Editor. 1996, Marcel Dekker, inc.: New York. p. 357.

Weiss, E. A., *Castor, sesame and safflower.* 1971, London: Leonard Hill. 286-298.

Welin-Klintström, S., R. Jansson, H. Elwing, *An off-null ellipsometer with lateral scanning capability for kinetic studies at liquid-solid interfaces.* J. Colloid & Interf. Sci., 1993. **157**: p. 498-503.

Wenten, I. G., A. Rasmussen, and G. Jonsson. *Membrane cleaning after beer clarification.* in *Fouling and cleaning in food processing.* 1994. Jesus college Cambridge:

Wolff, J., *Tailoring of ultrafiltration membranes by plasma treatment and their application for the desalination and concentration of water-soluble organic substances.* J. Membrane Sci, 1988. **36**: p. 207-214.

Yamagiwa, K., H. Kobayashi, and A. Ohkawa, *Membrane fouling in ultrafiltration of hydrophobic nonionic surfactants.* J. Chem. Eng. Japan, 1993. **26**(1): p. 13-18.

Yukawa, H., K. Shimura, A. Suda, and A. Maniwa, *Cross flow electro-ultrafiltration for colloidal solution of protein.* J. Chem. Eng. Japan, 1983. **16**(4): p. 305-311.

Zeman, L. J., *Adsorption effects in rejection of macromolecules by ultrafiltration membranes.* J. Membr. Sci., 1983. **15**(3): p. 213-30.

Zha, F. F., A.G. Fane, C.J.D. Fell, R.W., Schofield, *Critical displacement pressure of a supported liquid membrane.* J. Membrane Sci., 1992. **75**: p. 69-80.

Zhang, W., M. Wahlgren, B. Sivik, *Membrane characterization by the captive angle technique. II. Characterization of UF-membranes and comparison between the captive bubble and sessile drop as methods to obtain water contact angles.* Desalination, 1989. **72**: p. 263-273.

Zhang, W., B. Hallström, *Membrane characterization using the captive bubble technique. I. Methodology of the captive bubble technique.* Desalination, 1990. **79**: p. 1-12.

Zschocke, P. and D. Quellmalz, *Novel ion exchange membranes based on an aromatic polyethersulfone.* J. Membrane Sci., 1985. **22**: p. 325-332.

Zydney, A. L. and C. K. Colton, *A concentration polarization model for the filtrate flux in cross-flow microfiltration of particulate suspensions.* Chem. Eng. Commun., 1986. **47**: p. 1-21.

Appendix A

A new way in synthesising TEP/SO_3-complex

A.1 Introduction

A method found in literature (Johnson *et al.*, 1984) to synthesise the TEP/SO_3-complex has the disadvantage that a lot of moisture is introduced to the system, which introduces the formation of sulfuric acid. To overcome this problem, a new set-up has been developed.

A.2 Theory

Sulfonation of aromates or molecules containing a phenyl-group is an often used reaction in the chemical industry. The reason for this, is the widespread use of sulfuric acid and the relative simplicity of the reaction. Sulfonation can be carried out by several chemical agents, such as (fuming) sulfuric acid, chlorosulfonic acid, fluorosulfonic acid, sulfur trioxide and sulphite in the presence of an oxidator (LeRoi Nelson, 1964).

Several researchers (Arnold and Assink, 1988; Johnson *et al.*, 1984; Zschocke and Quellmalz, 1985) prefer sulfonation with a complex of sulfurtrioxide with triethylenephosphate. The advantage of this sulfonation agent is that the SO_3-reactivity can be controlled (Noshay and Robeson, 1976). The complex is in equilibrium with free SO_3, which is very reactive but only present in very small amounts, because of a low equilibrium constant in various solvents, such as pyridine, triethyleneamine, trimethylamine and triethylenephosphate (TEP).

$$TEP/SO_3 \rightleftharpoons TEP + SO_3 \tag{A.1}$$

Crosslinking reactions due to side-reactions can therefore be avoided with a different TEP and SO_3 ratio, which determines the degree of sulfonation.

Sulfonation of a PSf surface will result in a change in the surface tension properties of the surface. Sulfone-groups ($-SO_3^{\ominus}$) will be introduced to the surface, resulting in a charged surface.

Sulfonation by TEP/SO_3-complexes appears to be an effective way to sulfonate PSf surfaces. The mechanism of this reaction is by electrophilic substitution of the reactive free sulfurtrioxide molecules to the benzene-ring at the 2-2 diphenylpropyl-unit of the PSf backbone. This was found from H-NMR studies by Arnold et al. (Arnold and Assink, 1988). This mechanism is shown in Figure A.1.

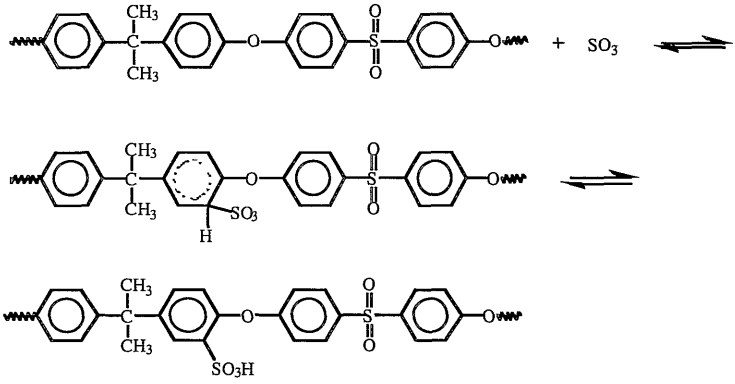

Figure A.1: The mechanism of sulfonation a PSf surface

A.3 Experimental part

A.3.1 Materials

Sulfurtrioxide (Aldrich chemicals) was first purified by a precipitation procedure. A closed container with SO_3 was put into an Argon-saturated set-up with two vessels connected to each other with a tube with two closed valves. The container with SO_3-was opened in one of the vessels and freezed with liquid nitrogen in about two hours. The system was put under vacuum and the valves were opened. Now the other vessel was freezed with liquid nitrogen and the SO_3 vaporised from the first vessel which was heated at 80 °C by an Eurotherm (Philips infrafil 125 W) into the cooled one in about four hours. In this way SO_3 was purified. After this, the vessels were put under vacuum and put into an Argon atmosphere to prevent a reaction with the moisture in air.

A.3.2 Method

The set-up to prepare TEP/SO_3 is shown in Figure A.2. Two containers were connected with an U-tube (connections were sealed with Teflon-tape). In container B (see Figure A.2) a certain amount of triethylenephosphate (Merck) was present in 200 ml cyclohexane dependent on the desired TEP/SO_3-ratio. The total set-up was saturated with an Argon stream which also transported vapour from container A to B. After saturation,

the purified SO_3 was put in container A, which was put into an oil-bath of about 30 °C . After about 4 days all the SO_3 had been evaporated and reacted with the TEP in container B. Two phases were observed in this container with the heavier brownish complex at the bottom.

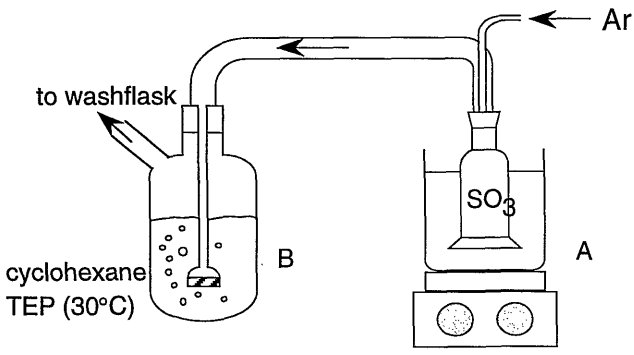

Figure A.2: The set-up to prepare TEP/SO_3

A.3.3 Characterisation

The TEP/SO_3 synthesis was carried out three times. The samples consisted of two phases, a heavier complex and cyclohexane phase. The synthesised complex was analysed by three different techniques; gaschromatography, infrared spectroscopy and elementary analysis. The purity of the lighter cyclohexane phase was investigated by gaschromatography.

Gaschromatography

The concentration and purity of the synthesised samples of TEP/SO_3 can be determined by gaschromatography, in which separation took place on the basis of a difference in affinity with a mobile gas phase and a stationary liquid or solid phase. The stationary phase was present in the gaschromatography column which is a liquid (10 % SE-30) on a inert carrier material present in the column (chrom. W. HP with a mesh size of 80/100). The column temperature was set to 50 °C and increased to 190 °C with 20°C min. The injection and detector temperatures were 220 °C . The injection volume was 0.2 $\mu\ell$.

IR-spectroscopy

The chemical bonds can be elucidated with IR spectroscopy. Because the bond between TEP and SO_3 is not a strong bond, a peak was expected at low wavenumbers of about 600 cm^{-1}.

Elementary analysis

From elementary analysis the TEP/SO_3-ratio can be calculated. In this technique an exact amount of the complex was burnt and analysed.

A.4 Results and discussion

A.4.1 Gaschromatography

The results of the gaschromatography measurements are given in Table A.1. The synthesised heavier TEP/SO_3 phase was rather constant in composition for the three samples. The fraction of pure TEP/SO_3 was > 50 %, the pure TEP-fraction was about 30 % for the first attempt (not measured for the second and third attempt) and the cyclohexane fraction was < 6.4 %. The purity of the cyclohexane phase is 98.6 %.

Because TEP/SO_3 formed an emulsion-phase with cyclohexane, other solvents were used to dissolve the complex. It was found, however, for DOP and ethanol as eluent fluids, that TEP/SO_3 degraded.

Table A.1: The results of gaschromatography measurements of three different TEP/SO_3 batches

	1st [%]	2nd [%]	3rd [%]	lighter phase [%]
cyclohexane	2.7	6.1	6.4	98.6
TEP	32.8	[a]	[a]	[a]
TEP/SO_3	> 60	> 50	> 50	[a]
rest	< 4.5	[a]	[a]	1.4

[a] not been measured

A.4.2 IR-spectroscopy

A IR-spectrum has been obtained and can be seen in Figure A.3. In this graph the chemical bonds were added and the weak $SO_3 \cdot O$ bond was located at 500 cm^{-1}, which indicated that it is a weak bond.

A.4.3 Elementary analysis

To determine the fractions of atoms in the synthesised TEP/SO_3, elementary analysis was carried out. The results of this analysis are shown in Table A.2. Theoretical atom fractions are calculated from the structural formula of TEP/SO_3 (see Figure A.4).

From this table, it was calculated that the TEP/SO_3-ratio for the first, second and third synthesis was respectively 1 : 1.4, 1 : 1.63 and 1 : 1.74.

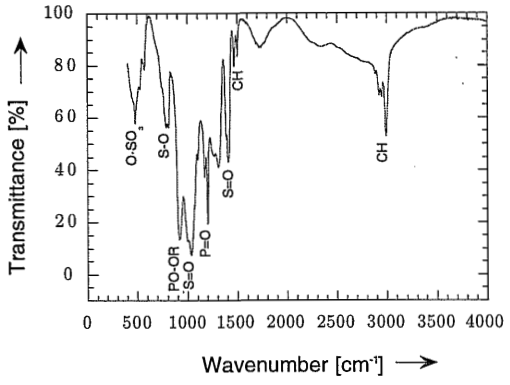

Figure A.3: An IR-spectrum from synthesised 1 : 1 TEP/SO_3

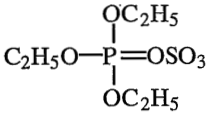

Figure A.4: The structural formula of TEP/SO_3

Table A.2: The theoretical determined and measured atom fractions from three different TEP/SO_3 batches

	theoretical [%]	1st [%]	2nd [%]	3rd [%]
C	21.0	30.18 ± 0.35	24.33 ± 0.01	23.42 ± 0.29
H	4.4	6.48 ± 0.22	5.17 ± 0.01	5.19 ± 0.14
N	0	0.13 ± 0.13	0.03 ± 0.00	0.03 ± 0.01
O	46.8	[a]	[a]	[a]
P	9.1	[a]	[a]	[a]
S	18.8	8.86 ± 0.05	15.8 ± 0.07	16.77 ± 0.11

[a] not been measured

A.5 Conclusions

A new technique was used to synthesise TEP/SO_3 Three samples were obtained of the TEP/SO_3-complex in cyclohexane which were not miscible. The TEP/SO_3 phase was heavier and was analysed by gaschromatography, IR-spectroscopy and elementary analysis. The cyclohexane phase was analysed by only gaschromatography.

The TEP/SO_3 content in the heavy phase was higher than 50 % for all the three sam-

ples. A small fraction of cyclohexane was present in the TEP/SO_3-phase. The chemical bond were elucidated with IR-spectroscopy and a weak bond at 500 cm^{-1} was present between the TEP and SO_3 molecules. The ratio between TEP/SO_3 was measured with elementary analysis and was about $1 : 1.5$.

Appendix B

Determination of the non oil bound surfactant concentration

Introduction

An emulsion consists of surfactant stabilised oil-droplets, free surfactant molecules and clustered surfactant molecules, known as micelles. A schematic picture of such an emulsion is given in Figure B.1. The non oil bound surfactant part in the emulsion is of interest during filtration of the emulsion. It is expected, that only free surfactants can permeate freely through the ultrafiltration membranes (Scamehorn *et al.*, 1989). Another phenomenon is the interaction between the free surfactants and the membrane surface. It has been seen in Chapter 4 of this thesis, that this interaction mainly occurs with the hydrophobic tailgroup of surfactants in our case. Therefore, it is of interest to determine the concentration of free surfactants in solution.

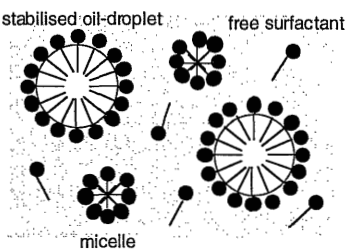

Figure B.1: Schematic drawing of the emulsion feed-solution

B.1 Method

Diffusion cell measurements

Diffusion experiments of emulsions were carried out in a diffusion cell containing two compartments of 120 *ml* each, separated by a GR40PP membrane. The feed compartment

contained the emulsion with a known composition (3.33 $g \cdot \ell^{-1}$ Castor oil and 1.33 $g \cdot \ell^{-1}$ NP9 in water) and the permeate compartment contained ultrapure water. Free surfactants alone were able to permeate the membrane. The concentration of the surfactants at the permeate side was analysed by measuring the absorption intensity at 280 nm (UV-spectroscopy, Philips PU 8720) under the assumption that the permeate contains no oil droplets (Lipp *et al.*, 1988). It was assumed that after three weeks, the free and clustered surfactant molecules will be in equilibrium in both compartments.

Samples were taken from the permeate side and analysed by UV/VIS spectroscopy for about three weeks. The feed side could not be analysed in this way because of oil droplets which were present.

B.2 Results

The surfactant concentration in the permeate compartment is plotted as a function of the time in Figure B.2.

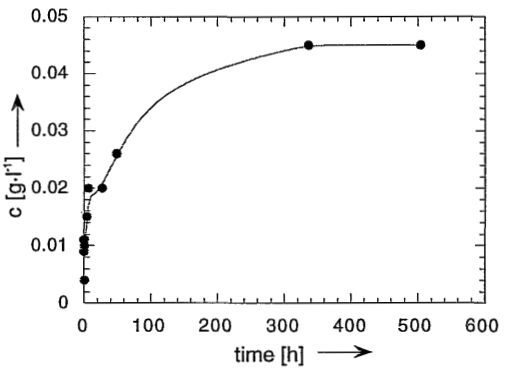

Figure B.2: Concentration profile at the permeate side of a diffusion cell with an emulsion solution at the feed side

From this graph it is clear that the surfactant concentration reached a plateau-value after 300 hours at a value of 0.045 $g \cdot \ell^{-1}$. It has been assumed that the amount of oil bound surfactants remains constant. Therefore the total non-oil bound surfactant concentration of the original emulsion was 0.09 $g \cdot \ell^{-1}$, which was 6.8 % of the total surfactant concentration in the emulsion solution. The critical micelle concentration of Synperonic NP9 was 0.06 $g \cdot \ell^{-1}$, which means that 0.03 $g \cdot \ell^{-1}$ of the surfactants were present in micelles (2.3 % of the total surfactant concentration). About 93.2 % of the surfactant molecules present in the emulsion solution was bound to the oil droplets.

If we assume monodisperse oil droplets with a particle diameter of 0.22 μm, it can be calculated that $2 \cdot 10^6$ surfactant molecules were present per oil droplet, which was

fully covered with surfactants. If furthermore it is assumed that only one monolayer of surfactants covered the oil droplets, the surface area per surfactant molecule can be calculated and was 7.8 $\AA^2$. This value was approximately five times too low with respect to contactable surface areas found in literature (Oss, 1993) for this surfactant.

membrane fouling.

Another way to prevent emulsion cake-layer formation which leads to irreversible membrane fouling is using membranes in the cross-flow configuration at low transmembrane pressures. This is the topic of Chapter 8. A critical transmembrane pressure was observed for both ultra- and microfiltration PSf and PVDF membranes, below which no flux decline during cross-flow filtration was found. These critical transmembrane pressures are linearly dependent on the membrane resistance and are higher for PSf than for PVDF membranes. This is due to larger adsorption effects onto PVDF which are not prevented by working at $\Delta P < \Delta P_c$. Nevertheless, operation below the ΔP_c of a membrane will lead to a longer membrane lifetime, owing to a reduction in membrane fouling because of a prevention of a gel or cake-layer.

A third attempt to reduce or prevent membrane fouling by formation of an emulsion gel or cake-layer is the use of electric forces perpendicular to the membrane surface in cross-flow filtration. An electric field (with the anode in the membrane feed channel) is expected to hinder the formation of a gel or cake-layer of emulsion droplets, which were found to be slightly negatively charged. A constant directly applied electric field enhanced the migration of particles from the membrane surface, resulting in higher filtration fluxes, but did not prevent irreversible fouling for two different types of PSf UF membranes.

Summarising, in this thesis emulsion filtration with polysulfone ultrafiltration membranes is studied leading to membrane fouling. The main mechanism of fouling is the formation of an irreversible gel or cake-layer on top of the membrane. This can be prevented or reduced by the use of prefilters, working at low transmembrane pressures in cross-flow filtration and using electric forces.

Samenvatting

Het grootste probleem tijdens de filtratie van afvalwaswater met behulp van ultra- en microfiltratie membranen is concentratie polarisatie en membraanvervuiling, welke leiden tot een verlies in membraanperformance en membraan levensduur. Membraanvervuiling is de depositie van componenten in de voeding op het membraanoppervlak, meestal als gevolg van een accumulatie van deze componenten aan het oppervlak (dit is het verschijnsel concentratie polarisatie). Membraanvervuiling bestaat uit porieverstopping, porie vernauwing, niet reversibele gel of koeklaag opbouw en adsorptie. Membraanvervuiling is daarom een complex verschijnsel dat afhangt van voedingseigenschappen (zoals de concentratie, pH, ionsterkte en interacties van componenten onderling), membraaneigenschappen (zoals de hydrofiliciteit, lading, ruwheid, porie grootte (verdeling) en porositeit van het membraan) en proceseigenschappen (zoals temperatuur, transmembraan druk en langsstroomsnelheid). De reductie of het voorkomen van membraanvervuiling vindt eveneens plaats op de bovengenoemde drie niveaus. Allereerst, is er in dit werk gekozen voor een model voor het afvalwater. Daarnaast op het niveau van het membraan is er zowel een membraan materiaal als structuur selectie uitgevoerd. Bovendien zijn de membraanoppervlakken gemodificeerd. Op het procesniveau is gebruik gemaakt van voorfilters, is er gewerkt onder lage transmembraandrukken en zijn er elektrische krachten gebruikt om membraanvervuiling tegen te gaan.

De **samenstelling** van afvalwater van huishoudelijke wasmachines wordt behandeld in Hoofdstuk 1. De hoofdbestanddelen hiervan zijn het wasmiddel (oppervlakte actieve stoffen, waterontharders en een bleeksysteem), vuil en water. Een gemiddelde wasmachine gebruikt 75 ℓ water per wasbeurt, dat na gebruik eindigt als afvalwater met daarin ongeveer $50 - 200$ g wasmiddel en ongeveer 100 g vuil. De belangrijkste bestanddelen voor wat betreft membraanvervuiling van deze complexe afvalwater stromen zijn oliën en vetten. Daarom is er gekozen voor een olie in water emulsie als model voor het afvalwater. Emulsies zijn bereid in een geroerd vat met Castor olie in water in aanwezigheid van een niet ionogene oppervlakteactieve stof (nonylfenolpoly(9)ethyleenoxide) en bleken minstens één jaar stabiel te zijn. Standaard emulsies met een gemiddelde druppelgrootte verdeling van 0.22 μm zijn bereid in een halfgevuld vat met een roersnelheid van 2000 omwentelingen per minuut gedurende 90 minuten. De samenstelling van deze standaard emulsies is 90 $g \cdot \ell^{-1}$ NP9 in 300 ml ultrapuur water en zijn in dit werk gebruikt als model vervuilende stof.

De selectie van het **membraan** materiaal en de structuur van het membraan is beschreven in Hoofdstuk 4. Verschillende dunne polymeerfilmpjes zijn bereid, waarop randhoekmetingen zijn verricht met water, glycerol en α-broomnaftaleen. Deze randhoeken zijn nodig in een theorie ontwikkeld door Van Oss om de niet-polaire en polaire oppervlaktespanningscomponenten te bepalen van de polymere materialen. Deze oppervlaktespanningscomponenten worden gecombineerd met die van polyethyleenoxide (PEO) en nonaan (gevonden in de literatuur). De laatste twee stoffen zijn als model genomen voor de twee delen van een molecuul van een oppervlakte actieve stof. Op deze manier kan de vrije energie van interactie worden bepaald, dat als maat is genomen voor de mate van adsorptie vervuiling van een membraan. Cellulose acetaat (CA) en polyacrylonitril (PAN) oppervlakken bleken de minste adsorptie te vertonen van PEO en nonaan. Dit volgde ook uit adsorptievervuilingsexperimenten met emulsies aan verschillende polymere membranen. In deze laatstgenoemde experimenten zijn de hoogste 'flux recovery' waarden gevonden voor de beide materialen en polyvinylideenfluoride (PVDF). Op basis van beide experimenten en op basis van de chemische en thermische stabiliteit van polymeren, is polysulfon (PSf) gekozen als meest optimaal membraan materiaal in dit werk. Een ultrafiltratie membraan (100 kDa) is gekozen voor verder onderzoek, vanwege de laagste afname in de schoonwaterflux, grootste retentie voor de emulsies en grootste waarde voor de 'flux recovery' vergeleken met microfiltratie membranen.

In Hoofdstuk 5 worden er verschillende oppervlaktemodificatietechnieken bestudeerd met als doel de mate van adsorptie te reduceren (door onder andere de hydrofiliciteit te verhogen) van PSf oppervlakken en tegelijkertijd de chemische en thermische stabiliteit te behouden. Plasma modificatie met NH_3-plasma's leidde tot een verhoging van de hydrofiliciteit, maar resulteerde ook in een beschadiging van de structuur van het membraan. Hetzelfde werd gevonden met sulfonatie van PSf membranen met TEP/SO_3, sulfonatie met $ClSO_3H$ leidde ook tot een verhoging van de hydrofiliciteit, maar resulteerde niet in een structuurbeschadiging van het membraanoppervlak.

Het mechanisme van membraanvervuiling tijdens dead-end filtratie met emulsies is het onderwerp van Hoofdstuk 6. Dit mechanisme bleek de vorming van een gel of koeklaag op het membraanoppervlak te zijn. Een koeklaag bestaande uit individuele oliedruppels wordt gevormd na een initiële fase van porieverstopping. Uit emulsiefiltratie experimenten met transmembraandrukken onder $\Delta P = 5\ bar$, volgde dat deze koeklagen incompressibel zijn en niet coalesceerden in dit drukbereik. Bovendien resulteerden de koeklagen in een niet reversibele membraanvervuiling van de ultrafiltratie membranen, wat volgde uit een daling in de 'flux recovery'.

Om membraanvervuiling te reduceren of zelfs te voorkomen op het **procesniveau**, zijn er in dit werk drie manieren toegepast. Allereerst is er in Hoofdstuk 7 gebruik gemaakt van voorfilters. Verschillende soorten voorfilters (namelijk zeolieten, calciumcarbonaat en polystyreenlatices) zijn op het membraan (UF PSf) aangebracht voorafgaande aan het eigenlijk dead-end filtratie experiment. Het gebruik van voorfilters bleek effectief te zijn om membraanvervuiling te reduceren, wat bleek uit een verhoging in de 'flux recovery' waarde bij het gebruik van voorfilters. Een kritische voorfilterdikte was echter nodig ten einde effectief membraanvervuiling te voorkomen. Hiernaast bestond er bij

een constante voorfilterdikte een tijdseffect voor de emulsies om het membraanoppervlak te vervuilen. Beide observaties kunnen worden geïnterpreteerd aan de hand van een dieptefilter mechanisme van de voorfilter op het membraan.

Een tweede methode om koeklaagvorming van emulsiedruppels op het membraanoppervlak te voorkomen is om lage transmembraandrukken te gebruiken tijdens langsstroomfiltratie. Dit is het onderwerp van Hoofdstuk 8. Een kritische membraandruk bestaat voor zowèl ultra- als microfiltratie PSf en PVDF membranen waaronder geen afname in de flux is waargenomen tijdens langsstroomfiltratie. Deze kritische transmembraandrukken hangen lineair af van de membraanweerstand en zijn hoger voor PSf in vergelijking met PVDF membranen. De oorzaak hiervan is een groter adsorptie-effect van emulsies op PVDF, wat niet kan worden voorkomen door te werken onder de kritische transmembraandruk. Desalniettemin zal het werken onder de kritische transmembraandruk leiden tot een verhoogde levensduur van het membraan, door de reductie van membraanvervuiling als gevolg van het voorkomen van een gel of koeklaag.

Een derde methode ter voorkoming of reductie van membraanvervuiling door koeklaag vorming is gebruik te maken van elektrische krachten loodrecht op het membraanoppervlak tijdens langsstroomfiltratie. Een elektrisch veld (met de anode in het voedingscompartiment van de membraanmodule) zal de vorming van een gel of koeklaag van emulsiedruppels hinderen. De emulsiedruppels bleken namelijk negatief geladen te zijn. Een constant elektrisch veld bleek de migratie van emulsiedruppels op het membraanoppervlak te beïnvloeden en resulteerde in een hogere filtratieflux. Helaas kon membraanvervuiling niet worden voorkomen voor de verschillende PSf UF membranen.

Samenvattend is in dit werk de membraanvervuiling tijdens emulsiefiltratie bestudeerd aan de hand van PSf UF membranen. Het mechanisme van deze vervuiling is hoofdzakelijk de vorming van een niet-reversibele gel of koeklaag op het membraan. Dit kan voorkomen of gereduceerd worden door het gebruik van voorfilters, het werken bij lage transmembraandrukken tijdens langsstroomfiltratie en door gebruik te maken van elektrische krachten.

Levensloop

Emile Cornelissen werd geboren op 11 augustus 1968 te Apeldoorn, alwaar hij in 1986 zijn VWO diploma behaalde aan het Katholiek Veluws College. In hetzelfde jaar begon hij de studie Chemische Technologie aan de toenmalige Technische Hogeschool Twente, nu Universiteit Twente te Enschede. Zijn doctoraalstage vervulde hij bij DSM Resins te Zwolle, waar hij heeft gewerkt aan een reokinetisch model voor het uithardingsgedrag van poederverf systemen. In het kader van de internationale studiereizen heeft hij in 1989 meegewerkt aan de door C.T.S.G. Alembic georganiseerde reis naar Zweden en Denemarken. In 1992 verrichtte hij zijn doctoraalopdracht in de vakgroep Fysische Scheidingen bij prof.dr.ir. T. Reith met als onderwerp, "Modellering van multicomponent membraanscheiding in holle vezel modules", waarmee hij zijn doctoraaldiploma Chemische Technologie behaalde.

In de periode van 1 november 1992 tot 2 januari 1997 was hij werkzaam als assistent in opleiding bij de onderzoeksgroep Membraantechnologie onder leiding van prof.dr.ir. H. Strathmann en verrichtte hij het onderzoek beschreven in dit proefschrift.